NASA Contractor Report 198462

# Computational Study of a Contoured Plug-Nozzle as a Supersonic Jet Noise Suppressor

I.S. Das
*Pennsylvania State University*
*University Park, Pennsylvania*

A. Khavaran
*NYMA, Inc.*
*Brook Park, Ohio*

A.P. Das
*Youngstown State University*
*Youngstown, Ohio*

June 1996

Prepared for
Lewis Research Center
Under Grant NAG3–1563


National Aeronautics and
Space Administration

# TABLE OF CONTENTS

# 1. SUMMARY

This report summarizes a computational study to examine the effectiveness of a scale model of an axially symmetric ideal contoured plug-nozzle (CPN) as a supersonic jet noise suppressor. The CPN has an exit diameter of 45mm and the geometrical configuration is such that the jet flow is shockless at the design pressure ratio of $\xi_d = 3.62$ (equivalent to a Mach number of 1.49). The gasdynamics of the jet flows have been predicted using the CFD code, NPARC with k-ε turbulence model; these data are then used as inputs to perform the noise computations based on the modified version of the General Electric MGB code. The study covers a range of pressure ratio, $2.0 \leq \xi \leq 5.0$ (over-, fully-, and under-expanded jet flows). The agreement of the computational aeroacoustic results with the reported experimental data is favorable. The computational results indicate consistent noise reduction effectiveness of the CPN at all pressure ratios (design and off-design) when compared to the equivalent convergent and convergent-divergent nozzles. At the design pressure ratio (shockless flow), the codes predict the noise levels within 3.0dB of the experimental data. But at the off-design pressure ratios (flows with shocks), the agreement is rather mixed. The modeling, in general, predicts the noise levels at off-design supercritical pressure ratios within 5.0dB except at very high frequencies, particularly at pressure ratios far away from the design pressure ratio, when deviations up to 8.0dB are noted. A qualitative difference in directivity trends between the prediction and the reported measurements is observed. The mechanism of shock formations in the CPN jet flows is noted to be basically different from those in the convergent and convergent-divergent nozzle jet flows. The modified GE/MGB noise code in conjunction with the CFD code, NPARC with k-ε turbulence model, is noted to be a satisfactory prediction tool for a comparative assessment of jet noise suppression; however, the noise code needs to be further modified to accommodate for shock formations in cases involving the presence of a plug in propulsion nozzles.

# 2. INTRODUCTION

A need for development of a supersonic cruise aircraft has lately been felt by the commercial aircraft industry, and several key environmental issues (community noise, sonic boom, atmospheric emissions, etc.) must be addressed to meet this goal [1,2]. The problem of noise suppression is of utmost severity - for example, the Federal Aviation Administration FAR 36 Stage III noise regulations require removal of as much as 99% of the jet noise (20 EPNdB) with acceptable thrust penalty. The magnitude of challenge could be appreciated by noting that the four Olympus engines of the Concorde produce noise levels in excess of 12, 18, and 13 EPNdB, respectively, for sideline, cutback and approach. The earlier jet noise suppression researches in the 1970's and 1980's under the NASA Supersonic Cruise Aircraft Research (SCAR) could achieve noise reductions of the order of only 2 EPNdB per percent thrust loss [3] whereas the present regulations would require a noise reduction of the order of 4 EPNdB per percent thrust loss [3].

In shock-free cold jet flows, the noise mechanism is primarily due to turbulent mixing, and the aerodynamic noise generated depends upon the mean flow speed, the flow velocity gradients just downstream of the nozzle exit, and the turbulence and mixing characteristics [4]. Imperfectly expanded supersonic jet flows contain repetitive shock cells which interact with the turbulence fluctuations generating: (a) harmonically related discrete tones of noise often termed "screech" [5], and (b) broadband but strongly peaked shock-associated noise [6-10]. It is generally recognized that contribution of shock-associated noise to the total noise is dominant at off-design supercritical pressure ratios, at lower temperatures, and at higher angles to the downstream jet axis. Also, it has been found that the mixing noise and the shock-associated noise components are often coupled. Intensity of the shock-associated noise is known to be dependent upon (i) the strength and the spacing of the repetitive shock cells, and (ii) the strength and coherence of the flow fluctuations convected through the shock fronts. Therefore, to suppress aerodynamic noise components radiated by shock containing jets, these characteristics

associated with shock structures need to be modified such that the contributing noise sources and the effectiveness of their noise generating mechanism are both reduced.

It is reported that multi-stream co-axial nozzles [11, 12] and convergent-divergent nozzles when operated close to the design pressure ratio [6, 13] strongly inhibit the shock noise. Rectangular geometry supersonic nozzle [14] and elliptical geometry supersonic nozzle [15] have also been examined as jet noise suppressors. Also, the use of the Pratt & Whitney ejector-mixer nozzle concept with ejector shrouds has also been considered as a strong possibility [16]. Some recent experimental acoustic studies of supersonic jet flows from plug-nozzles have also shown appreciable noise suppression effects [17-21]. In some of these studies, the plugs were rather long cylindrical center-bodies [17-18] and comparatively long plugs are likely to result in aerodynamic and weight penalties. In some others [19, 21], the plug surfaces were un-contoured and pointed or truncated, and consequently, in these cases the jet flows would be plagued with flow separation and wake shock formations . The preliminary experimental study of a *contoured* plug-nozzle with a *pointed* termination (CPN) as a jet noise suppressor [20] reported substantial reductions in the overall sound pressure levels as compared to the equivalent convergent nozzle - these reductions were noted at all observation angles and at all pressure ratios, off-design (flows with shocks) and design (shockless flow). The contoured plug-nozzle jet flows were found to considerably inhibit the growth and the strength of shock structures when operated at off-design supercritical pressure ratios, thereby greatly reducing the intensity of shock-associated noise component. The noise suppression effectiveness of such a *minimum length* contoured plug-nozzle jet was observed to be of the same order as that of an equivalent contoured convergent-divergent nozzle jet at the same design pressure ratio (shockless flows); but at the off-design pressure ratios of operation (flows with shocks), the noise suppression effectiveness of the CPN was reported to be better than that of the equivalent CD nozzle.

The evidence is thus clear (though limited because of a small number of reported studies) that the presence of a suitable plug results in considerable jet noise suppression through weakening/elimination of repetitive shock cells, and, possibly, also through slightly enhanced mixing. A simple single-stream plug-nozzle on its own may not be able

to meet the stringent demands of the present FAA noise regulations. However, a plug of suitable geometry can be incorporated inside practically any single- or multi-stream nozzle, circular convergent and convergent-divergent nozzles, non-circular (rectangular or elliptical) nozzles, circular or non-circular co-axial nozzles, ejector- mixer nozzles, etc. Placement of suitable plug(s) could add to the noise suppression effectiveness of the nozzles without plugs which are being considered for meeting the jet noise suppression requirement with acceptable thrust penalty.

The only reported study of a contoured plug-nozzle jet noise is a preliminary experimental investigation of rather limited scope [20]. The present investigation aims at a computational study of the gasdynamics and the far-field noise radiation of an ideal contoured plug-nozzle. It is hoped that this will help in further evaluation of the role of a contoured plug in jet noise suppression.

# 3. CONTOURED PLUG-NOZZLE JET FLOW

A fully external-expansion contoured plug-nozzle (CPN) is a modification of the conventional convergent-divergent (CD) nozzle. It combines a convergent nozzle and a contoured plug, where the supersonic expansion downstream of the sonic throat of the convergent nozzle occurs externally over the plug surface. Unlike the CD nozzle, the CPN jet flow in part is controlled by the ambient pressure and not by the nozzle wall. Therefore, the free jet boundary downstream of the CPN throat is self-adjusting. At the design pressure ratio, the CPN jet flow at the exit is uniform, axial, and shockless (see Fig. 1). The design of the isentropic plug profile for an axially symmetric, fully external expansion CPN is based on the following key considerations.

The expansion waves are assumed to be centered at the nozzle lip L (Fig. 1). For the free jet flow boundary at the lip to be straight and parallel to the nozzle axis, the convergent lip has to have an inclination $\alpha$, equal and opposite to the Prandtl-Meyer angle for the design Mach number $M_d$; in the expansion over the shoulder of an axially symmetric body, the flow in the limit is given by the two-dimensional Prandtl-Meyer theory.

The expansion waves emanating as a fan from the nozzle lip and incident on the plug surface are all canceled by suitable compression turns provided at the plug surface. The leading expansion wave of the P-M fan (corresponding to the design Mach number $M_d$) must end at the plug tip and is straight, being the start of the uniform flow region. The plug contour as such is a streamline of the potential (isentropic) flow issuing from the plug-nozzle. A methodology of designing an isentropic supersonic inlet plug using the method of characteristics was developed by Connors & Meyer [22]. To avoid the computational difficulty near the flow center line (radial co-ordinate $\rightarrow$ 0), they assumed a finite plug-tip angle and a finite strength oblique shock extending from the plug tip to the nozzle lip (throat). The plug contours were predicted for relatively high design pressure ratios. It was suggested that this approach for the inlet plug design would also be applicable to the prediction of the plug contour of an externally expanded plug-nozzle.

For a convergent lip of a given exit radius $R_N$, the maximum length of the contoured plug, $L_{max}$ is fixed for a given design Mach number $M_d$. Moreover, for an ideal contoured plug-nozzle, the annulus radius ratio K ( ratio of the plug radius at the sonic point to the radius of the nozzle lip) is a unique function of the design Mach number [23]. At a high design pressure ratio (ie, high $M_d$ ), the corresponding value of K is large, resulting in small annulus width of the throat $W_t$. Therefore, the assumption made by Connors and Meyer [22] that the sonic line at the throat is straight, is reasonably satisfied only at high design pressure ratios. The present study, however, focuses on plug-nozzles of lower design pressure ratios normally encountered in turbojet engines for supersonic jet propulsion. This range of low pressure ratios was not covered in the earlier predictions of contours of inlet plugs [22]. At lower deign pressure ratios $\xi_d$, the annulus radius ratio K of the plug-nozzle is smaller, and consequently the annulus width $W_t$ is comparatively larger. Also, because of considerably different slopes of the inner and outer walls at the throat, the flow at the throat is essentially non-uniform. The sonic line would thus have an appreciable curvature. Consequently, a prediction of the exact curved sonic line is necessary for obtaining a truly isentropic plug profile of a minimum length contoured plug-nozzle.

The design parameters that must be determined for the start of a numerical solution scheme are the annulus radius ratio K, the outer wall slope $\alpha$, the inner wall (plug) slope at the sonic point $\psi$, the maximum plug length $L_{max}$ and the exact shape of the sonic line. These parameters were estimated for a design Mach number $M_d = 1.49$ in an earlier study [20]. For design purposes, a set of charts showing the functional dependence of the overall geometric parameters K, $\alpha$, $\psi$ and $L_{max}$ on the design Mach number $M_d$ is provided in Appendix A (Figs. A1 & A2). A plug having an ideal contour (a pointed tip and isentropic profile) may not be a practical choice. In such cases, the geometry of a non-contoured plug should closely agree with the overall geometry of the ideal contoured plug in order to achieve the maximum possible noise reduction benefit through use of a plug.

# 4. PLUG-NOZZLE CONFIGURATION

The Syracuse study [20] is the only reported experimental study of a contoured (isentropic) plug-nozzle designed for operation at low to moderate supersonic pressure ratios. The nominal design number of this plug-nozzle is 1.5. The corresponding overall geometrical parameters (see Fig. 1) annulus radius ratio K, the lip angle $\alpha$, the plug-surface angle at the sonic point $\Psi$, and the maximum length to the lip radius ratio ($L_{max}/R_N$) are, respectively, 0.43, 11.91°, 28.4° and 1.30. The test contoured plug-nozzle has a lip radius of 45 mm and a lip thickness of 0.25 mm. The ratio of the converging nozzle inlet to exit area is 46. It was reported that the plug-nozzle jet was shockless at the design pressure ratio of $\xi_d = 3.62$ and the jet screech noise was noted to be absent. The scope of this experimental study was rather limited, at least from gasdynamics perspectives. For further details of the experimental setup, see Ref. 20.

The computational gasdynamics/noise study undertaken is carried for the contoured plug-nozzle geometry of the aforementioned experimental study [20]. This would enable comparison of the computational gasdynamics and noise data with the reported measurements. A profile of the contoured plug-nozzle studied is presented in Appendix A (Fig. A3). Also, a complete geometry of the annular flow boundaries (outer plug-stem surface is the inner boundary and inner surface of the converging nozzle is the outer boundary) is presented in Table A (Appendix A). The reference point (X=0, R=0) is located on the jet axis (an axis of symmetry) at the start of the converging section of the nozzle, X-axis is directed along the downstream jet axis, and the radial R-axis is perpendicular to the jet axis.

# 5. METHOD OF SOLUTION

The computational solution for the aeroacoustics of the contoured plug-nozzle jet noise is primarily based upon the methodology as developed in the GE/MGB code [24] and subsequently modified by the NASA Lewis researchers [25, 26]. In the earlier GE approach [24], the aerodynamic predictions were carried out by applying an extension of the Reichardt's model. The Reichardt's solution neglects radial mean flow and swirl, and the effect of shock structures, if present, on mixing and turbulence. This results in a relatively fast numerical scheme, but the predictions for complex geometry are found to be unsatisfactory. In the later modifications [25, 26], a two-stage algorithm was considered. The Reichardt's model was substituted by a CFD Navier-Stokes solver and the aerodynamic calculations were carried out independently. The resulting plume data were then used for the noise computations. Better gasdynamic representation of the flow field would, one may expect, lead to better predictions of the noise radiation. For full details of the NASA Lewis methodology (used in the present computational study) see, Ref. 25 & 26. In what follows, only a brief sketch is presented.

The flow field computation is based on the NPARC code [27] with k-ε turbulence model [28]. This code is an evolution of the PARC code developed by Arnold Engineering Development Center, which in turn was based upon the NASA Ames ARC code. This extensively validated code solves the complete Reynolds-averaged Navier-Stokes equations in conservative law form, using the Beam and Warming [29] approximate factorization algorithm. The first section briefly describes the application of the NPARC with k-ε turbulence model for computation of the source strength and spectrum, and explains the empirical constants used for the convection factor. The second section considers how the mean flow velocities and temperatures, obtained by the application of the CFD code, are to be used in the estimation of sound/flow interaction of the jet flow. The third section explains the shock noise prediction scheme.

## 5.1 Source Spectrum Model

Following Lighthill's approach [30, 31], the mean square acoustic pressure in the far-field in absence of convection and refraction may be written as,

$$\overline{p^2}(R, \theta, \phi) = \frac{R_i R_j R_k R_l}{16\pi^2 C_\infty^4 R^6} \int\int_{\vec{y}\,\vec{\xi}} \frac{\partial^4}{\partial \tau^4} \overline{(T_{ij} T'_{kl})}\, d\vec{\xi}\, d\vec{y} \tag{1}$$

The source strength is assumed to be dominated by the unsteady momentum flux, ie, $T_{ij} \sim \rho V_i V_j$. The separation vector $\vec{\xi}$ is the correlation between $\rho V_i V_j$ at $\vec{y}$ and $\rho' V_k' V_l'$ at $\vec{y}+\vec{\xi}$, and $\tau$ is the time delay correlation. The corresponding spectrum in terms of the Fourier transform of the autocorrelation function is,

$$\overline{p_\omega^2} = \frac{1}{2\pi} \int_{-\infty}^{\infty} \overline{p^2} e^{i\omega\tau}\, d\tau \tag{2}$$

As such, for a quasi-incompressible turbulence, the source strength is characterized by a two-point time-delayed fourth-order velocity correlation tensor. For a nearly parallel mean flow, contributions of the self-noise terms may be shown to be independent of the mean flow. Assuming a normal joint probability for turbulent velocity components [32] and following the Batchelor's model [33] for isotropic turbulence, the fourth-order correlation is a linear combination of the second-order correlations,

$$\overline{v_i v_j v'_k v'_l} = \overline{(v_i v'_k)}\,\overline{(v_j v'_l)} + \overline{(v_i v'_l)}\,\overline{(v_j v'_k)} + \overline{(v_i v'_j)}\,\overline{(v_k v'_l)} \tag{3}$$

By assuming the two-point velocity correlation to be separable in space/time factors [32],

$$\overline{v_i v'_j} = R_{ij}(\vec{\xi}) g(\tau), \tag{4}$$

the integration can be carried out in closed form. The space factor may be written as [33],

$$R_{ij}(\vec{\xi}) = T\left[\left(f + \frac{1}{2}\xi f'\right)\delta_{ij} - \frac{1}{2} f' \xi_i \xi_j / \xi\right] \tag{5}$$

where $T = \overline{(v_i v_i)}/3$ is the intensity of turbulence replacing the axial turbulence in the Reichardt's model and $f' = \partial f / \partial \xi$ and $f(\xi) = \exp[-\pi\xi^2/L^2]$, L being longitudinal macroscale of turbulence. The time factor of correlation may be expressed as,

$g(\tau) = \exp[-(\tau/\tau_0)^2]$, where $\tau_0$ is the characteristic time delay in moving reference frame. For axisymmetric jets, it has been shown that $\tau_0$ is proportional to the inverse of mean shear. Since the eddy length scale $L_\varepsilon$ is related to the kinetic energy of turbulence, $k=(\overline{v_i v_i})/2$, and its dissipation rate $\varepsilon$ as $L_\varepsilon = k^{3/2}/\varepsilon$, and assuming $L \sim L_\varepsilon$, it can be concluded that, $1/\tau_0 \sim \varepsilon/k$.

The first component of source/ spectrum correlation tensor is given by[24, 32],

$$I_{1111}(\Omega)=(3/8)\sqrt{\pi}\rho^2 k^{7/2}(\Omega\tau_0)^4\exp[-(\Omega\tau_0)^2/8] \tag{6}$$

which is used to compute the noise field in conjunction with the refraction effect of the mean flow. The Doppler effect relating the source frequency $\Omega$ and the observer frequency f is given by, $\Omega = 2\pi f\overline{C}$, where the eddy convection factor, $\overline{C} = (1\text{-}M_c\text{Cos}\theta)$. In the modified computational approach, the eddy convection factor is taken as,

$$\overline{C} = \sqrt{(1 - M_c\cos\theta)^2 + (\alpha_c\sqrt{k}/C_\infty)^2} \tag{7}$$

The empirical constant $\alpha_c$ has been assumed to be 0.5 and the convection Mach number is taken as a weighted average of the exit Mach number and the local Mach number,

$$M_c = 0.5M + \beta_c M_j \tag{8}$$

The convection constant $\beta_c$ in the range of 0.25 to 0.3 appears to yield the best results.

## 5.2 Sound / Flow Interaction

The effect of the surrounding mean flow on acoustic radiations caused by convecting multipole sources, which is not accounted for by the acoustic analogy approach, needs to be incorporated [34-38]. The sound/flow interaction effect considered in the code used in the present study is primarily based upon the formulation developed by Mani and Balsa [24]. The mean square acoustic pressure in the far field is given by,

$$\overline{p^2}(R, \theta, \Omega) = \int_{\bar{y}} \Lambda(a_{xx} + 4a_{xy} + 2a_{yy} + 2a_{yz})\, d\bar{y} \tag{9}$$

where $a_{xx},\ldots,a_{yz}$ are the directivity factors which describe the noise field due to each of the quadrupole contained within a turbulent eddy volume element. The weighting factors are those derived by Ribner [32]. Factor $\Lambda$, related to the source intensity and frequency, is:

$$\Lambda \approx \frac{\left(\frac{\rho_\infty}{\rho} - 1\right)^2 I_{1111}(\Omega)}{(4\pi R C_\infty C)^2 (1 - M\cos\theta)^2 (1 - M_c \cos\theta)^2} \tag{10}$$

The directivity factors are functions of the shielding function $g^2$ given by,

$$g^2(r) = \frac{(1 - M\cos\theta)^2 \left(\frac{C_\infty}{C}\right)^2 - (\cos\theta)^2}{(1 - M_c \cos\theta)^2} \tag{11}$$

The mean flow variables obtained from the CFD computation are used to estimate $g^2(r)$ and hence the directivity factors. The location where $g^2(r)$ changes sign is known as the turning point. A negative value of $g^2(r)$ between the source and the observer indicates the possibility of fluid shielding. The position of source with respect to the turning points of $g^2(r)$ contributes to the amount of shielding by a factor of

$$\exp\left[-2K\int_{r_1}^{r_2}\sqrt{|g^2(r)|}\,dr\right],$$

where the limits are determined by the source location with respect to the turning points, and $K = \Omega/C_\infty$, is the wave number.

A correction of one Doppler factor has been utilized for the source volume effects [39]. The correction for flight speed has been included using the flight dynamic factor, $(1 + M_\infty \cos\theta)^{-1}$, where $M_\infty$ is the flight number.

### 5.3 Shock Noise Prediction

The shock noise prediction methodology incorporated in the code follows the formulations of Tam and his associates [40-42]. The earlier formulation, based on the vortex sheet shock cell model of Pack [43], assumes a thin mixing layer. A later development considers multiple scales shock cell model which accounts for the spreading of the mean flow, and the shock cell structure is represented by a superposition of the wave guide modes of the jet flow. The mechanism is further elaborated in Tam's

stochastic model theory in which the large turbulence structures are represented by a superposition of the intrinsic instability waves of the mean jet flow. Combined with the multiple scales shock cell model, the stochastic model theory predicts both the near and far field spectra. The shock noise power spectral density at a point (r, θ) is given by,

$$S(r,\theta,f)=\frac{\Gamma L_w^2 A_j \bar{A}^2 \left(\frac{\rho_\infty^2 C_\infty^4 M_j^2}{f(fD_j/U_j)}\right)}{(1+\frac{\gamma-1}{2}M_d^2)r^2} \times \sum_{m=1}^{\infty}\frac{1}{\sigma_m^2 J_1^2(\sigma_m)}\exp\left\{-\left(\frac{(f_m-f)(1+M_c\cos\theta)\,L_W}{f\,(U_c/U_j)}\right)^2\frac{1}{2\ln 2}\right\} \tag{12}$$

where Γ is an unknown empirical constant and $L_w$ is the half-width of Tam's "similarity source model" and is related to the core length of the jet. Both parameters need to be determined by fitting the prediction formula to the experimental data. The fully-expanded jet diameter $D_j$ is related to the nozzle exit diameter D through the mass conservation equation as,

$$\frac{D_j}{D}=\left[\frac{1+\frac{\gamma-1}{2}M_j^2}{1+\frac{\gamma-1}{2}M_d^2}\right]^{\frac{\gamma+1}{4(\gamma-1)}}\left(\frac{M_d}{M_j}\right)^{1/2} \tag{13}$$

The parameter $\sigma_m$ is the $m^{th}$ root of the zeroth order Bessel function and $f_m$ is defined as,

$$f_m=\frac{U_c k_m}{2\pi\,(1+M_c\cos\theta)} \tag{14}$$

where $k_m$ corresponds to the wave number of the $m^{th}$ wave guidemode of the shock cell structure at maximum wave amplitude. $J_1$ is the Bessel function of order one. The quantity $\bar{A}^2$ which characterizes the shock cell strength (to be determined semi-empirically to improve the prediction) is given by,

$$\overline{A}^{\,2} = \left[ \left( \frac{M_j^2 - M_d^2}{1 + \frac{\gamma - 1}{2} M_d^2} \right)^2 \left( \frac{D}{D_j} \right)^2 \right] \div \left[ 1 + n_1 \left( \frac{M_j^2 - M_d^2}{1 + \frac{\gamma - 1}{2} M_d^2} \right)^{n_2} \right] \tag{15}$$

where $n_1 = 3.0$, $n_2 = 3.0$ for underexpanded flows and $n_1 = 6.0$, $n_2 = 5.0$ for overexpanded flows. It should be noted that these values in Tam's model are based upon the experimental studies of the convergent-divergent nozzle jet flows.

The prediction incorporates the hot jet effects and it has been further modified to accommodate the forward flight effect [44].

# 6. SCOPE OF COMPUTATIONAL DATA

The axisymmetric flow-field is represented by a computational domain consisting of a 151 x 351 grid which is highly clustered along the plug-nozzle lip line and along the plug surface (Fig. 2). The domain starts at the beginning of the converging inlet of the plug-nozzle and extends to a length of 33D and has an outer radius of 11D (plug-nozzle exit diameter D = 45 mm and aspect ratio = 3). The assumed ambient conditions are: Mach number = 0.05 and static temperature (also the reference temperature) = 294 K. The noise data are computed at a far-field station located on an arc of radius 3.05 m centered at a point on the jet axis in the exit plane of the plug-nozzle at the lip.

The gasdynamics and far-field noise of the CPN jet has been computed at pressure ratios of $\xi$ = 2.0, 2.5, 3.0, 3.62 (design), 4.0, 4.5 and 5.0. For a given pressure ratio, a run time of about five hours on the Cray Y-MP was needed to attain satisfactory convergence. However, once the CFD computation is completed for one pressure ratio (say, $\xi_{design}$ = 3.62), the run times for subsequent computations from one adjacent pressure ratio to another are of the order of only four hours. A complete set of computational acoustic data were obtained at angles, *measured from the inlet*, in multiples of 10° from 20° to 160°. These acoustic data are reproduced in tabular forms in Appendix B (note that *the angles in tables are referred to from the inlet jet axis*) .

# 7. RESULTS & DISCUSSIONS

A complete set of the gasdynamics and the far-field noise data for the contoured plug-nozzle is available. The available gasdynamics data consist of predicted numerical outputs of all the flow variables at the grid points along with the associated contour plots. The computational noise data include one-third octave sound pressure levels of mixing noise, shock noise and total noise in the full range of the investigated pressure ratio for various angles to the jet axis. Only some typical gasdynamics and far-field noise results, which help assess the role of a CPN as a supersonic jet noise suppressor, are presented as part of the discussion that follows.

## 7.1 Some Gasdynamic Features Of CPN Jet Flows

A typical contour plot of the turbulence intensity in the CPN jet flow at design condition, $\xi_d$ = 3.62, is presented in Fig. 3. The contour values are normalized with respect to the acoustic speed at 294 K. The turbulence intensity levels, which play a key role in generation of the mixing noise, are noted to be rather low (< 12.4%) at all pressure ratios. The computational data of the turbulence intensity levels at the supercritical pressure ratios studied need to be further interpreted and validated. However, there is no quantitative data available for an ideal contoured plug-nozzle jet to enable a satisfactory validation of the use of NPARC code for prediction of gasdynamics of such jet flows.

A typical Mach number contour plot for the jet flow at design pressure ratio (shockless flow condition: $\xi_d$ = 3.62), is provided in Fig. 4. The supersonic core of the jet is noted to extend about fourteen jet diameters downstream from the plug-nozzle lip. This is significantly different from the corresponding reported values of about twelve diameters for the convergent nozzle [45] and about eighteen diameters for the convergent-divergent nozzle ($\xi_d$ = 3.18) [25]. The computational gasdynamics data indicate a reasonably shock free flow for the CPN at $\xi_d$ = 3.62. As compared to the convergent nozzle, and even convergent-divergent nozzle, the plug-nozzle CFD data

indicate presence of relatively weak cellular shock structures at all off-design pressure ratios (both less than or greater than the design pressure ratio). Close to the design pressure ratio, at $\xi = 3.0$ or at $\xi = 4.0$, it is noted that the first few shock cells are too weak to repeat themselves farther downstream. The formations of the first shock cell in CPN jet flows occur relatively farther downstream, and the strength of the shock cells and their extents decay more rapidly. These observations are in agreement with the reported shadowgraph records of the contoured plug-nozzle jet flow [20]. It should be noted that the Mach number contour plot (shockless flow condition) indicates the presence of some small subsonic pockets embedded in the supersonic core of the jet near the jet axis. This is explained by the presence of a thin separated wake flow region starting from the plug tip (wake flow on account of a finite plug tip dimension). A similar fine wake flow was also noted in the shadowgraph of the CPN jet flow presented in Ref. 20. A significant wake flow is necessarily accompanied by a recompression shock which, if strong enough, could lead to the formation of its own repetitive shock structure. An ideally pointed plug, of course, will not generate a wake but then, this is not a practical proposition. Also, it may be noted that there is no evidence of formations of wake shock or Mach disc even at the highest pressure ratio ($\xi = 5.0$) in the present computational study, as was the case in the earlier experimental study [20]. The Mach disc formations are always encountered at high off-design supercritical pressure ratios in the convergent and convergent-divergent nozzle jet flows.

### 7.2 Mechanism Of Shock Formations In CPN Jet Flows

The operation of the CPN at a supercritical pressure ratio less than the design pressure ratio ($\xi < \xi_d$ or $M_j < M_d$) is designated here as the overexpanded mode of operation. In such flows (see Fig. 5(a)), all the expansion waves between the leading wave front (corresponding to $M = M_j$) and the tailing wave front ($M = 1$) of the expansion fan, centered at and emanating from the nozzle lip, are canceled at the contoured plug surface. However, the continued compression turnings of the contoured plug surface

downstream of the location, where the leading expansion wave ($M = M_j$) of the expansion fan is incident on the plug, generate a family of compression wave fronts on their own. If the fully expanded jet Mach number $M_j$, is much less than the design Mach number $M_d$, then these compression waves generated at the plug surface may coalesce together to form a weak oblique shock in the plug region close to the free jet boundary. For cases of $M_j$ not much less than $M_d$, the compression waves generated by the plug surface may not coalesce to form an oblique shock in the plug region. The compression fronts generated by the plug surface or the oblique shock formed by their coalescence in the plug region, reflect as weak expansions from the jet boundary; these expansion waves reflect as even weaker compressions from the opposite jet boundary; and, finally, the compression waves join together to form the first weak conical shock. Subsequent reflections then lead to formations of a train of weak repetitive shock cells. Such shock structure, on account of the compression waves originating from only a *part* of the plug surface near its tip, is weaker than the oblique shock structure of an underexpanded jet flow from an equivalent convergent nozzle operated at the same pressure ratio but formed by the coalescence of the compression waves due to reflection of the *entire* Prandtl-Meyer expansion fan from the free jet boundary. In jet flows when $M_j$ is not much less than $M_d$, the location of the first shock cell is relatively much farther downstream from the nozzle lip. These observations are validated by the reported shadowgraph records [23].

Typical shock formation in underexpanded CPN jet flows, ($M_j > M_d$) is shown in Fig. 5(b). In such jet flows, all of the expansion waves, corresponding to $M < M_d$, emanating from the nozzle lip are intercepted by the contoured plug surface and are canceled by the suitable compression turnings provided thereat. However, some expansion waves (corresponding to $M_j > M_d$) escape past the plug tip, meet the free jet boundary downstream, get reflected as compressions, and subsequently coalesce to form the first conical shock of the repetitive shock cell structure. Again, as in overexpanded cases, only a very small portion of the waves of the Prandtl-Meyer expansion fan centered at the nozzle lip play a role in shock formations; and, therefore, the train of shock cells formed is relatively weak. Also, the escaping expansion waves and their reflections as

compression waves from the jet boundary are relatively less steep, and, therefore, the first shock cell location is farther downstream and the shock cell spacings are larger. These observations are confirmed by the reported shadowgraph records [23].

It thus appears that the repetitive shock cell formations in contoured plug-nozzle jet flows, in both the underexpanded and overexpanded modes of operation, are relatively weak. The mechanism of shock formation is noted to be basically different from those in convergent nozzle and convergent-divergent nozzle jet flows.

### 7.3 Computational Noise Prediction

Some typical predicted one-third octave SPL spectra of the CPN jet flows for the fully expanded mode of operation ($\xi_d = 3.62$), for the overexpanded mode of operation ($\xi = 2.0, 2.5$ & $3.0$), and for the underexpanded mode of operation ($\xi = 4.0$ & $4.5$), are compared with the experimental values [20] in Figs. 6-11. Each figure shows spectra at four typical angles, *measured from the downstream jet axis,* $\theta = 30°, 60°, 90°$ and $120°$.

At the design pressure ratio ($\xi_d = 3.62$, shockless flow, Fig. 6), the agreement of the predicted SPL'S with the measurements may be considered to be, in general, very good, the deviations being of the order of 3dB. The agreement of the predicted values with the reported measurements are observed to be excellent at lower angles to the downstream jet axis throughout the entire range of frequencies except at the extreme upper ends. The code is noted to slightly underpredict the SPL's, generally at all angles. The deviations of the predictions from the measurements are noted to increase at higher angles to the jet axis, $\theta = 60°, 90°$ & $120°$. The maximum deviations are noted to be in the upper range of the one-third octave band center frequencies, these being of the order of 7dB or less; outside this range of frequencies, the agreement is noted to be very good. The SPL predictions at very high band center frequencies are noted to be poor at all angles to the jet axis. The computational scheme predicts the peak Strouhal numbers of the order of 0.3 ($f_{peak}\ D / U_j \cong 0.3$), which is nearly the same at all angles. However, the experimental data show that the peak Strouhal number increases with increasing angle up

to 60° and then levels off to a nearly constant value. A slight shift in the predicted peak frequency to a higher value, as compared to the measurements, is observed at almost all higher angles $\theta$. The general agreement of the 1/3-octave SPL predictions with the experimental data may be considered to be good though. Further, the agreement of predictions with the measurements in the present contoured plug-nozzle study is generally of the same order as that reported in an earlier computational study of the convergent-divergent nozzle [25]. The computational CPN gasdynamics data indicate that, at the design pressure ratio, the jet flow is nearly shockless and the dominant component of the noise generation mechanism is rather due to mixing alone. It thus appears that the combination of the NPARC CFD code and jet noise code GE/MGB [24] as modified by the NASA Lewis researchers [25], reasonably predicts the jet noise in situations where the mixing noise is the dominant noise component of the jet flow.

Now, the predicted noise spectra of the CPN jet in presence of shocks need to be examined. Repetitive shock cells are always present in jets at supercritical off-design pressure ratios. The one-third octave SPL's comparisons in the overexpanded modes of operation at $\xi$ = 2.0, 2.5 and 3.0 (see Figs. 7, 8 and 9, respectively), show a very reasonable agreement between predictions and measurements. At pressure ratios close to the design pressure ratio, the agreement of the predictions with the measurements are excellent in almost the entire range of frequencies, the deviations being of the order of 3 dB (see Figs. 8 & 9). With decreasing pressure ratio, however, the codes are noted to considerably overpredict the SPL's at very high frequencies. At the low pressure ratio farthest from the design condition, $\xi$ = 2.0, where one would expect relatively much pronounced repetitive shock structures in the jet flow field, an excellent agreement of the predictions with measurements (within 3 dB) is noted at all angles except at very high frequencies where deviations up to 10dB are noted (see Fig. 7). From the detailed numerical acoustic data (see, for example, Tables B-1, B-2 & B-3 in Appendix B), it may be concluded that the spectra are dominated by the mixing noise at almost all angles to the jet axis at all pressure ratios. However, at very low supercritical pressure ratio, the shock noise component is noted to dominate, in particular at very high frequencies and

larger angles to the jet axis. Therefore, the lack of good agreement in the overexpanded modes at very high frequencies may be attributed to the computational overprediction of shock noise. In the underexpanded modes also, for example at $\xi$ = 4.0 and 4.5, the predictions are noted to be quite satisfactory except at very low frequencies, deviations being of the order of within 3dB (see Figs. 10 and 11). For the lower range of one-third octave band center frequencies, the deviations are observed to be quite considerable, reaching values of up to 8dB. In general, the codes are noted to underpredict the SPL's in the underexpanded mode of operations whenever the deviations are significant. Using the same codes as in this study, a computational noise prediction study of a contoured CD nozzle ($\xi_d$ = 3.12) in imperfectly expanded modes of operation has been recently reported [26]. The agreement of the predicted CD nozzle jet SPL's with the measurements were noted to be quite fair except in the range of low one-third octave band center frequencies, where the deviations were found to be significant. It should be noted that according to the reported study [26], no noise suppression effectiveness of the CD nozzle, as compared to the equivalent underexpanded convergent nozzle, was observed at lower angles to the downstream jet axis at all frequencies. However, significant noise suppressions were reported for high frequencies at higher angles $\theta$ to the downstream jet axis where the shock associated noise is known to be the dominant component. Such is not the case for the contoured plug-nozzle of the present study where one notices noise suppression effectiveness at all pressure ratios (even at low supercritical off-design pressure ratios) for all angles to the downstream jet axis - at lower angles where mixing noise is the dominant component as well as at higher angles where the shock noise is the dominant component. It should be emphasized that the reported CPN experimental noise data [20] indicate little sensitivity to increases in the pressure ratio in the underexpanded mode close to the design pressure ratio. This may be attributed to the basically different shock formation mechanism in contoured plug-nozzle jet flows as explained in the earlier section. Thus, the underlying theories which form the basis of the noise code used in the present study need to be accordingly modified.

The predicted variation of the OASPL's vs $\theta$ for the CPN jet flow at the design pressure ratio, when the jet flow is shockless and the only noise is due to turbulent mixing, is compared with the CPN measurements in Fig. 12. The figure also shows the experimental noise data of an equivalent CD nozzle as derived from an earlier study [6]. The agreement of the computational CPN data with the CPN measurements are noted to be quite fair, deviations being of the order of 3dB in the middle range of angles to the downstream jet axis and slightly more in the range of higher and lower angles to the downstream jet axis. The predicted maximum OASPL is noted to be about 114.5dB at $\theta = 40°$ as compared to the corresponding measurement of 117dB at $\theta = 30°$. The codes always underpredict the OASPL's but the trend of variation seems to be well represented. Earlier measurements [20] have shown that the OASPL's of a contoured plug-nozzle ($M_d$ = 1.49, present case) are significantly lower than those of a contoured CD nozzle ($M_d$ = 1.48) at lower angles to the downstream jet axis [20, 6] where the mixing noise is known to be dominant. This trend is also indicated by the present computational study. Comparisons of the present CPN computational OASPL's vs $\theta$ prediction with a similar computational prediction for a CD nozzle (design pressure ratio, $\xi_d$ = 3.2) [25], when scaled down to a distance of 3.05m (present case) based on the inverse-square law variation and when adjusted for the nozzle exit area, also show the same trend. Thus, it may be concluded that the presence of a properly contoured plug may result in significant suppression of mixing noise also.

The computational OASPL's vs $\theta$ variations for some typical cases, when repetitive shock structures are present in the CPN jet flows, are compared with the experimental values in Fig. 13 for the supercritical pressure ratios less than $\xi_d$ (overexpanded mode of operation) and in Fig. 14 for supercritical pressure ratios greater than $\xi_d$ (underexpanded mode of operation). In the overexpanded mode of operation (Fig. 13), one notices a lack of a significant directivity pattern in the predicted noise radiation; the directivity pattern is noted to gradually emerge with increasing supercritical pressure ratio (being almost absent at $\xi$ = 2.0). Such a directivity pattern was not indicated in the reported measurements [20]. Further, the trend of noise directivity as

predicted by the computational study appears to be basically different at off-design supercritical pressure ratios: the measurements [20] consistently indicate a tapering off of the OASPL's from its highest value at the lowest angle $\theta$, to a gradual leveling off with increasing $\theta$. Another peculiarity of the computational modeling is that, for $\xi < \xi_d$, it underpredicts OASPL's at lower angles $\theta$ (region of the mixing noise dominance) and overpredicts them at higher angles $\theta$ (region of shock noise dominance); the magnitudes of deviations, however, are noted to be reasonable, being within 5dB.

The computational predictions of OASPL's vs $\theta$ variations for supercritical pressure ratios, $\xi > \xi_d$ (Fig. 14), exhibit directivity patterns which are, again, noted to be basically different in nature from the corresponding measurements. The predictions indicate well defined directivity pattern *always peaking at* $\theta \cong 40°$, whereas the measurements indicate practically no directivity pattern in the far-field noise radiation. Further, the computational modeling underpredicts OASPL's close to the design pressure and overpredicts the OASPL's farther away from the design pressure ratio in the entire range of the examined supercritical pressure ratios $\xi > \xi_d$; the maximum deviations, however, are observed to be quite reasonable, being well within 5dB. Thus, the computational modeling predictions are noted to be not as satisfactory in such situations.

### 7.4 Noise Suppression Effectiveness Of CPN

The variations of the predicted OASPL's at $\theta = 90°$ with the pressure ratio $\xi$ for the CPN jet flows are compared in Fig. 15 with the corresponding experimental data for the CPN [20] and the equivalent CD nozzle [6]. Neither the plug-nozzle prediction nor the reported plug-nozzle measurements show the typical "bucket" pattern as clearly exhibited by the reported CD nozzle studies. The "bucket" pattern refers to a dip in the variation of the OASPL's vs pressure ratio $\xi$ for the CD nozzle at and close to the shock-free design pressure ratio; the OASPL for the CD nozzle is 'lowest' at its design pressure ratio (shockless flow condition) and then quickly rises to the corresponding values for the conic nozzle at off-design pressure ratios on either side of the design pressure ratio. It is

important to note that the OASPL's at $\theta = 90°$ for the CPN jet as predicted by the codes are in general higher than the experimental values, but these values are still lower than the corresponding equivalent CD nozzle experimental values. In addition, the predicted OASPL's of the CPN jet are lower than the corresponding values for the equivalent convergent nozzle in the entire range of operating pressure ratio, whereas the OASPL's of CD nozzle jets at off-design pressure ratios approach those of the equivalent conic nozzle jets. That is, the computational scheme predicts that, as a jet noise suppressor, the contoured plug-nozzle is as good as a contoured CD nozzle, if not better.

The variation of computational OASPL's at $\theta = 90°$ (the angle to the jet axis where the shock-associated noise is known to be dominant) for the contoured plug-nozzle is also plotted as a function of the logarithmic Harper-Bourne & Fisher type shock parameter, $\log_{10}\beta$, where $\beta = (M_j^2 - M_d^2)^{1/2}$, in Fig. 16. For comparisons, the experimental data are also shown in the figure. The solid line in the figure is a linear fit to the experimental data [20]. It is well known that the underexpanded convergent nozzle jet flows follow the $\beta^4$-scaling law [7] where $\beta = (M_j^2-1)^{1/2}$. A similar $\beta^4$-scaling law, where $\beta = (M_j^2 - M_d^2)^{1/2}$ , for the imperfectly expanded CD nozzle jet flows is also known. As opposed to the convergent nozzle and the CD nozzle, the contoured plug-nozzle jet noise intensity, over the entire range of $M_j$, varies approximately as $\beta^2$ (as indicated by the solid line in the figure). Therefore, the OASPL's for the CPN increases comparatively less steeply than those for the convergent nozzle, or for the CD nozzle. The underlying physical reason for this behavior is provided by the earlier observations on shock formations in the CPN jet flows - the strength of the shock structures in the CPN jet flows in the over- and underexpanded modes are relatively weaker and the shock-cell spacings are relatively larger. Also, the typical phenomenon of oblique shock formation at the nozzle lip in the overexpanded CD nozzle jet flows is noted to be absent in the CPN jet flows. Consequently, the contributions of the shock-associated noise in the imperfectly expanded CPN jet flows are comparatively less.

The computational data of the present CPN jet noise do not indicate a $\beta^2$-scaling law, where $\beta = (M_j^2 - M_d^2)^{1/2}$. This may be attributed to the failure of the theoretical

scheme to predict shock noise at pressure ratios far removed from the design. The present jet noise code is based on the work of Tam and his associates [40-42] which account for only moderately imperfectly expanded supersonic jets.

Several factors need to be noted in regard to the application of the present computational approach to jet noise predictions. First, a number of empirical parameters ($\alpha$, $\alpha_c$, $\beta_c$, $\Gamma$, $L_w$, etc.) need to be used as inputs to the codes and these parameters are to be chosen based on the available experimental data as guide. In the present study, the choice of these parameters was primarily based upon the experimental data on the underexpanded convergent nozzle jet flows and fully- and imperfectly-expanded CD nozzle jet flows. No experimental data on contoured plug-nozzle jet flows are available to help determine a suitable set of values for the empirical constants. Second, the underlying mechanisms of the mixing noise and shock noise radiation used in the computational modeling are supported primarily by the studies on convergent nozzle and CD nozzle jet flows. As noted before, the mechanism of shock formations in a contoured plug-nozzle jet flows is basically different from those in the convergent nozzle or in the convergent-divergent nozzle jet flows. Also, as reported in experimental studies [6, 20], at design conditions of shockless flows, much lesser noise levels were noted at lower angles $\theta$ (region of mixing noise dominance) for the CPN than for the CD nozzle. Therefore, it is reasonable to conclude that in order to further modify the GE/MGB code, issues related to these need to be addressed. In addition, one should also take into consideration of possible coupling of the mixing noise and the shock noise radiation.

In general, the computational results well support the role of a contoured plug-nozzle as a supersonic jet noise suppressor. Further, the computational study validates the key findings of the experimental study [20] in regard to the noise suppression effectiveness of the contoured plug-nozzle.

# 8. CONCLUSIONS & RECOMMENDATIONS

## 8.1 Conclusions

Based on discussions of the results of the computational gasdynamic and far-field noise study of the contoured plug-nozzle jet flows, some important conclusions may be drawn as follows:

1. The prediction of noise levels of the contoured plug-nozzle jet flow at design condition (shockless flow) is noted to be good; the model often predicts the noise levels within 3dB of the reported experimental values. The trends as well as the magnitudes are well represented.

2. The modeling, in general, predicts the noise levels at off-design supercritical pressure ratios (flows with shocks) within 5dB except at very high frequencies, particularly at pressure ratios far away from the design, when deviations up to 8 dB are observed. A basic difference in the predicted directivity pattern and the reported experimental directivity pattern is noted.

3. The role of a contoured plug-nozzle as a jet noise suppresser for low to moderate supersonic pressure ratios is well supported by the computational study.

4. The computational noise prediction scheme consisting of a combination of the modified GE/MGB noise code and the NPARC CFD-code with k-ε turbulence model is noted to be a useful engineering tool for a comparative evaluation of jet noise suppression approaches.

## 8.2 Recommendations

The available gasdynamics data on the contoured plug-nozzle jet flows are very limited. This makes it difficult to assess the validity of the NPARC CFD-code with k-ε turbulence model in predicting the gasdynamics of such jet flows. A proper estimate of the empirical gasdynamic constants for use in the codes is rather difficult at this stage. The noise prediction code can at best be only as good as the CFD code that drives it. Therefore, there is a need for further experimental gasdynamics and acoustic data on the contoured plug-nozzle jet flows for a range of supercritical design pressure ratios.

The issues of possible different mechanisms for both the mixing noise and shock-associated noise radiations in contoured plug-nozzle jet flows need to be addressed for the future development of the GE/MGB code as modified at NASA Lewis.

It is suggested that the possibility of use of a suitably optimized plug in nozzle schemes competing for jet noise suppression be assessed.

# 9. NOMENCLATURE

| | |
|---|---|
| $A$ | area of the jet |
| $C$, $C_\infty$ | local and ambient speed of sound |
| $\overline{C}$ | eddy convection factor |
| $D$ | diameter |
| $f$ | observer frequency |
| $f_P$ | peak frequency |
| $I_{ijkl}$ | source correlation tensor |
| $J_1$ | Bessel function of order one |
| $k$ | turbulent kinetic energy |
| $k_m$ | wave number |
| $K$ | annulus radius ratio of the plug-nozzle ($= R_P/R_N$) |
| $L$ | longitudinal macroscale of turbulence |
| $L_\varepsilon$ | eddy length scale |
| $L_{max}$ | axial length of the plug from the sonic point to its tip |
| $L_W$ | half-width of Tam's similarity source model |
| $M$ | Mach number |
| $M_C$ | convection Mach number |
| $p$ | absolute pressure |
| $r$ | radial distance |
| $R$ | radius (also source to observer distance) |
| $R_i$ | observer co-ordinate |
| $R_P$ | radius of the plug at the sonic point |
| $R_N$ | radius of the nozzle lip at the exit |
| St | Strouhal number, fD/U |
| $U$ | mean velocity in the direction of the flow |

$V_i$ local velocity component

$v_i$ fluctuating velocity component

$T_{ij}$ unsteady momentum flux

$W_t$ annulus width of the throat from sonic point to the nozzle lip

$y$ source co-ordinate

$\alpha$ inclination of the plug-nozzle lip to the jet axis

$\beta$ Harper-Bourne & Fisher type parameters: $(M_j^2-1)^{1/2}$ for underexpanded convergent nozzles and $(M_j^2- M_d^2)^{1/2}$ for plug-nozzles and CD nozzles

$\alpha_C$, $\beta_C$ convection constants

$\delta_{ij}$ Kronecker delta

$\varepsilon$ dissipation rate of turbulent kinetic energy

$\gamma$ ratio of specific heats

$\Gamma$ empirical constant

$\mu$ Mach angle, $\sin^{-1}(1/M)$

$\nu$ Prandtl-Meyer angle

$\xi$ ratio of reservoir absolute pressure to the ambient absolute pressure

$\rho$ density

$\psi$ wall slope of the plug at the sonic point

$\sigma_m$ $m^{th}$ root of the zeroth order Bessel function

$\tau$ time delay correlation

$\tau_0$ characteristic time delay in moving reference frame

$\theta$ polar angle with respect to the downstream jet axis

$\Omega$ source frequency

**Subscripts:**

c convection

d design

j fully-expanded jet flow

## 10. REFERENCES


1. Stitt, L.E. , *Exhaust Nozzles for Propulsion Systems with Emphasis on Supersonic Cruise Aircraft*, NASA RP-1235, 1990.

2. Smith, M.J.T., et al., *Future Supersonic Transport Noise - Lessons from the Past*, AIAA Paper 88-2989, July 1988.

3. Seiner, J.M. and Krejsa, E.A., *Supersonic Jet Noise and the High Speed Civil Transport*, AIAA Paper 89-2358, July 1989.

4. Lighthill, M.J., *The Bakerian Lecture: Sound Generated Aerodynamically*, 1962 Proceedings of the Royal Society London A267, 147-182.

5. Powell, A., *On the Mechanism of Choked Jet Noise*, 1953 Proceedings of the Physical Society 66(12B), 1039-1056.

6. Yu, J.C. and Dosanjh, D.S., *Noise Field of a Supersonic Mach 1.5 Cold Model Jet*, Journal of the Acoustical Society of America 51, 1400-1410, 1972.

7. Harper-Bourne, M. and Fisher, M.J., *The Noise from Shock Waves in Supersonic Jets, Noise Mechanisms* - AGARD Conference on Propagation and Reduction of Jet Noise, AGARD CP-131, pp. 11-1 to 11-13, Paris 1973.

8. Seiner, J.M., *Advances in High Speed Jet Aeroacoustics*, AIAA Paper 84-2275, 1984.

9. Ribner, H.S., *Cylindrical Sound Waves Generated by Shock Vortex Interaction*, AIAA Journal , Vol. 43, pp. 1708-1715, Nov. 1985.

10. Tanna, H.K., An Experimental Study of Jet Noise, Part II: Shock Associated Noise, Journal of Sound & Vibration, Vol. 50, pp. 429-444, 1977.

11. Dosanjh, D.S., Bhutiani, P.K., and Ahuja, K.K., *Jet Noise suppression by Co-axial Cold/Heated Jet Flows*, AIAA Journal, vol. 16, No. 3, pp. 268-270, March 1978.

12. Tanna, H.K., Tam, C.K.W., and Brown, W.H., *Shock-Associated Noise Reduction from Inverted-Velocity Profile Coannular jets*, NASA CR-3454, 1981.

13. Tam, C.K.W. and Tanna, H.K., *Shock-Associated Noise of Supersonic Jets from Convergent-Divergent Nozzles*, Journal of Sound and Vibration, Vol. 81, No. 3, pp. 337-358, 1982.

14. Seiner, J.M., Ponton, M.K., *Acoustic Properties Associated with Rectangular Geometry Supersonic Nozzles*, AIAA Paper No. 86-1867, 1986.

15. Morris, P.J. and Bhat, T.R.S., *Supersonic Elliptic Jet Noise*, AIAA Paper No. 93-4409, 1993.

16. Krejsa, E.A., Cooper, B.A., Hall, D.G., and Khavaran, A., *Noise Measurements from an Ejector Suppressor Nozzle in the NASA Lewis 9- by 15-Foot Low Speed Wind Tunnel*, AIAA Paper No. 99-3983, NASA TM 103628, 1990.

17. Maestrello, L., *An Experimental study on Porous Plug Jet Noise Suppressor*, AIAA Paper No. 79-0673, 1979.

18. Kibens, V. and Wlezien, R.W., *Noise Reduction Mechanisms in Supersonic Jet with Porous Center-Bodies*, AIAA Journal, Vol. 23, No. 5, pp. 678-684, 1985.

19. Yamamoto, K., Brausch, J.F., Balsa, T.F., Janardan, B.A., and Knott, P.R., *Experimental Investigation of Shock-Cell Noise Reduction for Single Stream Nozzles in Simulated Flight*, NASA CR-3845, Dec. 1984.

20. Dosanjh, D.S. and Das, I.S., *Aeroacoustics of Supersonic Jet Flows from a Contoured Plug-Nozzle*, AIAA Journal, Vol. 26, No. 8, pp. 924-931, 1988.

21. Das, I.S., and Dosanjh, D.S., *Short Conical Solid/Perforated Plug-Nozzle as Supersonic Jet Noise Suppressor*, Journal of Sound and Vibration, 146(3), pp. 391-406, 1991.

22. Connors, J.F. and Meyer, R.C., *Design Criteria for Axisymmetric & Two-Dimensional Supersonic Inlets and Exits*, NASA TN 3589, Oct. 1956.

23. Dosanjh, D.S. and Das, I.S., *Aeroacoustics of Contoured and Solid/Porous Conical Plug Nozzle Supersonic jet Flows*, NASA CR-178095, Jan. 1987.

24. Mani, R., Balsa, T.E., Gliebe, P.R., Kantol, R.A., Stringas, E.J., and Wang, J.F.C., *High Velocity Jet Noise Source Location and Reduction, Task 2: Theoretical Developments and Basic Experiments*, FAA-Rd-76-79-2, 1977.

25. Khavaran, A., Krejsa, E.A., and Kim, C.M., *Computation of Supersonic Jet Mixing Noise for an Axisymmetric Convergent-Divergent Nozzle*, Journal of Aircraft, Vol. 31, No. 3, pp. 603-609, 1994.

26. Kim, C.M., Krejsa, E.A., and Khavaran, A., *Computation of Supersonic Jet Noise Under Imperfectly Expanded Conditions*, AIAA Paper No. 93-0735, Jan. 1993.

27. Cooper, G.K. and Sirbaugh, J.R., *PARC Code: Theory and Usage*, Arnold Engineering Development Center, Report No. AEDC-TR-89-15, 1989.

28. Chien, K.Y., *Prediction of Channel and Boundary Layer Flows with a Low Reynolds Number Turbulence*, AIAA Journal, Vol. 20, No.1, pp. 33-38, Jan. 1982.

29. Beam R. and Warming R.F., *An Implicit Finite Difference Algorithm for Hyperbolic Systems in Conservation Form*, Journal of Computational Physics, Vol. 22, No. 1, pp. 87-110, Sept. 1976.

30. Lighthill, M.J., *On Sound Generated Aerodynamically, I General Theory*, Proc. Royal Soc. of London, Vol. a211, pp. 564-587, 1952.

31. Lighthill, M.J., *On Sound Generated Aerodynamically, II Turbulence as a Source of Sound* , Proc. Royal Soc. of London, Vol. a222, pp. 1-32, 1954.

32. Ribner, H.S., *Quadrupole Corrections Governing the Pattern of Jet Noise*, Journal of Fluid Mechanics, Vol. 38, pp. 1, 1969.

33. Batchelor , G.K., *The Theory of Homogeneous Turbulence*, Cambridge University Press, 1953.

34. Mani, R., *The Influence of Jet Flow on Jet Noise, Part I The Noise of Unheated Jets*, Journal of Fluid Mechanics, Vol. 76, pp. 753-778, 1976.

35. Goldstein, M.E., *The Low Frequency Sound from Multipole Sources in Axisymmetric Shear Flows, Part II*, Journal of Fluid Mechanics, Vol. 75, pp. 17-28, 1976.

36. Balsa, T.F., *The Acoustic Field of Sources in Shear Flow with Application to Jet Noise: Convective Amplification*, J. of Fluid Mechanics, Vol. 79, pp. 33-47, 1977.

37. Tester, B.J. and Morfey, C.L., *Developments in Jet Noise Modeling - Theoretical Predictions and Comparisons with Measured Data*, J, of Sound and Vibration, Vol.46, pp. 79-103, 1976.

38. Pao, S.P., *Aerodynamic Noise Emission from Turbulent Shear Layers, J. of Fluid Mechanics*, Vol. 59, pp. 451, 1973.

39. Ffowcs-Williams, J.E., *The Noise from Turbulence Convected at High Speed*, Phil. Transactions of Roy. Soc. of London, Vol. A255, pp. 469-503, 1963.

40. Tam, C.K.W., Jackson, J.A., and Seiner, J.M., *A Multiple Scales Model of the Shock Cell Structure of Imperfectly Expanded Supersonic Jets*, Journal of Fluid Mechanics, Vol. 153, pp. 123-149, 1987.

41. Tam, C.K.W., *Stochastic Model Theory of Broad Band Shock Associated Noise from Supersonic Jets*, Journal of Fluid Mechanics, Vol. 153, pp. 123-149, 1987.

42. Tam, C.K.W., *Broadband Shock Associated Noise of Supersonic Jets*, Journal of Sound and Vibration, Vol. 140, pp. 55-71, 1990.

43. Pack, D.C., *A Note on Prandtl's Formula for the Wavelength of a Supersonic Gas Jet*, Quarterly J. of Mechanics and Applied Mathematics, Vol. 3, pp. 173-181, 1950.

44. Tam, C.K.W., *Forward Flight Effects on Broadband Shock Associated Noise of Supersonic Jets*, AIAA Paper No. 89-1088, 1989.

45. Nagamatsu, H. T., Sheer, R. F., and Horva, G., Supersonic Jet Noise Theory and Experiments, Basic Aerodynamic Research, Ed. Schwartz, I. R., NASA SP-207, pp. 17-51, 1969.

## 11. LIST OF FIGURES

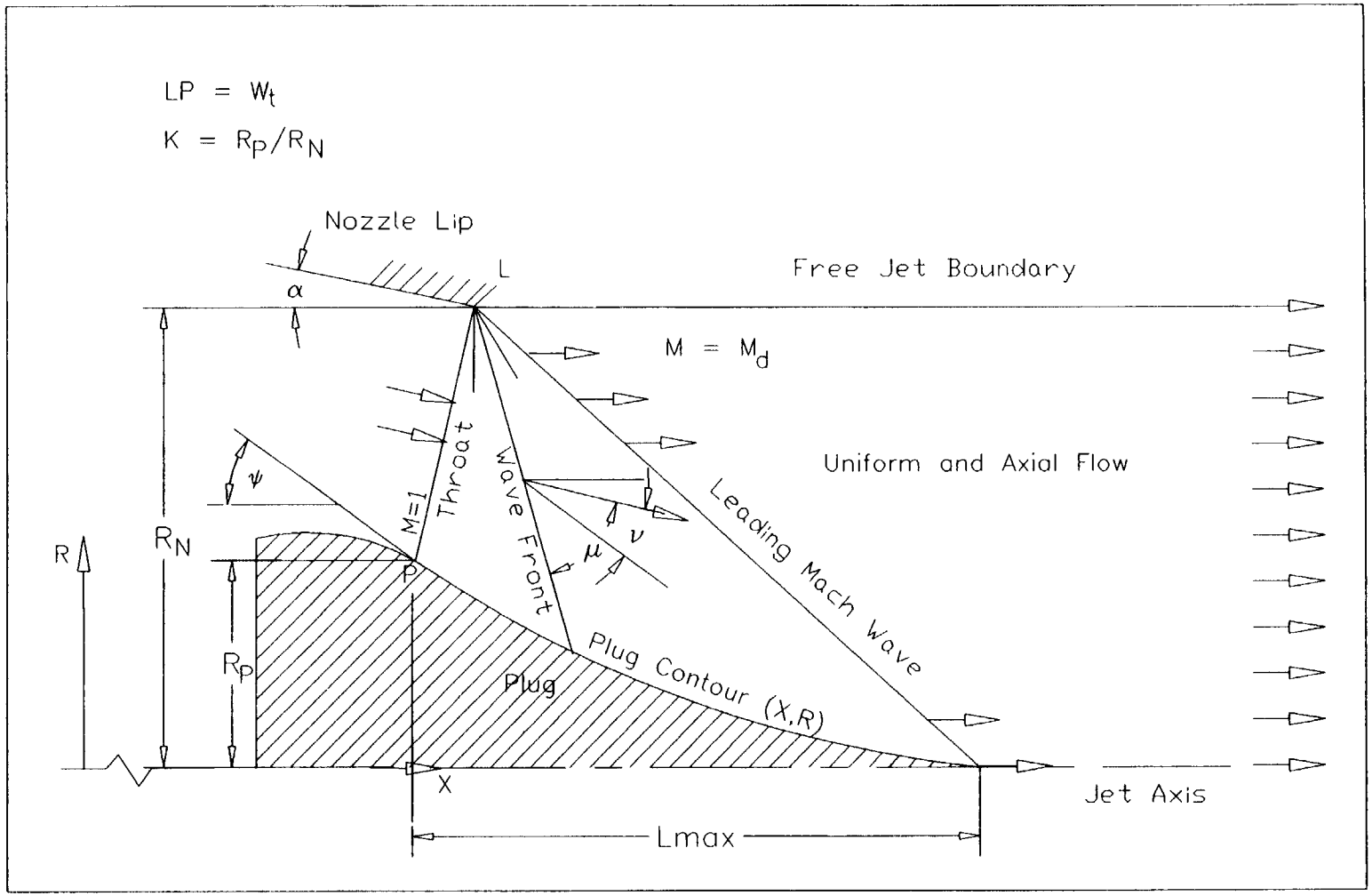


Fig.1 Fully expanded jet flow from an ideal contoured plug nozzle.

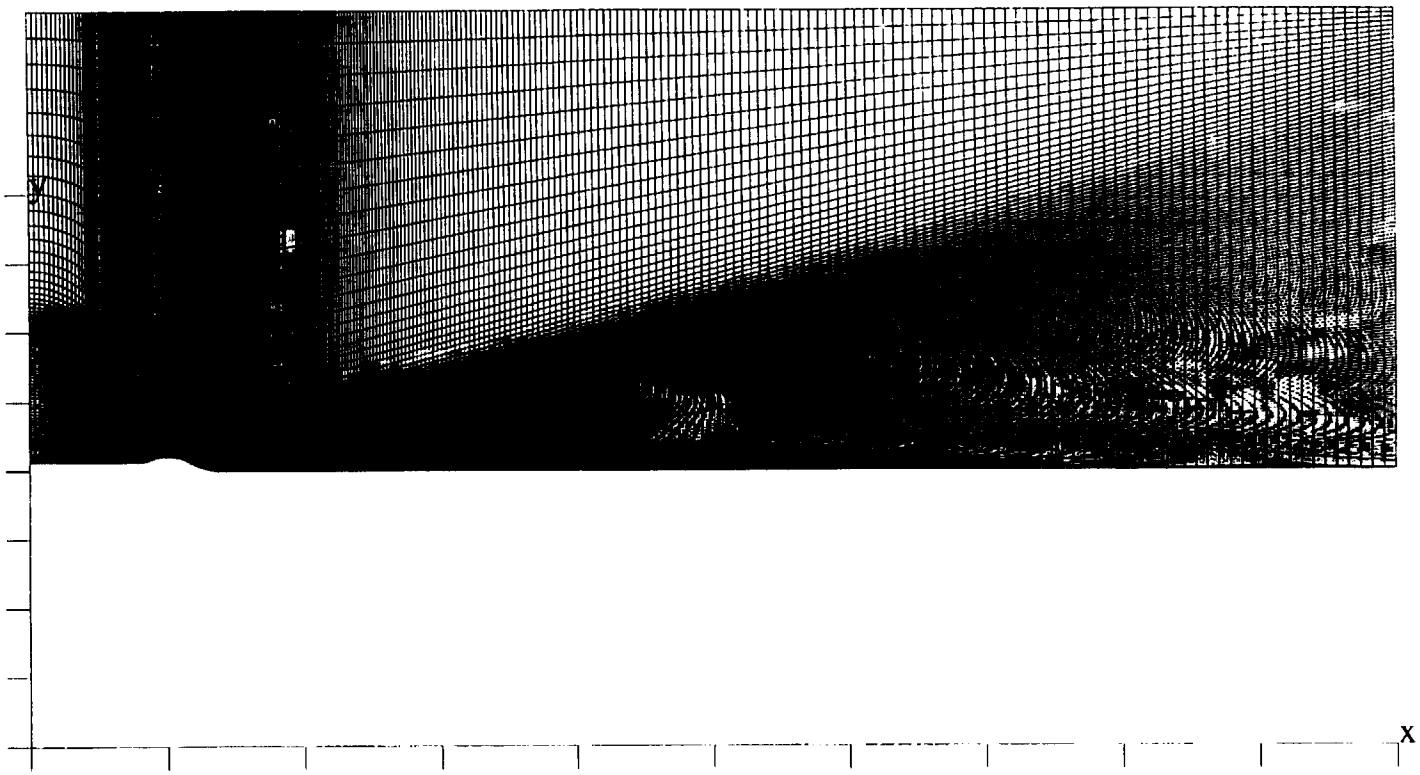


Fig. 2 Computational grid for the plug-nozzle (aspect ratio = 3, axial length = 33D).

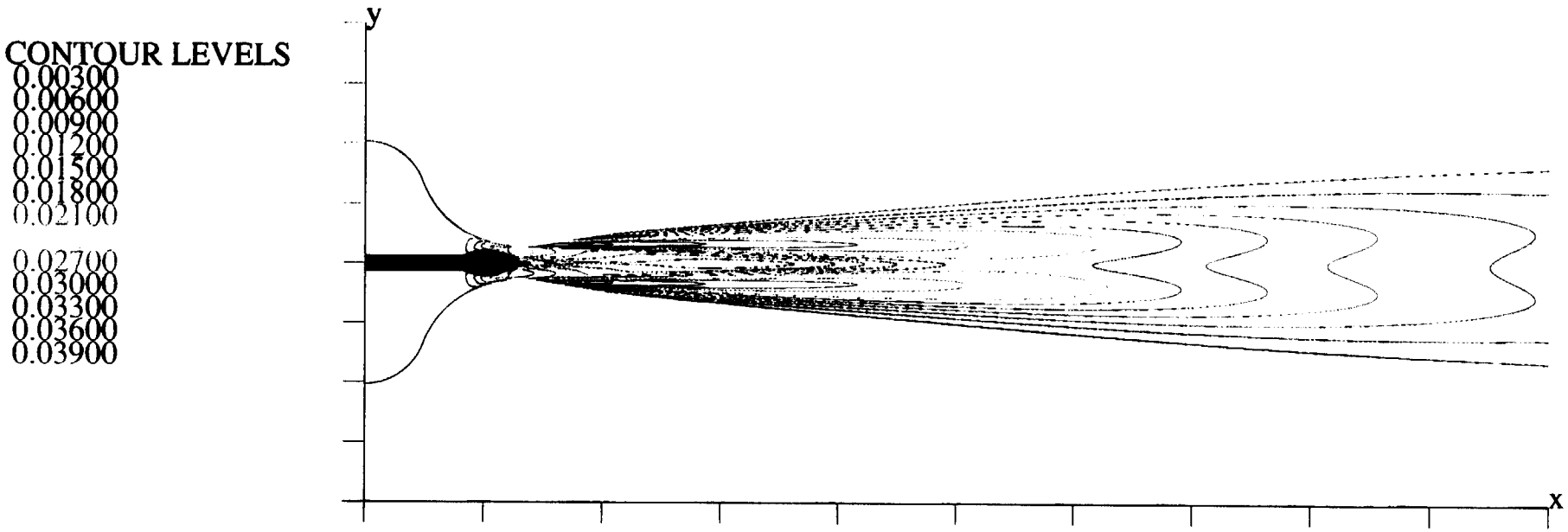


Fig. 3 Contour plot of turbulence intensity (pressure ratio = 3.62: design).

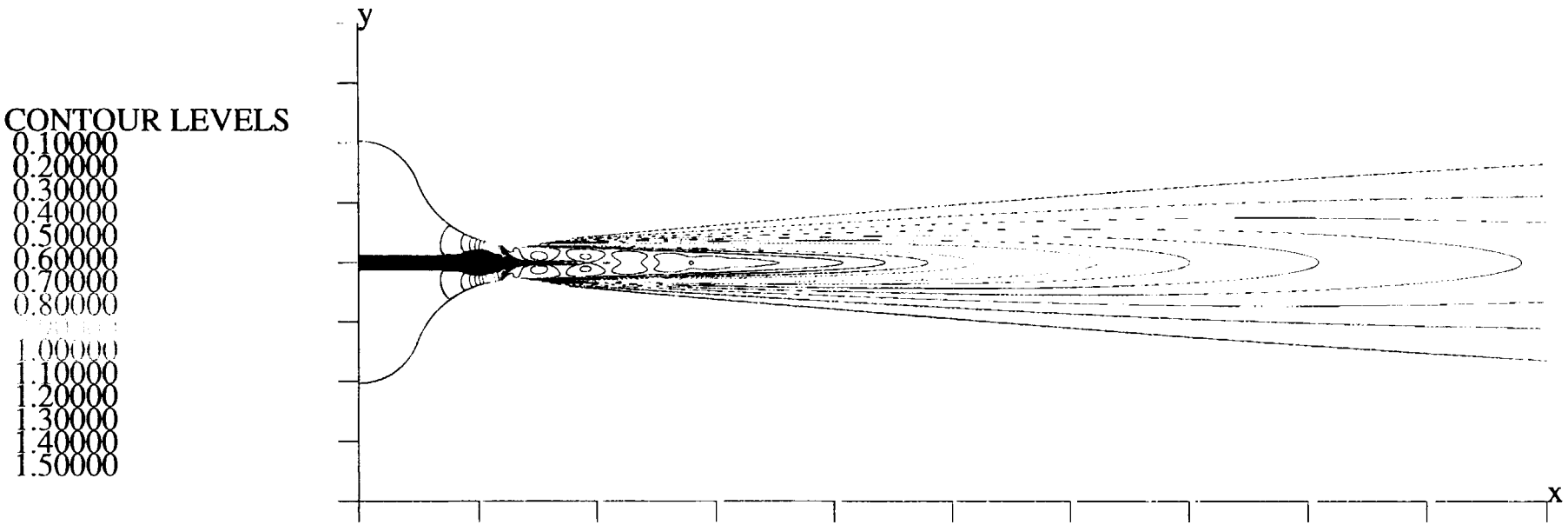


Fig. 4 Contour plot of flow field Mach number (pressure ratio = 3.62: design).

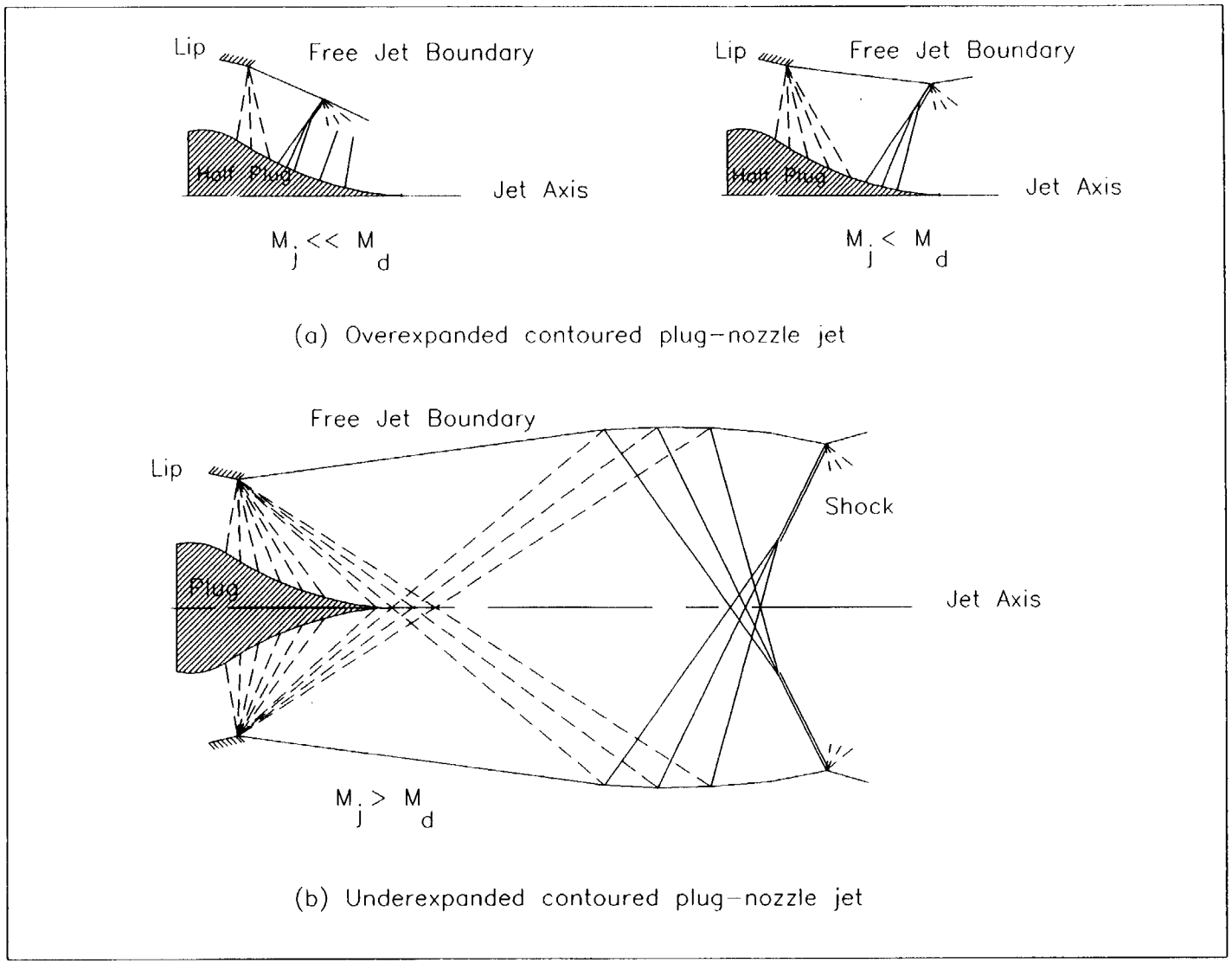


Fig. 5 Shock formations in over– and underexpanded contoured plug–nozzle jet flows.

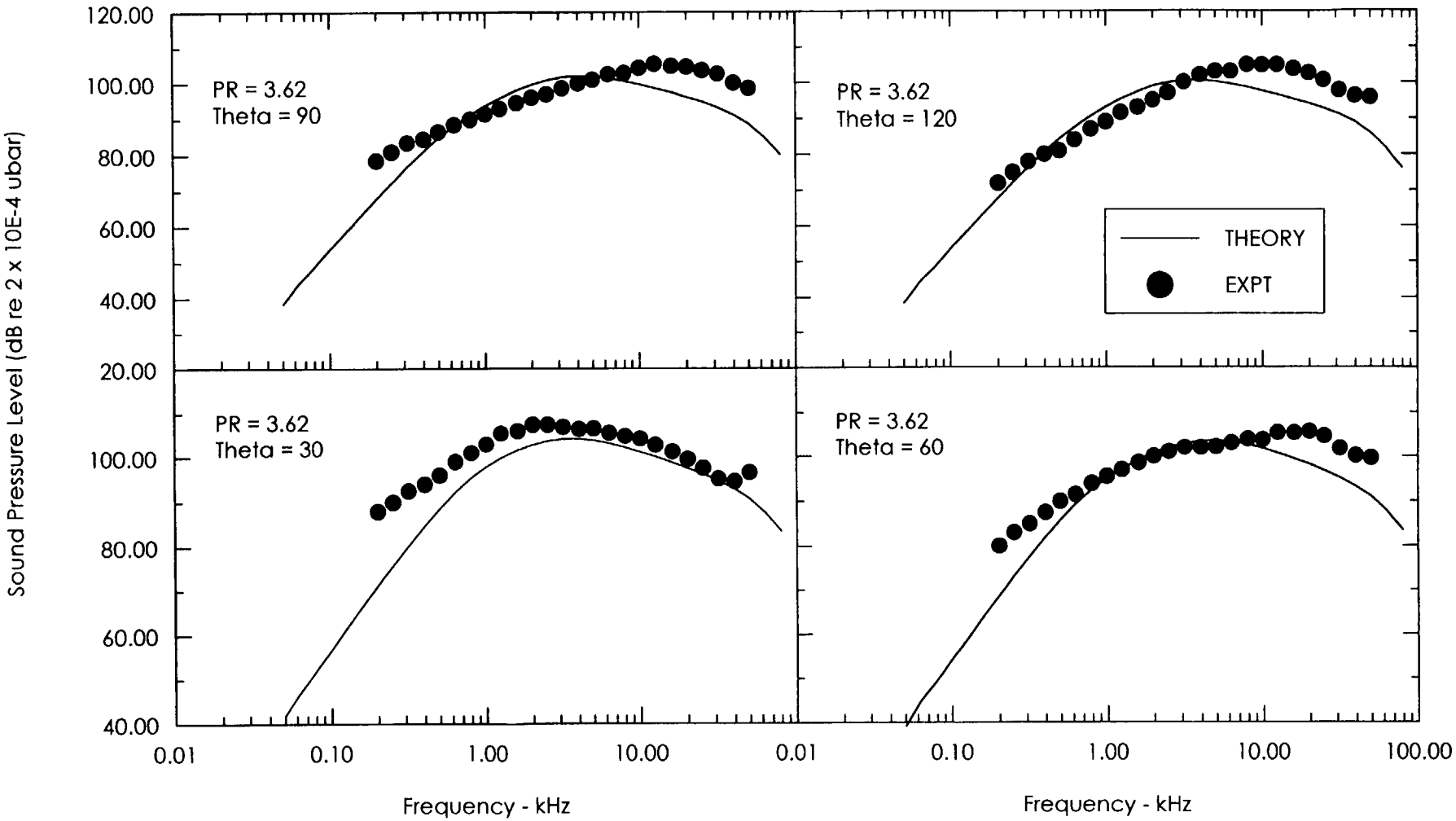


Fig. 6 Comparisons of 1/3-octave SPL spectra for the CPN jet flows at four typical angles theta (prediction vs measurements [20]; pressure ratio = 3.62).

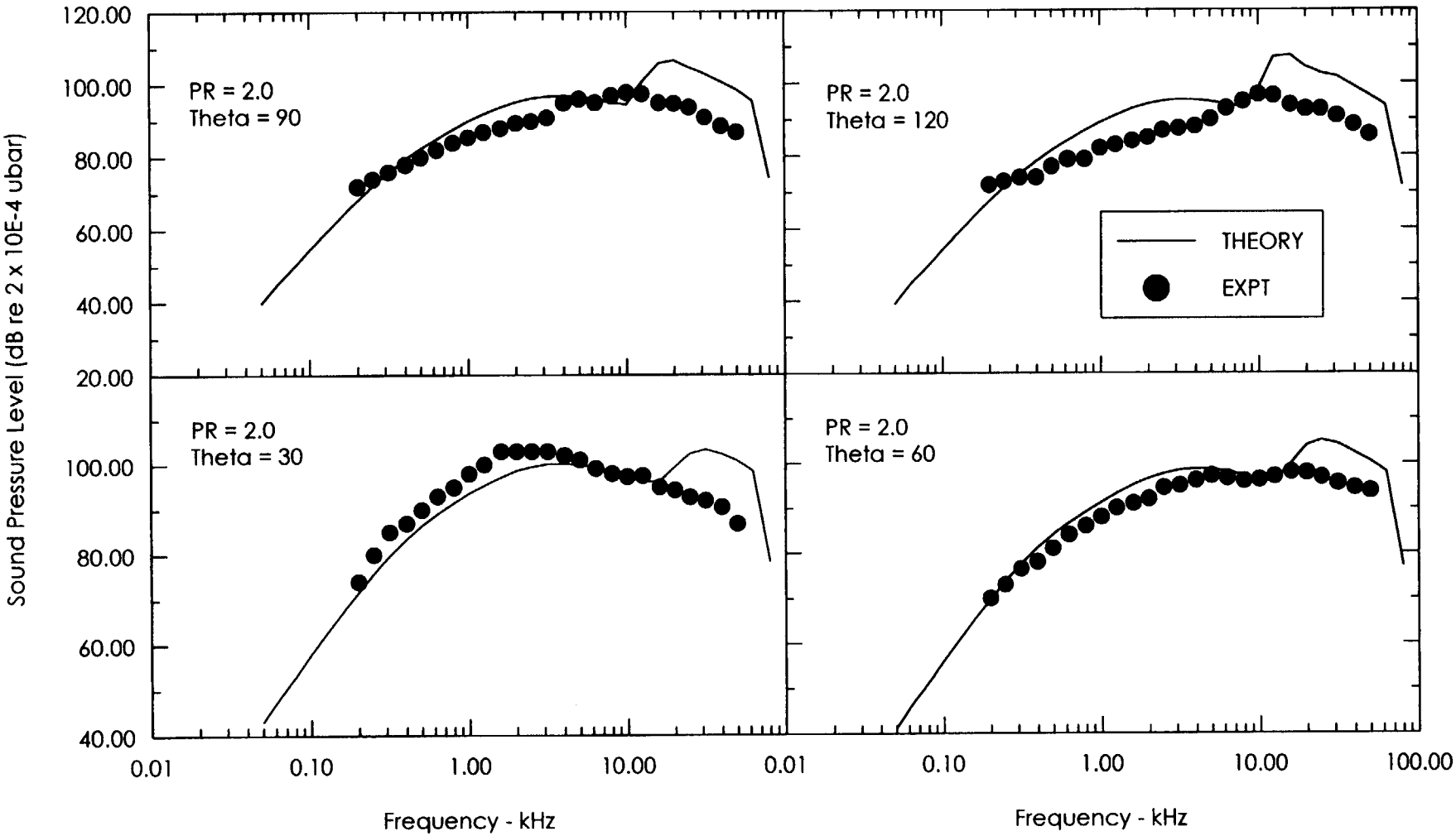


Fig. 7 Comparisons of 1/3-octave SPL for the CPN jet flows at four typical angles theta (prediction vs measurements [20]; pressure ratio = 2.0).

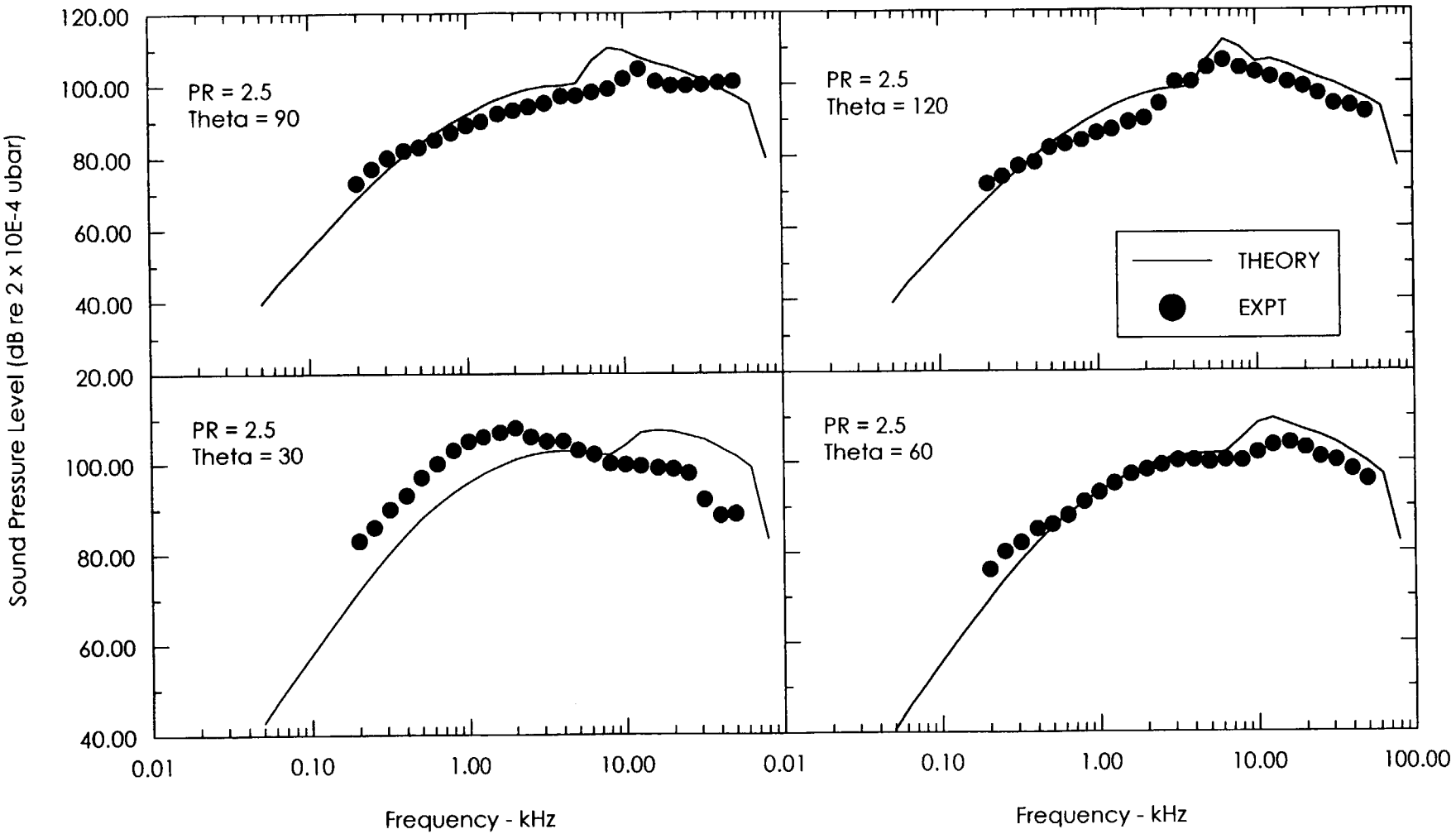


Fig. 8 Comparisons of 1/3-octave SPL for the CPN jet flows at four typical angles theta (prediction vs measurements [20]; pressure ratio = 2.5).

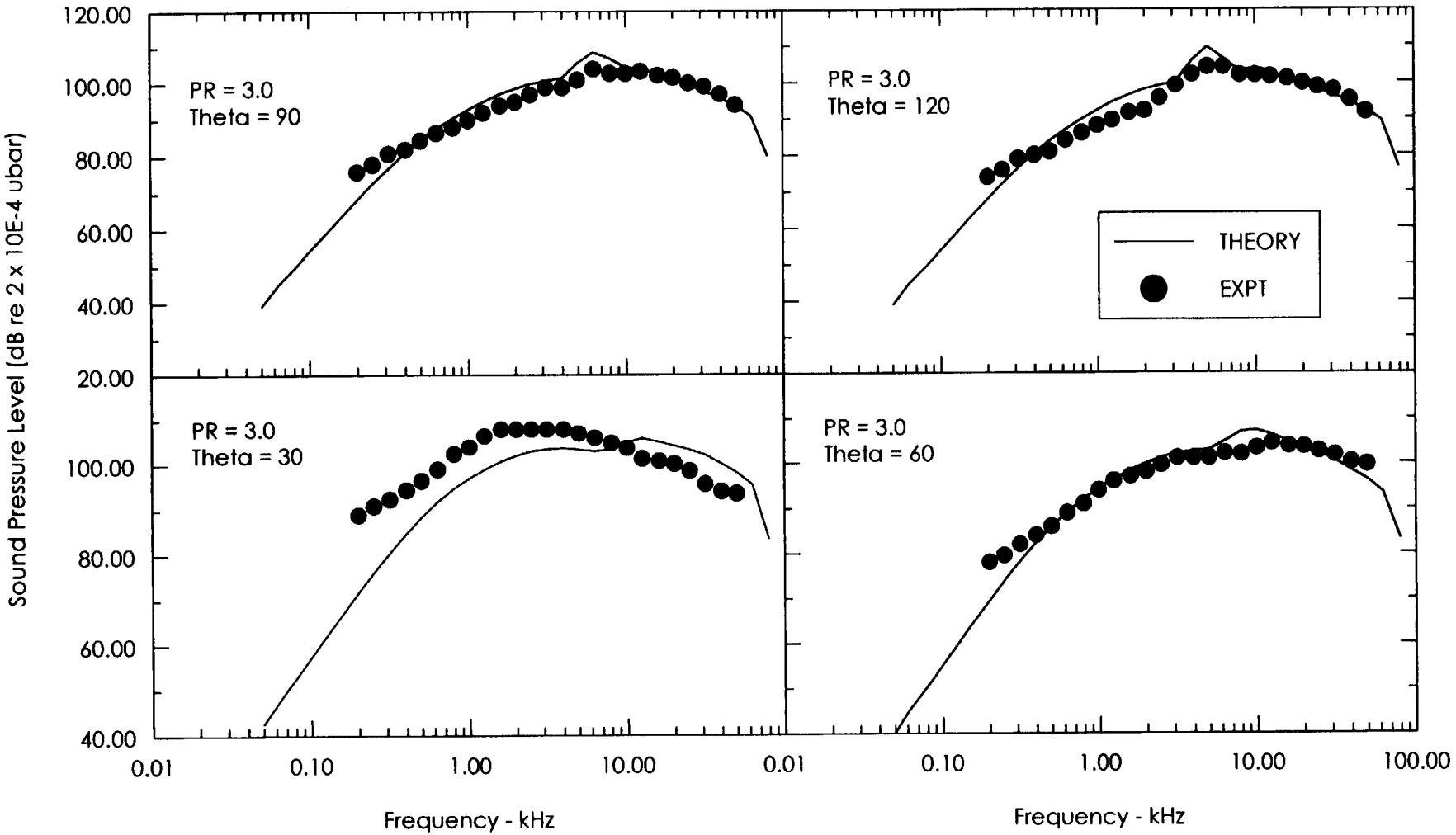


Fig. 9 Comparisons of 1/3-octave SPL for the CPN jet flows at four typical angles theta (prediction vs measurements [20]; pressure ratio = 3.0).

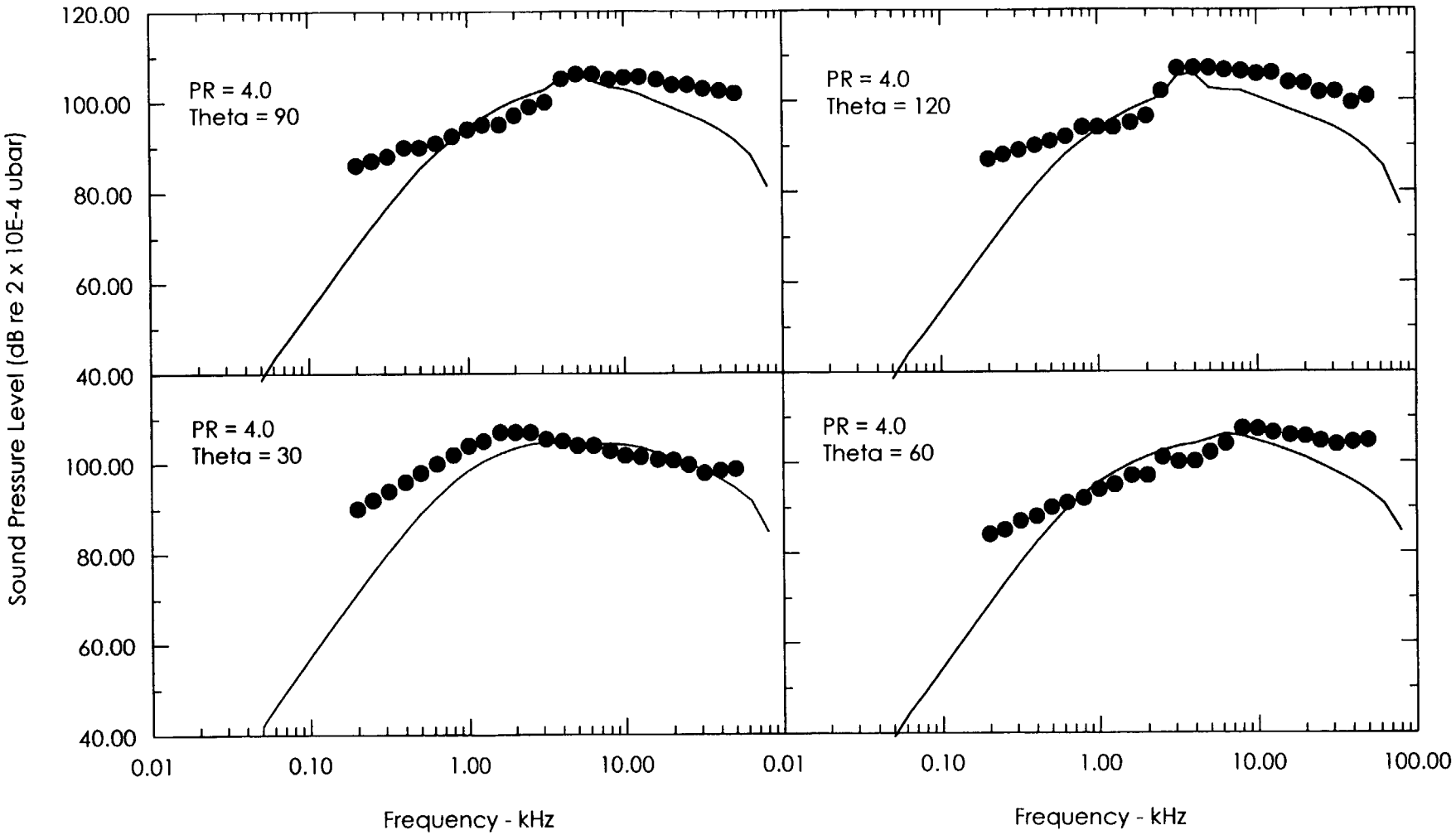


Fig. 10 Comparisons of 1/3-octave SPL for the CPN jet flows at four typical angles theta (prediction vs measurements [20]; pressure ratio = 4.0).

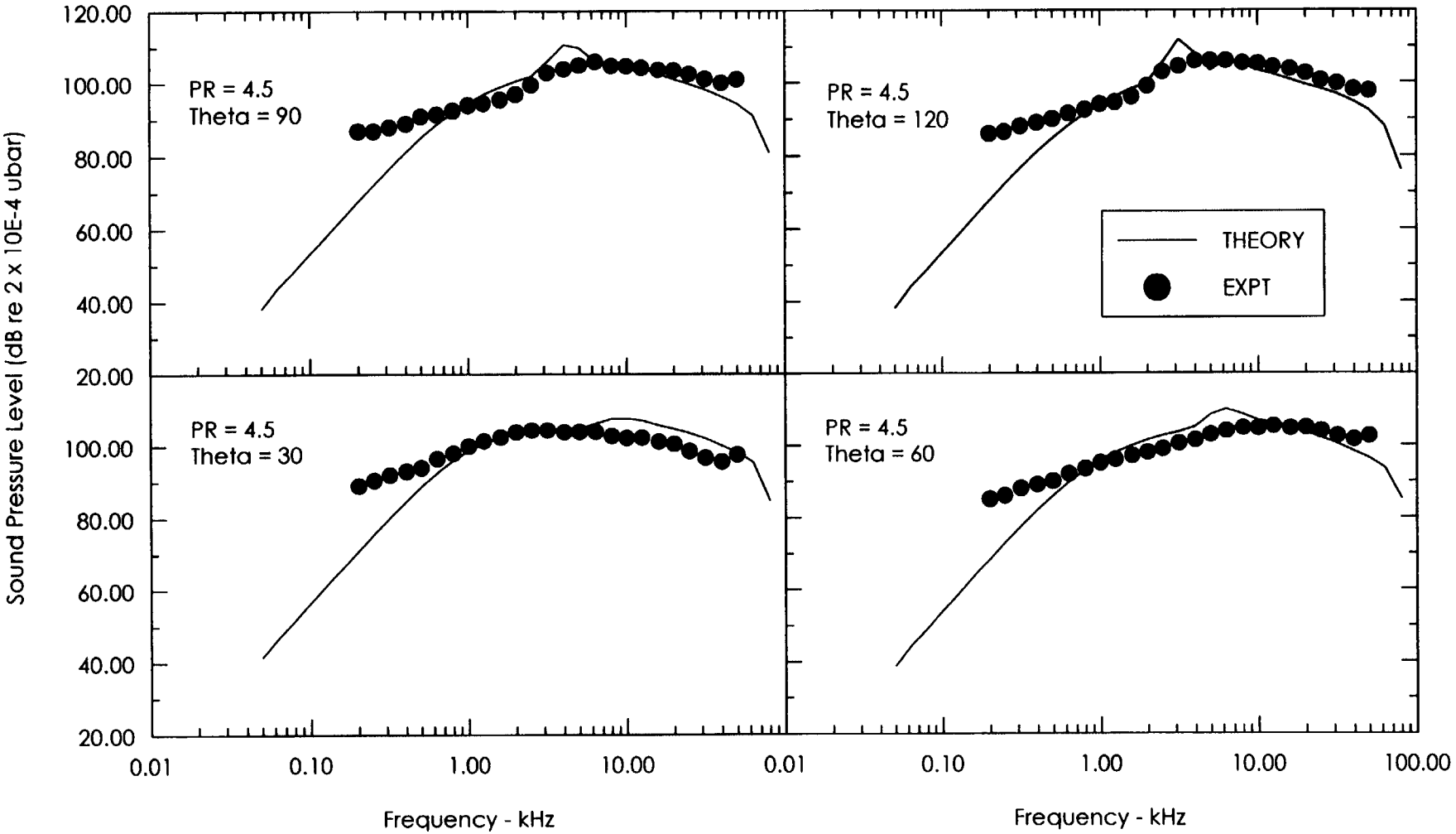


Fig. 11 Comparisons of 1/3-octave SPL spectra for the CPN jet flows at four typical angles theta (prediction vs measurements [20]; pressure ratio = 4.5).

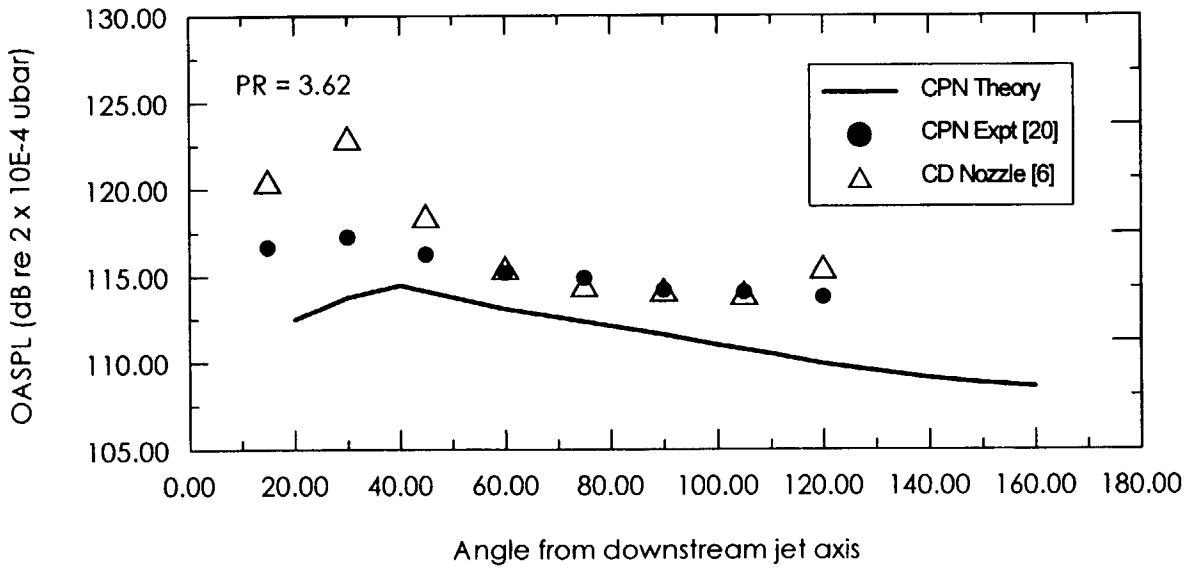


Fig. 12 Comparisons of overall sound pressure level directivity for the CPN prediction, the CPN measurements [20] and the CD nozzle measurements [6] at design pressure ratios.

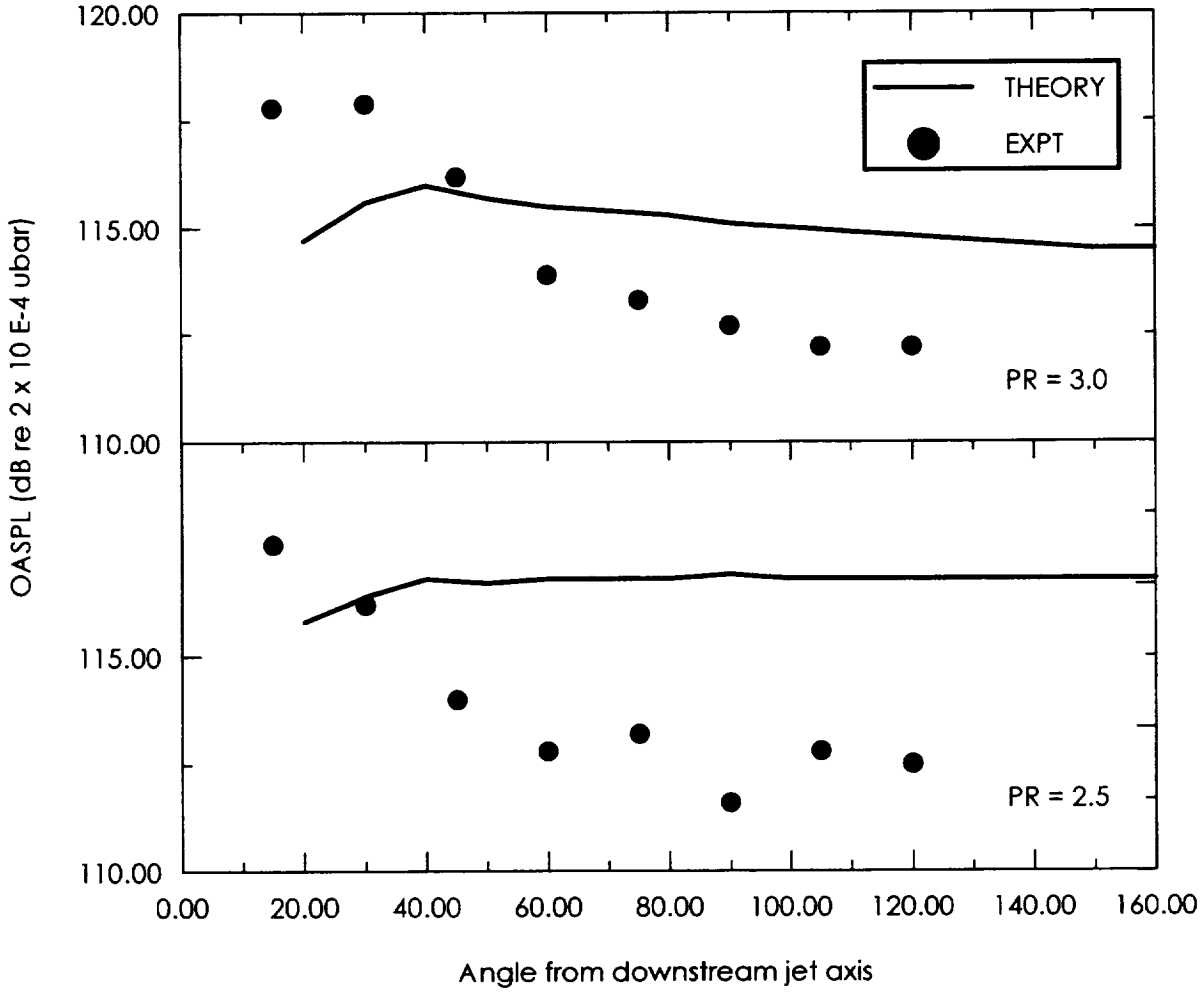


Fig. 13 Comparisons of overall sound pressure level directivity of the overexpanded CPN jet flows (prediction vs measurements [20]).

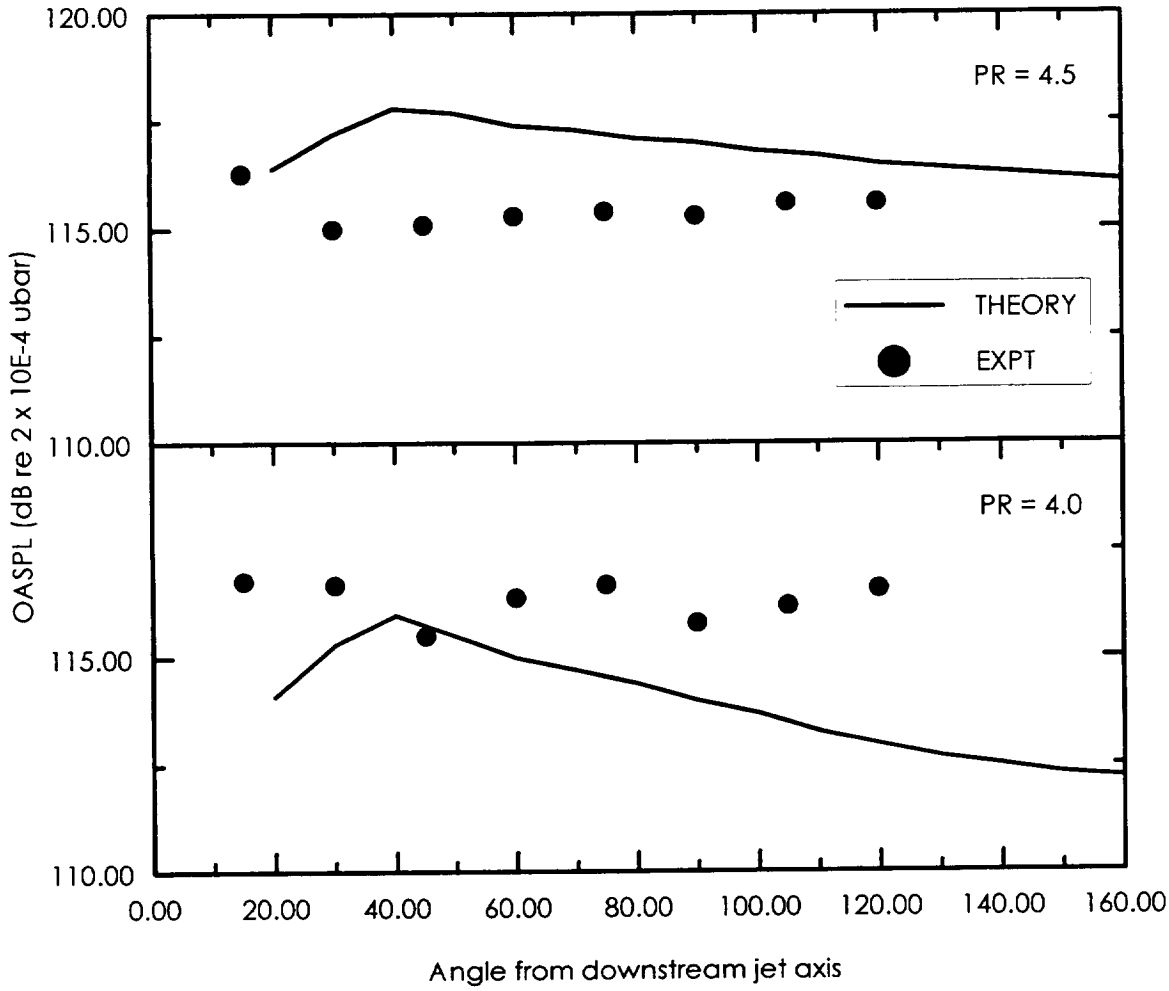


Figure 14: Comparisons of overall sound pressure level directivity of the underexpanded CPN jet flows (prediction vs measurements [20]).

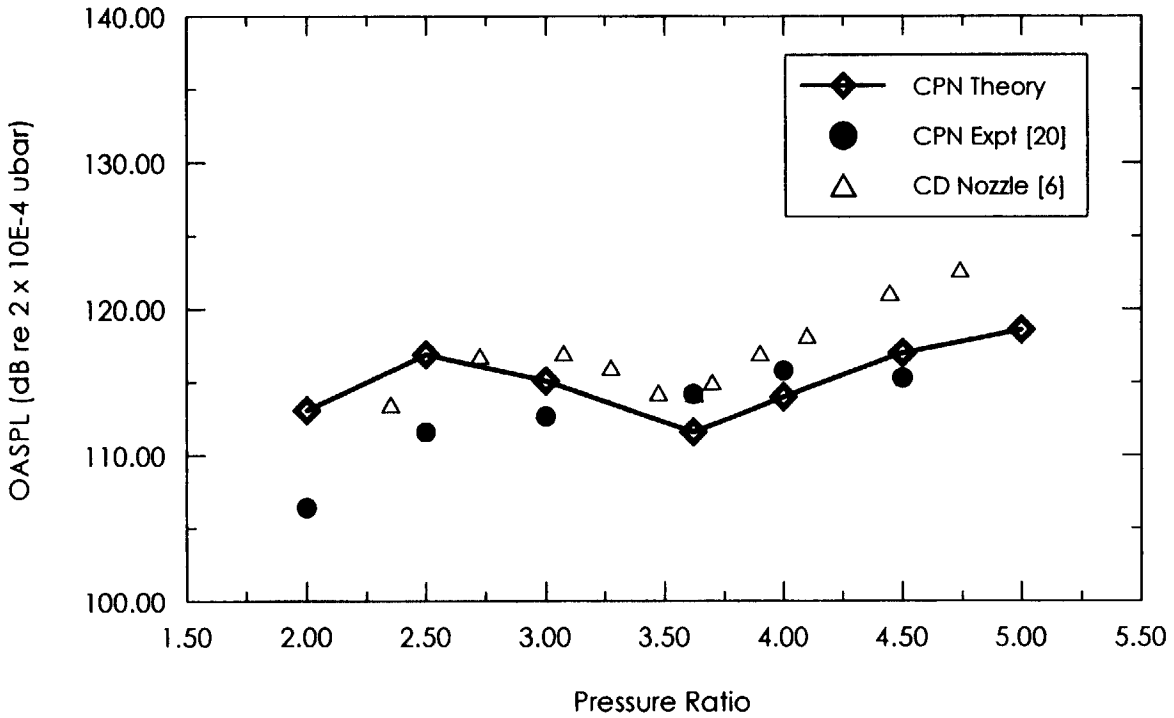


Fig. 15 Comparisons of overall sound pressure level variations with pressure ratio for the CPN prediction, the CPN measurements [20] and the CD nozzle measurements [6] (theta = 90).

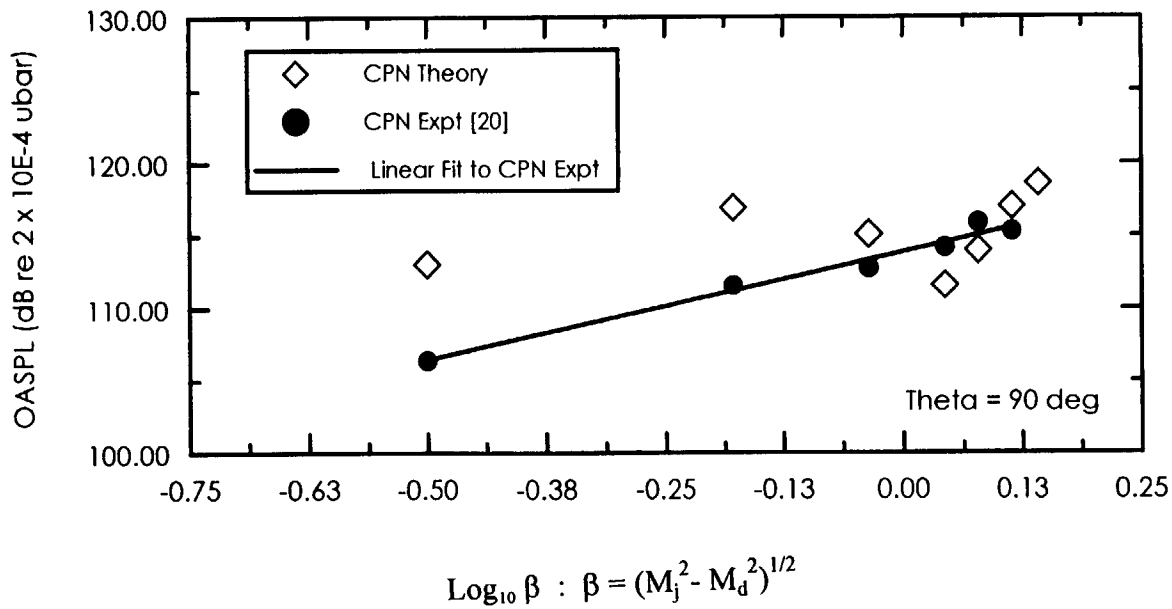


Fig. 16 Overall sound pressure level scaling in the CPN jet flows (the predicted data, experimental data [20] and linear fit to the experimental data).

# APPENDIX A

A brief methodology for prediction of the sonic line shape and the overall geometrical parameters is presented in what follows. The charts showing overall geometrical parameters (nozzle lip slope $\alpha$, the plug wall slope at the sonic point $\psi$, the annulus radius ratio K and the maximum axial length of the plug from the sonic point to its tip) as functions of the design Mach number $M_D$ are presented in Figs. A1 & A2. The profile of the contoured plug-nozzle, subject of the present computational study, is presented in Fig. A3 and the set of co-ordinates of the contoured plug-nozzle annulus is provided in Table A.

## Estimate of the Overall Design Parameters

For the free jet boundary to be straight and axial, the nozzle lip inclination $\alpha$ is related to the design Mach number $M_d$ through the Prandtl-Meyer function,

$$\alpha = \left(\frac{\gamma+1}{\gamma-1}\right)^{1/2} \tan^{-1}\sqrt{\frac{\gamma+1}{\gamma-1}\left(M_j^2-1\right)} - \tan^{-1}\sqrt{M_j^2-1}$$

The area of the throat for an infinitesimal interval is,

$$A_t = \pi\left(R_1^2 - R_2^2\right)/\cos\left(\frac{\omega_1+\omega_2}{2}\right)$$

where the mean flow direction, $\omega_1 \approx \omega_2$.

The geometrical condition of Mach gradient at the throat in the streamline direction being zero,

$$\frac{d A_t}{dL} = 0 \Rightarrow \omega_2 = \sin^{-1}\left(\frac{\sin \omega_1}{(R_2/R_1)}\right)$$

The mean flow direction is,

$$\omega_m = \frac{\omega_2 + \omega_1}{2}$$

Also, the infinitesimal element radius ratio is,

$$\frac{R_2}{R_1} = \sqrt{1 - \frac{\cos \omega_m}{(A_e/A_t)}}$$

where the area ratio ($A_e/A_t$) is given by the one dimensional area ratio for the isentropic flow.

The preceding set of equations may be used for establishing an iterative scheme, starting from the nozzle lip, to obtain the co-ordinates of the curved sonic line along with the values of the geometrical configuration factor K, and the slope of the sonic line at the plug $\psi$. The starting value of $\omega_1$ is given by, $\omega_1 = \alpha$. The iterative scheme is initiated by guessing a value of the radius ratio, $R_2/R_1$, and the process rapidly converges to yield co-ordinates of the points on the sonic line.

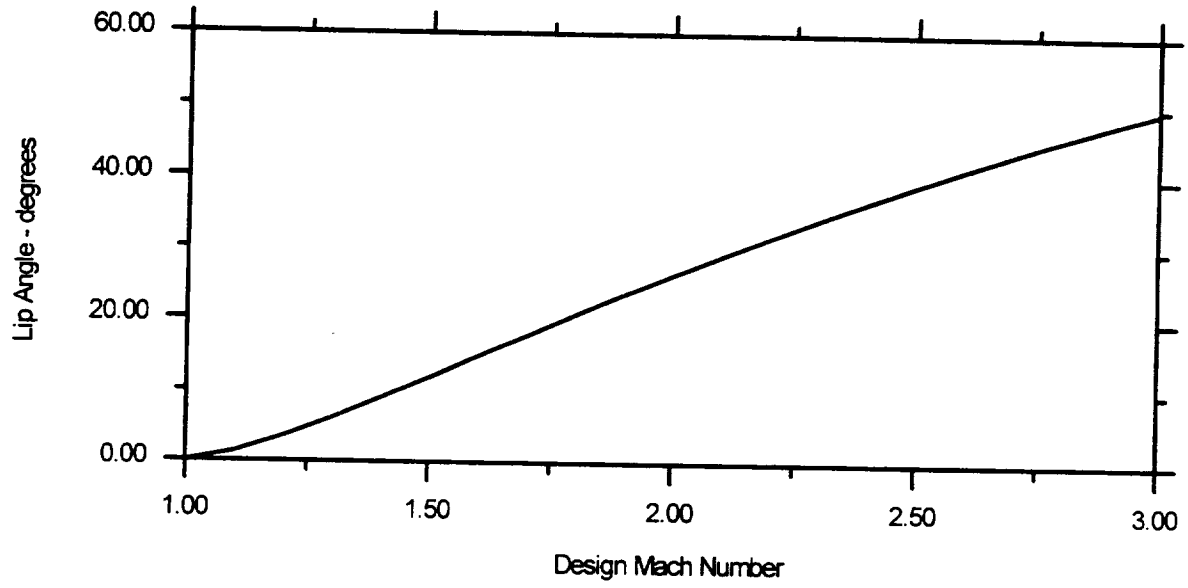


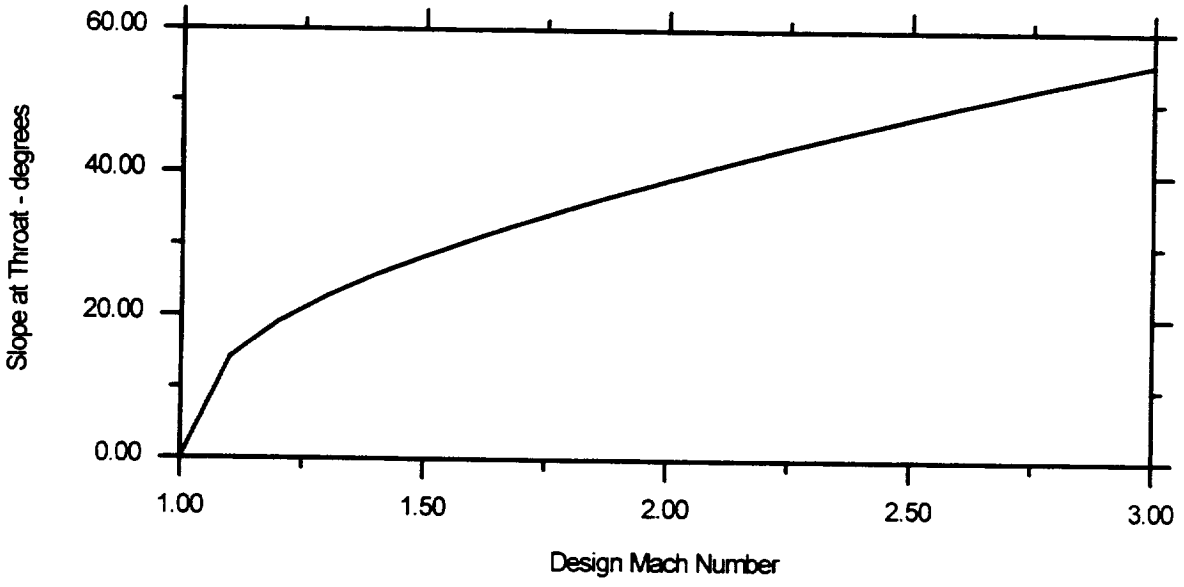


Fig. A1 Dependence of Overall Plug-Nozzle Geometry on Design Mach Number

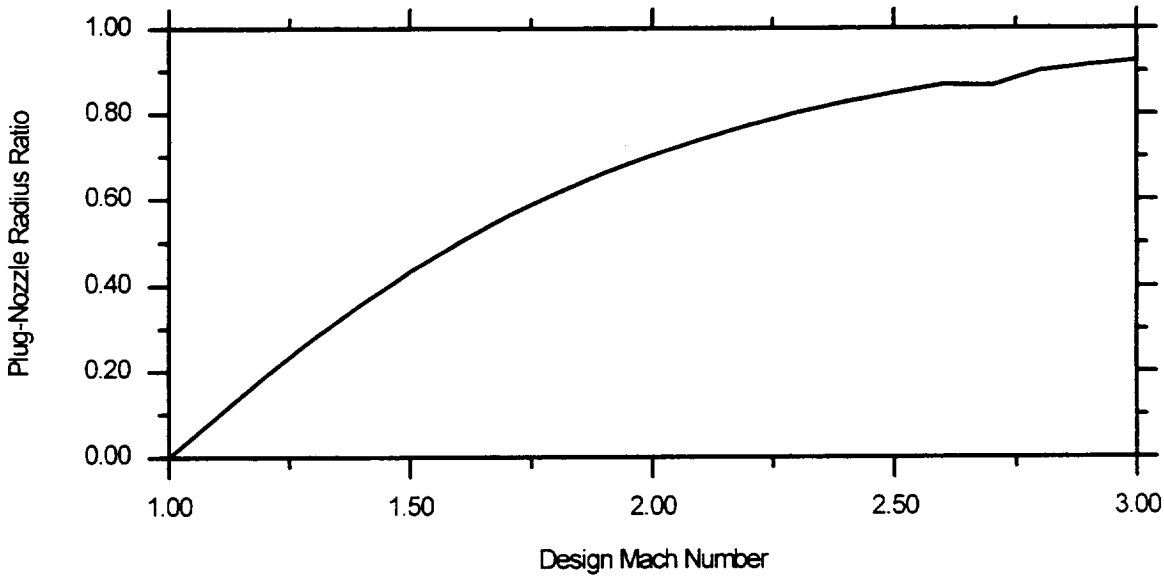


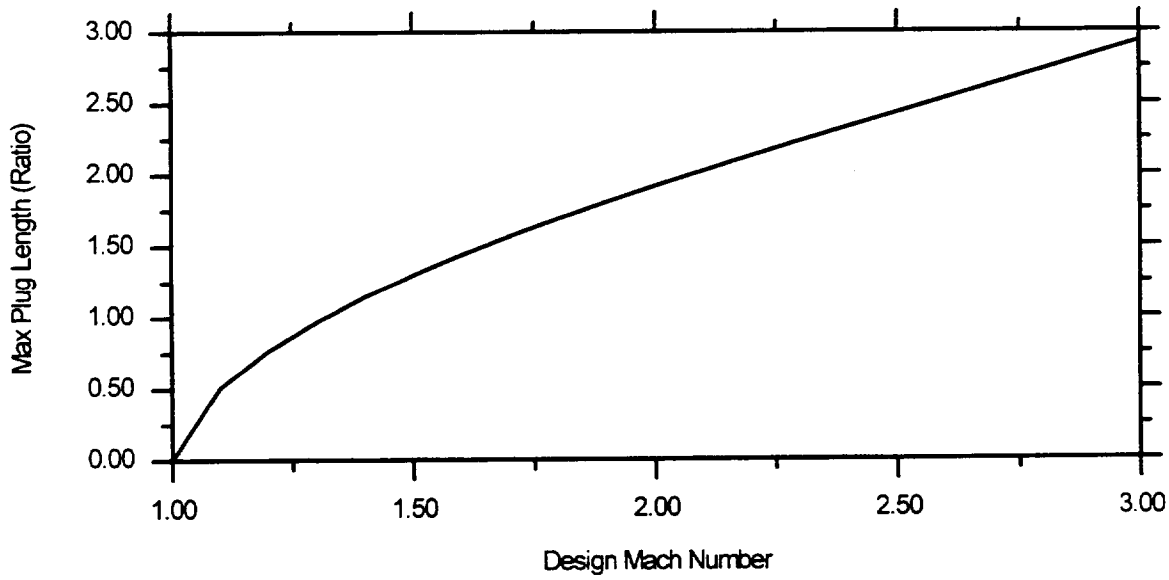


Fig. A2 Dependence of Overall Plug-Nozzle Geometry on Design Mach Number
(Lengths normalized with respect to Nozzle Lip Radius)

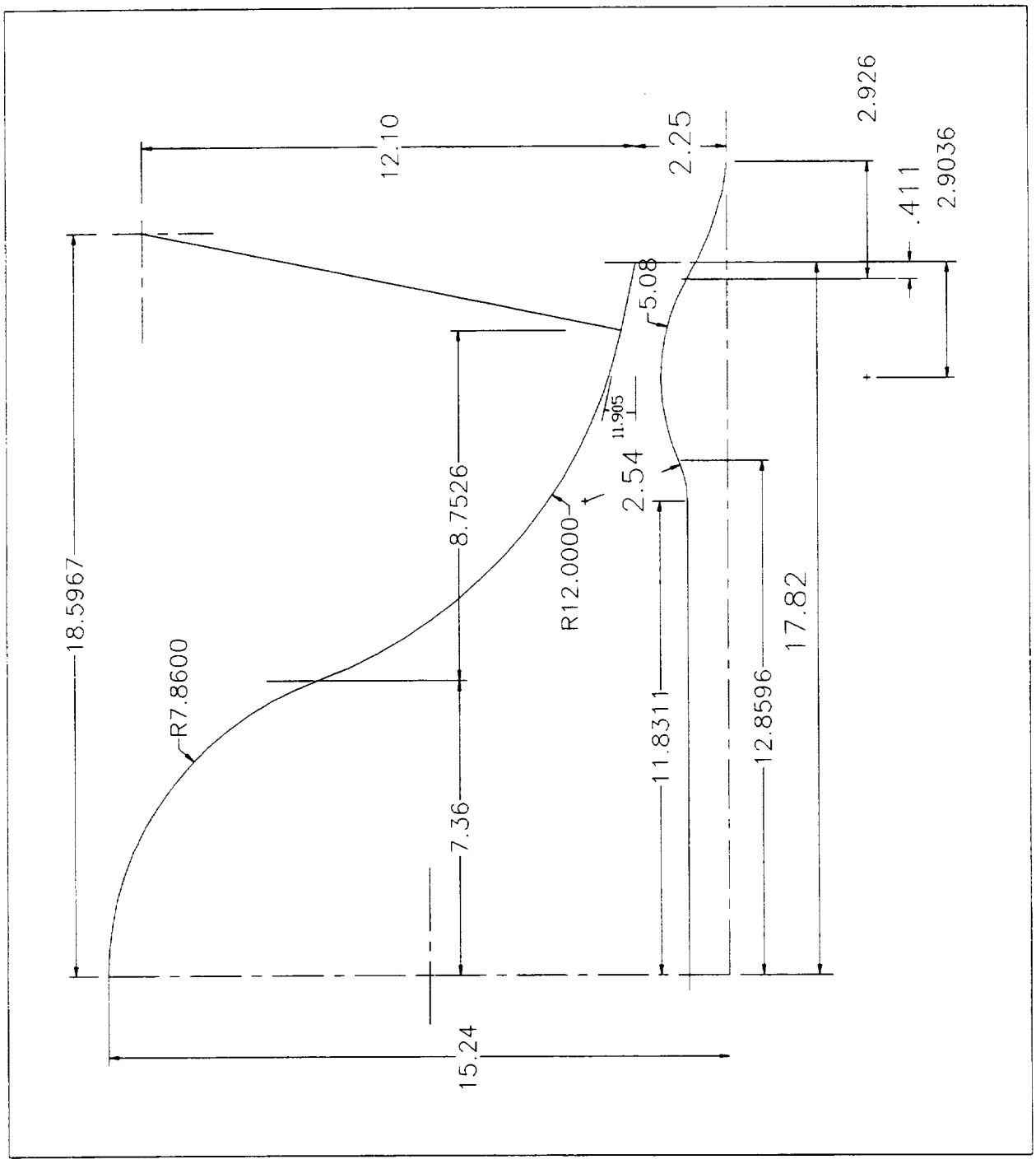


Fig. A3 Profile of the test contoured plug-nozzle (design Mach number = 1.5).

| X- PLUG | R- PLUG | X - NOZ | R - NOZ | | X- PLUG | R- PLUG | X - NOZ | R - NOZ |
|---|---|---|---|---|---|---|---|---|
| | | | | | | | | |
| 0 | 0.955 | 0 | 15.24 | | 10.5697 | 0.955 | 9.0882 | 7.03 |
| 0.2072 | 0.955 | 0.1782 | 15.238 | | 10.777 | 0.955 | 9.2664 | 6.8042 |
| 0.4145 | 0.955 | 0.3564 | 15.2319 | | 10.9842 | 0.955 | 9.4446 | 6.589 |
| 0.6217 | 0.955 | 0.5346 | 15.2218 | | 11.1915 | 0.955 | 9.6228 | 6.3836 |
| 0.829 | 0.955 | 0.7128 | 15.2076 | | 11.3987 | 0.955 | 9.801 | 6.1873 |
| 1.0362 | 0.955 | 0.891 | 15.1893 | | 11.606 | 0.955 | 9.9792 | 5.9994 |
| 1.2435 | 0.955 | 1.0692 | 15.1669 | | 11.8132 | 0.955 | 10.1574 | 5.8193 |
| 1.4507 | 0.955 | 1.2474 | 15.1404 | | 12.0205 | 0.955 | 10.3356 | 5.6466 |
| 1.658 | 0.955 | 1.4256 | 15.1096 | | 12.2277 | 0.9624 | 10.5138 | 5.4809 |
| 1.8652 | 0.955 | 1.6038 | 15.0746 | | 12.435 | 0.9869 | 10.692 | 5.3217 |
| 2.0725 | 0.955 | 1.782 | 15.0353 | | 12.6422 | 1.029 | 10.8702 | 5.1687 |
| 2.2797 | 0.955 | 1.9602 | 14.9916 | | 12.8495 | 1.0897 | 11.0484 | 5.0216 |
| 2.487 | 0.955 | 2.1384 | 14.9435 | | 13.0567 | 1.2033 | 11.2266 | 4.8802 |
| 2.6942 | 0.955 | 2.3166 | 14.8909 | | 13.264 | 1.2835 | 11.4048 | 4.7442 |
| 2.9015 | 0.955 | 2.4948 | 14.8336 | | 13.4712 | 1.3536 | 11.583 | 4.6133 |
| 3.1087 | 0.955 | 2.673 | 14.7715 | | 13.6785 | 1.4139 | 11.7612 | 4.4874 |
| 3.316 | 0.955 | 2.8512 | 14.7046 | | 13.8857 | 1.4649 | 11.9394 | 4.3662 |
| 3.5232 | 0.955 | 3.0294 | 14.6327 | | 14.093 | 1.5067 | 12.1176 | 4.2496 |
| 3.7305 | 0.955 | 3.2076 | 14.5557 | | 14.3002 | 1.5397 | 12.2958 | 4.1375 |
| 3.9377 | 0.955 | 3.3858 | 14.4734 | | 14.5075 | 1.564 | 12.474 | 4.0297 |
| 4.145 | 0.955 | 3.564 | 14.3855 | | 14.7147 | 1.5797 | 12.6522 | 3.926 |
| 4.3522 | 0.955 | 3.7422 | 14.292 | | 14.922 | 1.5869 | 12.8304 | 3.8264 |
| 4.5595 | 0.955 | 3.9204 | 14.1925 | | 15.1292 | 1.5856 | 13.0086 | 3.7307 |
| 4.7667 | 0.955 | 4.0986 | 14.0868 | | 15.3365 | 1.5759 | 13.1868 | 3.6388 |
| 4.974 | 0.955 | 4.2768 | 13.9746 | | 15.5437 | 1.5576 | 13.365 | 3.5506 |
| 5.1812 | 0.955 | 4.455 | 13.8555 | | 15.751 | 1.5308 | 13.5432 | 3.4661 |
| 5.3885 | 0.955 | 4.6332 | 13.7293 | | 15.9582 | 1.4952 | 13.7214 | 3.3851 |
| 5.5957 | 0.955 | 4.8114 | 13.5953 | | 16.1655 | 1.4506 | 13.8996 | 3.3076 |
| 5.803 | 0.955 | 4.9896 | 13.4532 | | 16.3727 | 1.3969 | 14.0778 | 3.2335 |
| 6.0102 | 0.955 | 5.1678 | 13.3023 | | 16.58 | 1.3337 | 14.256 | 3.1627 |
| 6.2175 | 0.955 | 5.346 | 13.1419 | | 16.7872 | 1.2606 | 14.4342 | 3.0952 |
| 6.4247 | 0.955 | 5.5242 | 12.9713 | | 16.9944 | 1.1772 | 14.6124 | 3.0309 |
| 6.632 | 0.955 | 5.7024 | 12.7895 | | 17.2017 | 1.0829 | 14.7906 | 2.9697 |
| 6.8392 | 0.955 | 5.8806 | 12.5952 | | 17.4089 | 0.977 | 14.9688 | 2.9116 |
| 7.0465 | 0.955 | 6.0588 | 12.3871 | | 17.409 | 0.977 | 15.147 | 2.8566 |
| 7.2537 | 0.955 | 6.237 | 12.1633 | | 17.609 | 0.87 | 15.3252 | 2.8046 |
| 7.461 | 0.955 | 6.4152 | 11.9215 | | 17.819 | 0.759 | 15.5034 | 2.7556 |
| 7.6682 | 0.955 | 6.5934 | 11.6586 | | 18.029 | 0.646 | 15.6816 | 2.7095 |
| 7.8755 | 0.955 | 6.7716 | 11.3706 | | 18.209 | 0.569 | 15.8598 | 2.6664 |
| 8.0827 | 0.955 | 6.9498 | 11.0515 | | 18.389 | 0.489 | 16.038 | 2.626 |
| 8.29 | 0.955 | 7.128 | 10.6923 | | 18.569 | 0.417 | 16.2162 | 2.5882 |
| 8.4972 | 0.955 | 7.3062 | 10.2781 | | 18.764 | 0.345 | 16.3944 | 2.5506 |
| 8.7045 | 0.955 | 7.4844 | 9.8212 | | 18.959 | 0.28 | 16.5726 | 2.513 |
| 8.9117 | 0.955 | 7.6626 | 9.4064 | | 19.214 | 0.202 | 16.7507 | 2.4755 |
| 9.119 | 0.955 | 7.8408 | 9.0299 | | 19.439 | 0.14 | 16.9289 | 2.4379 |
| 9.3262 | 0.955 | 8.019 | 8.6838 | | 19.604 | 0.099 | 17.1071 | 2.4003 |
| 9.5335 | 0.955 | 8.1972 | 8.363 | | 19.776 | 0.064 | 17.2853 | 2.3628 |
| 9.7407 | 0.955 | 8.3754 | 8.0636 | | 20.03 | 0.025 | 17.4635 | 2.3252 |
| 9.948 | 0.955 | 8.5536 | 7.7827 | | 20.234 | 0.005 | 17.6417 | 2.2876 |
| 10.1552 | 0.955 | 8.7318 | 7.5179 | | 20.335 | 0.00001 | | |
| 10.3625 | 0.955 | 8.91 | 7.2675 | | | | | |
| | | | | | | | | |
| | | | | | | | | |
| | | | | | | | | |

Table A. Co-ordinates of the Contoured Plug & Converging Nozzle Surfaces

# APPENDIX B

A complete set of the numerical noise data obtained as a result of the computational noise study of a contoured plug-nozzle of design Mach number 1.49 is presented in tabular forms in this Appendix. The tables consist of the mixing noise levels, the shock noise levels, and the total noise levels at pressure ratios, $\xi$ = 2.0, 2.5, 3.0, 3.62 (design), 4.0, 4.5, 5.0. The numerical gasdynamics data for the contoured plug-nozzle jet flows obtained as outputs of the NPARC code are not included herein but these are also available.

| ANGLE | 20 | 30 | 40 | 50 | 60 | 70 | 80 | 90 | 100 | 110 | 120 | 130 | 140 | 150 | 160 | PWL |
|---|---|---|---|---|---|---|---|---|---|---|---|---|---|---|---|---|
| FREQ | | | | | | | | | | | | | | | | |
| 50 | 38.8 | 38.8 | 38.9 | 39.0 | 39.1 | 39.3 | 39.5 | 39.8 | 40.2 | 40.6 | 41.1 | 41.6 | 42.2 | 43.0 | 44.4 | 68.4 |
| 63 | 43.7 | 43.7 | 43.8 | 43.9 | 44.1 | 44.2 | 44.5 | 44.8 | 45.1 | 45.5 | 46.0 | 46.5 | 47.1 | 48.0 | 49.4 | 73.3 |
| 80 | 48.7 | 48.8 | 48.9 | 49.0 | 49.1 | 49.3 | 49.5 | 49.8 | 50.2 | 50.6 | 51.1 | 51.6 | 52.2 | 53.0 | 54.4 | 78.4 |
| 100 | 53.4 | 53.4 | 53.5 | 53.6 | 53.8 | 54.0 | 54.2 | 54.5 | 54.9 | 55.3 | 55.8 | 56.3 | 56.9 | 57.7 | 59.1 | 83.1 |
| 125 | 57.9 | 57.9 | 58.0 | 58.2 | 58.3 | 58.5 | 58.8 | 59.1 | 59.5 | 59.9 | 60.4 | 60.9 | 61.5 | 62.4 | 63.7 | 87.7 |
| 160 | 62.7 | 62.8 | 62.9 | 63.0 | 63.2 | 63.4 | 63.7 | 64.0 | 64.4 | 64.8 | 65.3 | 65.9 | 66.5 | 67.4 | 68.7 | 92.6 |
| 200 | 66.8 | 66.9 | 67.0 | 67.2 | 67.4 | 67.6 | 67.9 | 68.2 | 68.6 | 69.1 | 69.6 | 70.2 | 70.8 | 71.7 | 73.0 | 96.8 |
| 250 | 70.7 | 70.8 | 70.9 | 71.1 | 71.3 | 71.5 | 71.8 | 72.2 | 72.6 | 73.1 | 73.7 | 74.3 | 74.9 | 75.8 | 77.1 | 100.9 |
| 315 | 74.3 | 74.4 | 74.6 | 74.7 | 75.0 | 75.2 | 75.6 | 76.0 | 76.4 | 77.0 | 77.5 | 78.1 | 78.8 | 79.7 | 81.0 | 104.7 |
| 400 | 77.8 | 77.9 | 78.0 | 78.2 | 78.4 | 78.7 | 79.1 | 79.5 | 80.0 | 80.5 | 81.1 | 81.7 | 82.4 | 83.4 | 84.6 | 108.2 |
| 500 | 80.7 | 80.8 | 80.9 | 81.1 | 81.3 | 81.6 | 82.0 | 82.4 | 82.9 | 83.4 | 84.0 | 84.6 | 85.3 | 86.4 | 87.5 | 111.1 |
| 630 | 83.5 | 83.6 | 83.7 | 83.9 | 84.1 | 84.4 | 84.7 | 85.1 | 85.6 | 86.1 | 86.7 | 87.3 | 87.9 | 89.1 | 90.0 | 113.8 |
| 800 | 86.2 | 86.3 | 86.5 | 86.6 | 86.8 | 87.1 | 87.4 | 87.7 | 88.1 | 88.6 | 89.1 | 89.7 | 90.3 | 91.5 | 92.2 | 116.3 |
| 1000 | 88.5 | 88.6 | 88.7 | 88.9 | 89.1 | 89.4 | 89.6 | 90.0 | 90.4 | 90.8 | 91.2 | 91.7 | 92.4 | 93.6 | 94.1 | 118.5 |
| 1250 | 90.5 | 90.6 | 90.7 | 90.9 | 91.1 | 91.4 | 91.7 | 92.0 | 92.4 | 92.8 | 93.2 | 93.6 | 94.3 | 95.4 | 95.8 | 120.5 |
| 1600 | 92.2 | 92.3 | 92.5 | 92.7 | 93.0 | 93.3 | 93.6 | 93.9 | 94.3 | 94.7 | 95.1 | 95.5 | 96.2 | 97.2 | 97.3 | 122.3 |
| 2000 | 93.3 | 93.5 | 93.7 | 93.9 | 94.2 | 94.6 | 94.9 | 95.3 | 95.7 | 96.1 | 96.5 | 96.9 | 97.7 | 98.6 | 98.3 | 123.6 |
| 2500 | 94.0 | 94.1 | 94.4 | 94.7 | 95.0 | 95.4 | 95.8 | 96.3 | 96.7 | 97.1 | 97.5 | 97.9 | 98.9 | 99.5 | 99.0 | 124.6 |
| 3150 | 94.1 | 94.3 | 94.6 | 95.0 | 95.4 | 95.9 | 96.3 | 96.8 | 97.3 | 97.8 | 98.3 | 98.7 | 99.7 | 100.1 | 99.2 | 125.2 |
| 4000 | 93.9 | 94.1 | 94.4 | 94.8 | 95.3 | 95.8 | 96.4 | 97.0 | 97.5 | 98.1 | 98.6 | 99.1 | 100.1 | 100.2 | 99.1 | 125.3 |
| 5000 | 93.3 | 93.5 | 93.9 | 94.3 | 94.8 | 95.4 | 96.0 | 96.7 | 97.3 | 97.9 | 98.5 | 99.0 | 100.1 | 99.9 | 98.6 | 125.1 |
| 6300 | 92.4 | 92.7 | 93.1 | 93.5 | 94.1 | 94.7 | 95.3 | 96.0 | 96.7 | 97.4 | 98.0 | 98.6 | 99.6 | 99.3 | 97.9 | 124.6 |
| 8000 | 91.4 | 91.7 | 92.1 | 92.5 | 93.1 | 93.7 | 94.4 | 95.1 | 95.8 | 96.5 | 97.2 | 97.8 | 98.8 | 98.4 | 96.9 | 123.7 |
| 10000 | 90.4 | 90.7 | 91.1 | 91.5 | 92.1 | 92.7 | 93.4 | 94.1 | 94.8 | 95.5 | 96.2 | 96.9 | 97.9 | 97.3 | 95.8 | 122.8 |
| 12500 | 89.3 | 89.6 | 90.0 | 90.4 | 91.0 | 91.6 | 92.3 | 93.0 | 93.7 | 94.4 | 95.1 | 95.8 | 96.7 | 96.2 | 94.7 | 121.8 |
| 16000 | 88.0 | 88.3 | 88.6 | 89.1 | 89.7 | 90.3 | 90.9 | 91.7 | 92.4 | 93.1 | 93.7 | 94.4 | 95.4 | 94.9 | 93.4 | 120.7 |
| 20000 | 86.7 | 87.0 | 87.3 | 87.8 | 88.3 | 89.0 | 89.6 | 90.3 | 91.1 | 91.8 | 92.4 | 93.1 | 94.1 | 93.6 | 92.1 | 119.6 |
| 25000 | 85.1 | 85.4 | 85.8 | 86.3 | 86.9 | 87.5 | 88.2 | 88.9 | 89.6 | 90.3 | 91.0 | 91.7 | 92.6 | 92.1 | 90.7 | 118.5 |
| 31500 | 83.0 | 83.3 | 83.8 | 84.3 | 84.9 | 85.6 | 86.4 | 87.1 | 87.9 | 88.6 | 89.3 | 90.0 | 90.9 | 90.4 | 89.0 | 117.3 |
| 40000 | 80.3 | 80.7 | 81.1 | 81.7 | 82.3 | 83.1 | 83.9 | 84.8 | 85.6 | 86.4 | 87.1 | 87.9 | 88.8 | 88.3 | 86.9 | 115.9 |
| 50000 | 77.5 | 77.8 | 78.2 | 78.8 | 79.5 | 80.3 | 81.1 | 82.0 | 82.9 | 83.8 | 84.6 | 85.3 | 86.3 | 85.8 | 84.3 | 114.3 |
| 63000 | 74.0 | 74.3 | 74.8 | 75.3 | 76.0 | 76.8 | 77.7 | 78.5 | 79.5 | 80.4 | 81.2 | 82.0 | 83.0 | 82.5 | 80.9 | 112.5 |
| 80000 | 69.5 | 69.9 | 70.4 | 71.0 | 71.7 | 72.5 | 73.3 | 74.3 | 75.2 | 76.1 | 77.0 | 77.8 | 78.8 | 78.3 | 76.8 | 110.5 |
| OVERALL | 103.6 | 103.8 | 104.1 | 104.5 | 104.9 | 105.4 | 105.9 | 106.5 | 107.1 | 107.6 | 108.2 | 108.7 | 109.7 | 109.8 | 108.9 | 135.1 |
| PNL | 116.1 | 116.3 | 116.6 | 116.9 | 117.3 | 117.7 | 118.2 | 118.8 | 119.3 | 119.8 | 120.3 | 120.8 | 121.8 | 122.1 | 121.4 | |
| PNLT | 116.1 | 116.3 | 116.6 | 116.9 | 117.3 | 117.7 | 118.2 | 118.8 | 119.3 | 119.8 | 120.3 | 120.8 | 121.8 | 122.1 | 121.4 | |

Table B-1. Computational Acoustic Data for Pressure Ratio 2.0 : Mixing Noise Component

| ANGLE | 20 | 30 | 40 | 50 | 60 | 70 | 80 | 90 | 100 | 110 | 120 | 130 | 140 | 150 | 160 | PWL |
|---|---|---|---|---|---|---|---|---|---|---|---|---|---|---|---|---|
| FREQ | | | | | | | | | | | | | | | | |
| 50 | 0.0 | 0.0 | 0.0 | 0.0 | 0.0 | 0.0 | 0.0 | 0.0 | 0.0 | 0.0 | 0.0 | 0.0 | 0.0 | 0.0 | 0.0 | 27.9 |
| 63 | 35.8 | 35.8 | 35.8 | 35.8 | 35.8 | 35.8 | 35.8 | 35.8 | 35.8 | 35.8 | 35.8 | 35.8 | 35.8 | 35.8 | 35.8 | 63.7 |
| 80 | 36.5 | 36.5 | 36.5 | 36.5 | 36.5 | 36.5 | 36.5 | 36.5 | 36.5 | 36.5 | 36.5 | 36.5 | 36.5 | 36.5 | 36.5 | 64.4 |
| 100 | 40.6 | 40.6 | 40.6 | 40.6 | 40.6 | 40.6 | 40.6 | 40.6 | 40.6 | 40.6 | 40.6 | 40.6 | 40.6 | 40.6 | 40.6 | 68.4 |
| 125 | 38.9 | 38.9 | 38.9 | 38.9 | 38.9 | 38.9 | 38.9 | 38.9 | 38.9 | 38.9 | 38.9 | 38.9 | 38.9 | 38.9 | 38.9 | 66.8 |
| 160 | 39.5 | 39.5 | 39.5 | 39.5 | 39.5 | 39.5 | 39.5 | 39.5 | 39.5 | 39.5 | 39.5 | 39.5 | 39.5 | 39.5 | 39.5 | 67.4 |
| 200 | 40.5 | 40.5 | 40.5 | 40.5 | 40.5 | 40.5 | 40.5 | 40.5 | 40.5 | 40.5 | 40.5 | 40.5 | 40.5 | 40.5 | 40.5 | 68.4 |
| 250 | 41.6 | 41.6 | 41.6 | 41.6 | 41.6 | 41.6 | 41.6 | 41.6 | 41.6 | 41.6 | 41.6 | 41.6 | 41.6 | 41.6 | 41.6 | 69.5 |
| 315 | 42.8 | 42.8 | 42.8 | 42.8 | 42.8 | 42.8 | 42.8 | 42.8 | 42.8 | 42.8 | 42.8 | 42.8 | 42.8 | 42.8 | 42.8 | 70.7 |
| 400 | 43.5 | 43.5 | 43.5 | 43.5 | 43.5 | 43.5 | 43.5 | 43.5 | 43.5 | 43.5 | 43.5 | 43.5 | 43.5 | 43.5 | 43.5 | 71.4 |
| 500 | 44.6 | 44.6 | 44.6 | 44.6 | 44.6 | 44.6 | 44.6 | 44.6 | 44.6 | 44.6 | 44.6 | 44.6 | 44.6 | 44.6 | 44.6 | 72.5 |
| 630 | 45.8 | 45.8 | 45.8 | 45.8 | 45.8 | 45.8 | 45.8 | 45.8 | 45.8 | 45.8 | 45.8 | 45.8 | 45.8 | 45.8 | 45.8 | 73.7 |
| 800 | 46.5 | 46.5 | 46.5 | 46.5 | 46.5 | 46.5 | 46.5 | 46.5 | 46.5 | 46.5 | 46.5 | 46.5 | 46.5 | 46.5 | 46.5 | 74.4 |
| 1000 | 47.4 | 47.4 | 47.4 | 47.4 | 47.4 | 47.4 | 47.4 | 47.4 | 47.4 | 47.4 | 47.4 | 47.4 | 47.4 | 47.4 | 47.4 | 75.4 |
| 1250 | 48.9 | 48.9 | 48.9 | 48.9 | 48.9 | 48.9 | 48.9 | 48.9 | 48.9 | 48.9 | 48.9 | 48.9 | 48.9 | 48.9 | 48.9 | 76.8 |
| 1600 | 49.5 | 49.5 | 49.5 | 49.5 | 49.5 | 49.5 | 49.5 | 49.5 | 49.5 | 49.5 | 49.5 | 49.5 | 49.5 | 49.5 | 49.5 | 77.4 |
| 2000 | 50.4 | 50.4 | 50.4 | 50.4 | 50.4 | 50.4 | 50.4 | 50.4 | 50.4 | 50.4 | 50.4 | 50.4 | 50.4 | 50.4 | 50.4 | 78.4 |
| 2500 | 51.6 | 51.6 | 51.6 | 51.6 | 51.6 | 51.6 | 51.6 | 51.6 | 51.6 | 51.6 | 51.6 | 51.6 | 51.6 | 51.6 | 51.6 | 79.5 |
| 3150 | 52.7 | 52.7 | 52.7 | 52.7 | 52.7 | 52.7 | 52.7 | 52.7 | 52.7 | 52.7 | 52.7 | 52.7 | 52.7 | 52.7 | 52.7 | 80.7 |
| 4000 | 53.4 | 53.4 | 53.4 | 53.4 | 53.4 | 53.4 | 53.4 | 53.4 | 53.4 | 53.4 | 53.4 | 53.4 | 53.4 | 53.4 | 53.4 | 81.4 |
| 5000 | 54.5 | 54.5 | 54.5 | 54.5 | 54.5 | 54.5 | 54.5 | 54.5 | 54.5 | 54.5 | 54.5 | 54.5 | 54.5 | 54.5 | 54.5 | 82.5 |
| 6300 | 58.0 | 56.5 | 55.7 | 55.7 | 55.7 | 55.7 | 55.7 | 55.7 | 55.7 | 55.7 | 55.7 | 55.7 | 55.7 | 55.7 | 55.7 | 83.8 |
| 8000 | 90.0 | 87.9 | 84.9 | 80.9 | 75.8 | 69.8 | 63.1 | 57.6 | 56.3 | 56.3 | 56.3 | 56.3 | 56.3 | 56.3 | 56.3 | 107.6 |
| 10000 | 104.9 | 103.8 | 102.3 | 100.1 | 97.2 | 93.5 | 89.0 | 83.8 | 77.9 | 71.6 | 65.3 | 60.1 | 57.6 | 57.2 | 57.2 | 124.6 |
| 12500 | 109.0 | 108.9 | 108.6 | 107.9 | 106.9 | 105.2 | 102.9 | 99.9 | 96.4 | 92.3 | 88.0 | 83.6 | 79.5 | 76.0 | 73.2 | 132.1 |
| 16000 | 104.9 | 105.5 | 106.3 | 107.0 | 107.4 | 107.4 | 106.8 | 105.6 | 103.8 | 101.4 | 98.7 | 95.7 | 92.8 | 90.3 | 88.2 | 133.2 |
| 20000 | 101.9 | 102.0 | 102.3 | 103.1 | 104.2 | 105.3 | 106.1 | 106.3 | 106.0 | 105.0 | 103.6 | 101.8 | 99.9 | 98.1 | 96.7 | 132.9 |
| 25000 | 102.2 | 102.2 | 102.2 | 102.3 | 102.4 | 102.8 | 103.6 | 104.5 | 105.1 | 105.2 | 104.9 | 104.1 | 103.1 | 102.0 | 101.1 | 132.8 |
| 31500 | 100.3 | 100.5 | 100.8 | 101.2 | 101.5 | 101.8 | 102.1 | 102.6 | 103.3 | 103.8 | 104.1 | 104.0 | 103.6 | 103.1 | 102.6 | 132.3 |
| 40000 | 97.3 | 97.6 | 97.9 | 98.3 | 98.9 | 99.5 | 100.0 | 100.6 | 101.1 | 101.7 | 102.1 | 102.3 | 102.3 | 102.1 | 101.8 | 131.1 |
| 50000 | 95.2 | 95.4 | 95.6 | 95.9 | 96.4 | 97.0 | 97.7 | 98.4 | 99.1 | 99.8 | 100.3 | 100.6 | 100.8 | 100.7 | 100.6 | 130.2 |
| 63000 | 92.6 | 92.8 | 93.0 | 93.3 | 93.6 | 94.1 | 94.6 | 95.5 | 96.1 | 97.0 | 97.8 | 98.2 | 98.6 | 98.3 | 98.4 | 129.2 |
| 80000 | 0.0 | 0.0 | 0.0 | 0.0 | 0.0 | 0.0 | 0.0 | 0.0 | 0.0 | 0.0 | 0.0 | 0.0 | 0.0 | 0.0 | 0.0 | 27.9 |
| OVERALL | 112.9 | 112.8 | 112.8 | 112.7 | 112.6 | 112.4 | 112.2 | 112.0 | 111.7 | 111.3 | 110.8 | 110.2 | 109.6 | 108.9 | 108.5 | 141.0 |
| PNL | 109.3 | 108.3 | 106.8 | 104.7 | 101.9 | 98.6 | 94.6 | 90.3 | 86.0 | 82.0 | 78.6 | 76.9 | 76.7 | 76.7 | 76.7 | |
| PNLT | 110.7 | 109.6 | 107.7 | 104.7 | 101.9 | 100.2 | 97.7 | 93.7 | 89.4 | 84.4 | 80.0 | 76.9 | 76.7 | 76.7 | 76.7 | |
| | | | | | | | | | | | | | | | | |
| | | | | | | | | | | | | | | | | |
| | | | | | | | | | | | | | | | | |

Table B-2. Computational Acoustic Data for Pressure Ratio 2.0 : Shock Noise Component

| ANGLE | 20 | 30 | 40 | 50 | 60 | 70 | 80 | 90 | 100 | 110 | 120 | 130 | 140 | 150 | 160 | PWL |
|---|---|---|---|---|---|---|---|---|---|---|---|---|---|---|---|---|
| FREQ | | | | | | | | | | | | | | | | |
| 50 | 38.8 | 38.8 | 38.9 | 39.0 | 39.1 | 39.3 | 39.5 | 39.8 | 40.2 | 40.6 | 41.1 | 41.6 | 42.2 | 43.0 | 44.4 | 68.4 |
| 63 | 44.3 | 44.4 | 44.5 | 44.5 | 44.7 | 44.8 | 45.0 | 45.3 | 45.6 | 46.0 | 46.4 | 46.9 | 47.4 | 48.2 | 49.5 | 73.8 |
| 80 | 49.0 | 49.0 | 49.1 | 49.2 | 49.3 | 49.5 | 49.8 | 50.0 | 50.4 | 50.8 | 51.2 | 51.8 | 52.3 | 53.1 | 54.5 | 78.6 |
| 100 | 53.6 | 53.6 | 53.7 | 53.8 | 54.0 | 54.2 | 54.4 | 54.7 | 55.0 | 55.4 | 55.9 | 56.4 | 57.0 | 57.8 | 59.2 | 83.2 |
| 125 | 57.9 | 58.0 | 58.1 | 58.2 | 58.4 | 58.6 | 58.8 | 59.1 | 59.5 | 59.9 | 60.4 | 61.0 | 61.5 | 62.4 | 63.7 | 87.7 |
| 160 | 62.7 | 62.8 | 62.9 | 63.0 | 63.2 | 63.4 | 63.7 | 64.0 | 64.4 | 64.8 | 65.4 | 65.9 | 66.5 | 67.4 | 68.7 | 92.6 |
| 200 | 66.8 | 66.9 | 67.0 | 67.2 | 67.4 | 67.6 | 67.9 | 68.2 | 68.6 | 69.1 | 69.6 | 70.2 | 70.8 | 71.7 | 73.0 | 96.8 |
| 250 | 70.7 | 70.8 | 70.9 | 71.1 | 71.3 | 71.5 | 71.8 | 72.2 | 72.6 | 73.1 | 73.7 | 74.3 | 74.9 | 75.8 | 77.1 | 100.9 |
| 315 | 74.3 | 74.4 | 74.6 | 74.7 | 75.0 | 75.3 | 75.6 | 76.0 | 76.4 | 77.0 | 77.5 | 78.2 | 78.8 | 79.7 | 81.0 | 104.7 |
| 400 | 77.8 | 77.9 | 78.0 | 78.2 | 78.4 | 78.7 | 79.1 | 79.5 | 80.0 | 80.5 | 81.1 | 81.7 | 82.4 | 83.4 | 84.6 | 108.2 |
| 500 | 80.7 | 80.8 | 80.9 | 81.1 | 81.3 | 81.6 | 82.0 | 82.4 | 82.9 | 83.4 | 84.0 | 84.6 | 85.3 | 86.4 | 87.5 | 111.1 |
| 630 | 83.5 | 83.6 | 83.7 | 83.9 | 84.1 | 84.4 | 84.7 | 85.1 | 85.6 | 86.1 | 86.7 | 87.3 | 87.9 | 89.1 | 90.0 | 113.8 |
| 800 | 86.2 | 86.3 | 86.5 | 86.6 | 86.8 | 87.1 | 87.4 | 87.7 | 88.1 | 88.6 | 89.1 | 89.7 | 90.3 | 91.5 | 92.2 | 116.3 |
| 1000 | 88.5 | 88.6 | 88.7 | 88.9 | 89.1 | 89.4 | 89.6 | 90.0 | 90.4 | 90.8 | 91.2 | 91.7 | 92.4 | 93.6 | 94.1 | 118.5 |
| 1250 | 90.5 | 90.6 | 90.7 | 90.9 | 91.1 | 91.4 | 91.7 | 92.0 | 92.4 | 92.8 | 93.2 | 93.6 | 94.3 | 95.4 | 95.8 | 120.4 |
| 1600 | 92.2 | 92.3 | 92.5 | 92.7 | 93.0 | 93.3 | 93.6 | 93.9 | 94.3 | 94.7 | 95.1 | 95.5 | 96.2 | 97.2 | 97.3 | 122.3 |
| 2000 | 93.3 | 93.5 | 93.7 | 93.9 | 94.2 | 94.6 | 94.9 | 95.3 | 95.7 | 96.1 | 96.5 | 96.9 | 97.7 | 98.6 | 98.3 | 123.6 |
| 2500 | 94.0 | 94.1 | 94.4 | 94.7 | 95.0 | 95.4 | 95.8 | 96.3 | 96.7 | 97.1 | 97.5 | 97.9 | 98.9 | 99.5 | 99.0 | 124.6 |
| 3150 | 94.1 | 94.3 | 94.6 | 95.0 | 95.4 | 95.9 | 96.3 | 96.8 | 97.3 | 97.8 | 98.3 | 98.7 | 99.7 | 100.1 | 99.2 | 125.1 |
| 4000 | 93.9 | 94.1 | 94.4 | 94.8 | 95.3 | 95.8 | 96.4 | 97.0 | 97.5 | 98.1 | 98.6 | 99.1 | 100.1 | 100.2 | 99.1 | 125.3 |
| 5000 | 93.3 | 93.5 | 93.9 | 94.3 | 94.8 | 95.4 | 96.0 | 96.7 | 97.3 | 97.9 | 98.5 | 99.0 | 100.1 | 99.9 | 98.6 | 125.0 |
| 6300 | 92.4 | 92.7 | 93.1 | 93.5 | 94.1 | 94.7 | 95.3 | 96.0 | 96.7 | 97.4 | 98.0 | 98.6 | 99.6 | 99.3 | 97.9 | 124.4 |
| 8000 | 93.8 | 93.2 | 92.8 | 92.8 | 93.2 | 93.7 | 94.4 | 95.1 | 95.8 | 96.5 | 97.2 | 97.8 | 98.8 | 98.4 | 96.9 | 123.6 |
| 10000 | 105.0 | 104.1 | 102.6 | 100.7 | 98.4 | 96.1 | 94.7 | 94.5 | 94.9 | 95.5 | 96.2 | 96.9 | 97.9 | 97.3 | 95.8 | 126.6 |
| 12500 | 109.0 | 108.9 | 108.6 | 108.0 | 107.0 | 105.4 | 103.3 | 100.7 | 98.2 | 96.5 | 95.9 | 96.0 | 96.8 | 96.2 | 94.7 | 132.1 |
| 16000 | 104.9 | 105.6 | 106.4 | 107.1 | 107.5 | 107.5 | 107.0 | 105.8 | 104.1 | 102.0 | 99.9 | 98.1 | 97.3 | 96.2 | 94.6 | 132.8 |
| 20000 | 102.0 | 102.1 | 102.5 | 103.2 | 104.3 | 105.4 | 106.2 | 106.5 | 106.1 | 105.2 | 103.9 | 102.3 | 100.9 | 99.4 | 98.0 | 132.3 |
| 25000 | 102.3 | 102.3 | 102.3 | 102.4 | 102.5 | 103.0 | 103.7 | 104.6 | 105.2 | 105.4 | 105.0 | 104.3 | 103.4 | 102.4 | 101.4 | 131.7 |
| 31500 | 100.4 | 100.6 | 100.9 | 101.2 | 101.6 | 101.9 | 102.2 | 102.8 | 103.4 | 103.9 | 104.2 | 104.1 | 103.8 | 103.3 | 102.8 | 130.7 |
| 40000 | 97.4 | 97.6 | 98.0 | 98.4 | 99.0 | 99.6 | 100.1 | 100.7 | 101.3 | 101.8 | 102.2 | 102.4 | 102.5 | 102.3 | 102.0 | 128.7 |
| 50000 | 95.3 | 95.4 | 95.7 | 96.0 | 96.5 | 97.1 | 97.7 | 98.5 | 99.2 | 99.9 | 100.4 | 100.8 | 101.0 | 100.8 | 100.7 | 126.7 |
| 63000 | 92.7 | 92.9 | 93.1 | 93.4 | 93.7 | 94.2 | 94.7 | 95.5 | 96.2 | 97.1 | 97.9 | 98.3 | 98.7 | 98.4 | 98.5 | 124.0 |
| 80000 | 69.5 | 69.9 | 70.4 | 71.0 | 71.7 | 72.5 | 73.3 | 74.3 | 75.2 | 76.1 | 77.0 | 77.8 | 78.8 | 78.3 | 76.8 | 103.0 |
| OVERALL | 113.4 | 113.4 | 113.3 | 113.3 | 113.3 | 113.2 | 113.2 | 113.1 | 113.0 | 112.8 | 112.7 | 112.5 | 112.6 | 112.4 | 111.7 | 140.9 |
| PNL | 118.1 | 117.7 | 117.1 | 117.3 | 117.5 | 117.9 | 118.3 | 118.8 | 119.3 | 119.8 | 120.3 | 120.8 | 121.8 | 122.1 | 121.4 | |
| PNLT | 119.7 | 119.4 | 118.8 | 118.7 | 118.6 | 117.9 | 118.3 | 118.8 | 119.3 | 119.8 | 120.3 | 120.8 | 121.8 | 122.1 | 121.4 | |

Table B-3. Computational Acoustic Data for Pressure ratio 2.0 : Total Noise Levels

| ANGLE | 20 | 30 | 40 | 50 | 60 | 70 | 80 | 90 | 100 | 110 | 120 | 130 | 140 | 150 | 160 | PWL |
|---|---|---|---|---|---|---|---|---|---|---|---|---|---|---|---|---|
| FREQ | | | | | | | | | | | | | | | | |
| 50 | 38.8 | 38.8 | 38.9 | 38.9 | 39.0 | 39.1 | 39.3 | 39.5 | 39.8 | 40.1 | 40.6 | 41.0 | 41.6 | 42.7 | 44.3 | 69.1 |
| 63 | 43.8 | 43.8 | 43.8 | 43.9 | 44.0 | 44.1 | 44.3 | 44.5 | 44.8 | 45.1 | 45.5 | 46.0 | 46.6 | 47.7 | 49.3 | 74.0 |
| 80 | 48.8 | 48.9 | 48.9 | 49.0 | 49.1 | 49.2 | 49.4 | 49.6 | 49.9 | 50.2 | 50.7 | 51.1 | 51.7 | 52.8 | 54.4 | 79.1 |
| 100 | 53.5 | 53.6 | 53.6 | 53.7 | 53.8 | 53.9 | 54.1 | 54.3 | 54.6 | 55.0 | 55.4 | 55.9 | 56.5 | 57.5 | 59.1 | 83.9 |
| 125 | 58.2 | 58.2 | 58.2 | 58.3 | 58.4 | 58.6 | 58.7 | 59.0 | 59.3 | 59.7 | 60.1 | 60.6 | 61.1 | 62.2 | 63.8 | 88.5 |
| 160 | 63.1 | 63.2 | 63.2 | 63.3 | 63.4 | 63.6 | 63.8 | 64.0 | 64.3 | 64.7 | 65.2 | 65.7 | 66.2 | 67.4 | 68.8 | 93.6 |
| 200 | 67.5 | 67.5 | 67.6 | 67.7 | 67.8 | 68.0 | 68.2 | 68.4 | 68.8 | 69.2 | 69.6 | 70.1 | 70.7 | 71.8 | 73.3 | 98.0 |
| 250 | 71.5 | 71.6 | 71.7 | 71.8 | 71.9 | 72.1 | 72.4 | 72.7 | 73.0 | 73.4 | 73.9 | 74.4 | 75.1 | 76.2 | 77.6 | 102.3 |
| 315 | 75.5 | 75.6 | 75.6 | 75.8 | 75.9 | 76.2 | 76.4 | 76.8 | 77.1 | 77.6 | 78.1 | 78.6 | 79.3 | 80.4 | 81.8 | 106.4 |
| 400 | 79.2 | 79.3 | 79.4 | 79.5 | 79.7 | 80.0 | 80.3 | 80.6 | 81.0 | 81.5 | 82.0 | 82.6 | 83.3 | 84.5 | 85.7 | 110.3 |
| 500 | 82.3 | 82.4 | 82.5 | 82.7 | 82.9 | 83.1 | 83.4 | 83.8 | 84.3 | 84.8 | 85.3 | 85.9 | 86.6 | 87.9 | 89.0 | 113.5 |
| 630 | 85.3 | 85.3 | 85.5 | 85.6 | 85.8 | 86.1 | 86.4 | 86.8 | 87.2 | 87.7 | 88.3 | 88.9 | 89.7 | 90.9 | 91.9 | 116.5 |
| 800 | 88.1 | 88.2 | 88.3 | 88.4 | 88.6 | 88.8 | 89.1 | 89.5 | 89.9 | 90.4 | 90.9 | 91.5 | 92.3 | 93.6 | 94.3 | 119.2 |
| 1000 | 90.5 | 90.6 | 90.7 | 90.8 | 91.0 | 91.2 | 91.5 | 91.8 | 92.2 | 92.7 | 93.1 | 93.7 | 94.5 | 95.8 | 96.2 | 121.4 |
| 1250 | 92.6 | 92.7 | 92.8 | 93.0 | 93.2 | 93.4 | 93.7 | 94.0 | 94.3 | 94.7 | 95.2 | 95.7 | 96.5 | 97.7 | 97.9 | 123.5 |
| 1600 | 94.6 | 94.7 | 94.8 | 95.0 | 95.2 | 95.5 | 95.8 | 96.1 | 96.4 | 96.8 | 97.2 | 97.6 | 98.5 | 99.5 | 99.4 | 125.5 |
| 2000 | 95.9 | 96.0 | 96.2 | 96.4 | 96.7 | 97.0 | 97.3 | 97.6 | 98.0 | 98.3 | 98.7 | 99.1 | 100.1 | 100.9 | 100.5 | 127.0 |
| 2500 | 96.6 | 96.8 | 97.1 | 97.4 | 97.7 | 98.1 | 98.5 | 98.8 | 99.2 | 99.6 | 100.0 | 100.4 | 101.5 | 101.9 | 101.2 | 128.1 |
| 3150 | 96.9 | 97.2 | 97.5 | 97.8 | 98.2 | 98.7 | 99.2 | 99.6 | 100.1 | 100.5 | 100.9 | 101.4 | 102.5 | 102.6 | 101.6 | 128.9 |
| 4000 | 96.8 | 97.0 | 97.4 | 97.8 | 98.3 | 98.8 | 99.4 | 99.9 | 100.5 | 101.0 | 101.4 | 102.0 | 103.0 | 102.8 | 101.5 | 129.2 |
| 5000 | 96.3 | 96.6 | 97.0 | 97.4 | 97.9 | 98.5 | 99.1 | 99.8 | 100.4 | 101.0 | 101.5 | 102.1 | 103.1 | 102.7 | 101.2 | 129.1 |
| 6300 | 95.7 | 95.9 | 96.3 | 96.8 | 97.3 | 97.9 | 98.6 | 99.3 | 100.0 | 100.6 | 101.2 | 101.9 | 102.8 | 102.1 | 100.5 | 128.7 |
| 8000 | 94.8 | 95.1 | 95.5 | 96.0 | 96.5 | 97.1 | 97.8 | 98.5 | 99.2 | 99.9 | 100.5 | 101.3 | 102.1 | 101.3 | 99.6 | 128.0 |
| 10000 | 94.0 | 94.2 | 94.6 | 95.1 | 95.6 | 96.3 | 97.0 | 97.7 | 98.4 | 99.1 | 99.7 | 100.5 | 101.3 | 100.4 | 98.7 | 127.3 |
| 12500 | 92.9 | 93.2 | 93.6 | 94.1 | 94.6 | 95.3 | 96.0 | 96.7 | 97.4 | 98.1 | 98.8 | 99.5 | 100.3 | 99.4 | 97.7 | 126.4 |
| 16000 | 91.4 | 91.7 | 92.2 | 92.7 | 93.3 | 94.0 | 94.7 | 95.5 | 96.2 | 96.9 | 97.6 | 98.3 | 99.1 | 98.2 | 96.5 | 125.4 |
| 20000 | 90.0 | 90.3 | 90.7 | 91.2 | 91.8 | 92.5 | 93.3 | 94.1 | 94.9 | 95.6 | 96.3 | 97.1 | 97.9 | 97.0 | 95.3 | 124.3 |
| 25000 | 88.6 | 88.9 | 89.3 | 89.7 | 90.3 | 91.0 | 91.7 | 92.5 | 93.3 | 94.1 | 94.8 | 95.6 | 96.4 | 95.5 | 93.8 | 123.2 |
| 31500 | 86.9 | 87.2 | 87.6 | 88.1 | 88.7 | 89.4 | 90.1 | 90.8 | 91.6 | 92.3 | 93.0 | 93.8 | 94.6 | 93.7 | 92.1 | 122.0 |
| 40000 | 84.8 | 85.1 | 85.5 | 86.0 | 86.6 | 87.3 | 88.1 | 88.9 | 89.6 | 90.3 | 91.0 | 91.8 | 92.6 | 91.8 | 90.1 | 120.8 |
| 50000 | 82.4 | 82.7 | 83.1 | 83.7 | 84.3 | 85.0 | 85.7 | 86.6 | 87.4 | 88.1 | 88.8 | 89.6 | 90.5 | 89.7 | 88.0 | 119.6 |
| 63000 | 79.0 | 79.3 | 79.8 | 80.5 | 81.2 | 82.0 | 82.8 | 83.6 | 84.4 | 85.2 | 86.0 | 86.8 | 87.7 | 86.9 | 85.3 | 118.3 |
| 80000 | 74.2 | 74.6 | 75.2 | 75.9 | 76.7 | 77.6 | 78.6 | 79.6 | 80.5 | 81.4 | 82.2 | 83.0 | 83.9 | 83.2 | 81.5 | 116.7 |
| OVERALL | 106.5 | 106.7 | 107.0 | 107.4 | 107.9 | 108.4 | 108.9 | 109.5 | 110.0 | 110.6 | 111.1 | 111.7 | 112.7 | 112.5 | 111.4 | 139.1 |
| PNL | 118.8 | 119.0 | 119.3 | 119.6 | 120.0 | 120.5 | 121.0 | 121.5 | 122.0 | 122.5 | 123.0 | 123.6 | 124.6 | 124.6 | 123.7 | |
| PNLT | 118.8 | 119.0 | 119.3 | 119.6 | 120.0 | 120.5 | 121.0 | 121.5 | 122.0 | 122.5 | 123.0 | 123.6 | 124.6 | 124.6 | 123.7 | |
| | | | | | | | | | | | | | | | | |
| | | | | | | | | | | | | | | | | |
| | | | | | | | | | | | | | | | | |

Table B-4. Computational Acoustic Data for Pressure Ratio 2.5 : Mixing Noise Component

| ANGLE | 20 | 30 | 40 | 50 | 60 | 70 | 80 | 90 | 100 | 110 | 120 | 130 | 140 | 150 | 160 | PWL |
|---|---|---|---|---|---|---|---|---|---|---|---|---|---|---|---|---|
| FREQ | | | | | | | | | | | | | | | | |
| 50 | 0.0 | 0.0 | 0.0 | 0.0 | 0.0 | 0.0 | 0.0 | 0.0 | 0.0 | 0.0 | 0.0 | 0.0 | 0.0 | 0.0 | 0.0 | 28.9 |
| 63 | 35.8 | 35.8 | 35.8 | 35.8 | 35.8 | 35.8 | 35.8 | 35.8 | 35.8 | 35.8 | 35.8 | 35.8 | 35.8 | 35.8 | 35.8 | 64.6 |
| 80 | 36.5 | 36.5 | 36.5 | 36.5 | 36.5 | 36.5 | 36.5 | 36.5 | 36.5 | 36.5 | 36.5 | 36.5 | 36.5 | 36.5 | 36.5 | 65.4 |
| 100 | 40.6 | 40.6 | 40.6 | 40.6 | 40.6 | 40.6 | 40.6 | 40.6 | 40.6 | 40.6 | 40.6 | 40.6 | 40.6 | 40.6 | 40.6 | 69.4 |
| 125 | 38.9 | 38.9 | 38.9 | 38.9 | 38.9 | 38.9 | 38.9 | 38.9 | 38.9 | 38.9 | 38.9 | 38.9 | 38.9 | 38.9 | 38.9 | 67.8 |
| 160 | 39.5 | 39.5 | 39.5 | 39.5 | 39.5 | 39.5 | 39.5 | 39.5 | 39.5 | 39.5 | 39.5 | 39.5 | 39.5 | 39.5 | 39.5 | 68.4 |
| 200 | 40.5 | 40.5 | 40.5 | 40.5 | 40.5 | 40.5 | 40.5 | 40.5 | 40.5 | 40.5 | 40.5 | 40.5 | 40.5 | 40.5 | 40.5 | 69.3 |
| 250 | 41.6 | 41.6 | 41.6 | 41.6 | 41.6 | 41.6 | 41.6 | 41.6 | 41.6 | 41.6 | 41.6 | 41.6 | 41.6 | 41.6 | 41.6 | 70.5 |
| 315 | 42.8 | 42.8 | 42.8 | 42.8 | 42.8 | 42.8 | 42.8 | 42.8 | 42.8 | 42.8 | 42.8 | 42.8 | 42.8 | 42.8 | 42.8 | 71.6 |
| 400 | 43.5 | 43.5 | 43.5 | 43.5 | 43.5 | 43.5 | 43.5 | 43.5 | 43.5 | 43.5 | 43.5 | 43.5 | 43.5 | 43.5 | 43.5 | 72.3 |
| 500 | 44.6 | 44.6 | 44.6 | 44.6 | 44.6 | 44.6 | 44.6 | 44.6 | 44.6 | 44.6 | 44.6 | 44.6 | 44.6 | 44.6 | 44.6 | 73.5 |
| 630 | 45.8 | 45.8 | 45.8 | 45.8 | 45.8 | 45.8 | 45.8 | 45.8 | 45.8 | 45.8 | 45.8 | 45.8 | 45.8 | 45.8 | 45.8 | 74.6 |
| 800 | 46.5 | 46.5 | 46.5 | 46.5 | 46.5 | 46.5 | 46.5 | 46.5 | 46.5 | 46.5 | 46.5 | 46.5 | 46.5 | 46.5 | 46.5 | 75.4 |
| 1000 | 47.4 | 47.4 | 47.4 | 47.4 | 47.4 | 47.4 | 47.4 | 47.4 | 47.4 | 47.4 | 47.4 | 47.4 | 47.4 | 47.4 | 47.4 | 76.3 |
| 1250 | 48.9 | 48.9 | 48.9 | 48.9 | 48.9 | 48.9 | 48.9 | 48.9 | 48.9 | 48.9 | 48.9 | 48.9 | 48.9 | 48.9 | 48.9 | 77.8 |
| 1600 | 49.5 | 49.5 | 49.5 | 49.5 | 49.5 | 49.5 | 49.5 | 49.5 | 49.5 | 49.5 | 49.5 | 49.5 | 49.5 | 49.5 | 49.5 | 78.4 |
| 2000 | 50.4 | 50.4 | 50.4 | 50.4 | 50.4 | 50.4 | 50.4 | 50.4 | 50.4 | 50.4 | 50.4 | 50.4 | 50.4 | 50.4 | 50.4 | 79.3 |
| 2500 | 51.6 | 51.6 | 51.6 | 51.6 | 51.6 | 51.6 | 51.6 | 51.6 | 51.6 | 51.6 | 51.6 | 51.6 | 51.6 | 51.6 | 51.6 | 80.5 |
| 3150 | 73.8 | 70.2 | 65.2 | 59.0 | 53.8 | 52.7 | 52.7 | 52.7 | 52.7 | 52.7 | 52.7 | 52.7 | 52.7 | 52.7 | 52.7 | 91.0 |
| 4000 | 101.4 | 99.5 | 96.7 | 92.8 | 87.7 | 81.4 | 73.8 | 65.2 | 56.8 | 53.4 | 53.4 | 53.4 | 53.4 | 53.4 | 53.4 | 120.1 |
| 5000 | 111.5 | 110.9 | 109.8 | 108.2 | 105.7 | 102.3 | 97.9 | 92.5 | 86.2 | 79.3 | 72.0 | 64.8 | 58.8 | 55.5 | 54.6 | 133.0 |
| 6300 | 110.8 | 111.3 | 111.8 | 111.9 | 111.6 | 110.5 | 108.7 | 105.9 | 102.3 | 97.9 | 93.1 | 88.1 | 83.3 | 79.0 | 75.7 | 136.9 |
| 8000 | 104.0 | 104.9 | 106.3 | 108.0 | 109.5 | 110.4 | 110.7 | 110.1 | 108.6 | 106.2 | 103.3 | 100.0 | 96.6 | 93.6 | 91.1 | 136.7 |
| 10000 | 105.7 | 105.4 | 105.0 | 104.8 | 105.3 | 106.8 | 108.4 | 109.5 | 109.7 | 109.1 | 107.7 | 105.8 | 103.7 | 101.6 | 99.9 | 136.3 |
| 12500 | 105.5 | 105.7 | 105.9 | 106.0 | 106.0 | 105.9 | 106.3 | 107.3 | 108.4 | 109.1 | 109.0 | 108.4 | 107.3 | 106.1 | 105.0 | 136.5 |
| 16000 | 102.8 | 103.1 | 103.5 | 104.0 | 104.5 | 104.9 | 105.2 | 105.6 | 106.2 | 107.0 | 107.5 | 107.7 | 107.4 | 106.8 | 106.2 | 135.3 |
| 20000 | 101.0 | 101.2 | 101.5 | 101.9 | 102.5 | 103.2 | 103.9 | 104.5 | 105.1 | 105.7 | 106.3 | 106.7 | 106.8 | 106.6 | 106.3 | 134.4 |
| 25000 | 99.8 | 99.9 | 100.1 | 100.4 | 100.8 | 101.3 | 102.1 | 102.9 | 103.7 | 104.5 | 105.2 | 105.7 | 105.9 | 106.0 | 105.9 | 133.6 |
| 31500 | 98.4 | 98.5 | 98.7 | 99.0 | 99.3 | 99.7 | 100.3 | 101.0 | 101.9 | 102.8 | 103.7 | 104.3 | 104.8 | 105.0 | 105.0 | 132.6 |
| 40000 | 96.3 | 96.4 | 96.6 | 96.9 | 97.2 | 97.6 | 98.1 | 98.7 | 99.5 | 100.4 | 101.4 | 102.2 | 102.7 | 103.1 | 103.2 | 131.3 |
| 50000 | 94.4 | 94.5 | 94.7 | 94.9 | 95.3 | 95.7 | 96.1 | 96.7 | 97.4 | 98.3 | 99.2 | 100.1 | 100.8 | 101.3 | 101.4 | 130.4 |
| 63000 | 91.9 | 92.0 | 92.2 | 92.4 | 92.7 | 93.1 | 93.5 | 94.0 | 94.7 | 95.5 | 96.5 | 97.3 | 98.2 | 98.7 | 98.8 | 129.3 |
| 80000 | 0.0 | 0.0 | 0.0 | 0.0 | 0.0 | 0.0 | 0.0 | 0.0 | 0.0 | 0.0 | 0.0 | 0.0 | 0.0 | 0.0 | 0.0 | 28.9 |
| OVERALL | 116.3 | 116.3 | 116.3 | 116.3 | 116.2 | 116.2 | 116.1 | 116.0 | 115.8 | 115.6 | 115.4 | 115.0 | 114.6 | 114.2 | 113.8 | 145.3 |
| PNL | 125.7 | 125.2 | 124.9 | 124.8 | 124.3 | 123.3 | 121.6 | 120.0 | 118.3 | 115.9 | 113.9 | 111.7 | 109.4 | 107.2 | 105.5 | |
| PNLT | 132.3 | 128.8 | 128.3 | 127.9 | 126.9 | 125.6 | 122.9 | 121.5 | 120.5 | 117.1 | 114.5 | 112.7 | 110.3 | 108.0 | 106.0 | |

Table B-5. Computational Acoustic Data for Pressure Ratio 2.5 : Shock Noise Component

| ANGLE | 20 | 30 | 40 | 50 | 60 | 70 | 80 | 90 | 100 | 110 | 120 | 130 | 140 | 150 | 160 | PWL |
|---|---|---|---|---|---|---|---|---|---|---|---|---|---|---|---|---|
| FREQ | | | | | | | | | | | | | | | | |
| 50 | 38.8 | 38.8 | 38.9 | 38.9 | 39.0 | 39.1 | 39.3 | 39.5 | 39.8 | 40.2 | 40.6 | 41.0 | 41.6 | 42.7 | 44.3 | 69.1 |
| 63 | 44.4 | 44.4 | 44.4 | 44.5 | 44.6 | 44.7 | 44.8 | 45.0 | 45.3 | 45.6 | 46.0 | 46.4 | 46.9 | 48.0 | 49.5 | 74.5 |
| 80 | 49.1 | 49.1 | 49.1 | 49.2 | 49.3 | 49.4 | 49.6 | 49.8 | 50.1 | 50.4 | 50.8 | 51.3 | 51.8 | 52.9 | 54.5 | 79.3 |
| 100 | 53.7 | 53.8 | 53.8 | 53.9 | 54.0 | 54.1 | 54.3 | 54.5 | 54.8 | 55.1 | 55.5 | 56.0 | 56.6 | 57.6 | 59.2 | 84.0 |
| 125 | 58.2 | 58.2 | 58.3 | 58.4 | 58.5 | 58.6 | 58.8 | 59.0 | 59.3 | 59.7 | 60.1 | 60.6 | 61.2 | 62.3 | 63.8 | 88.6 |
| 160 | 63.2 | 63.2 | 63.2 | 63.3 | 63.4 | 63.6 | 63.8 | 64.0 | 64.4 | 64.7 | 65.2 | 65.7 | 66.3 | 67.4 | 68.8 | 93.6 |
| 200 | 67.5 | 67.5 | 67.6 | 67.7 | 67.8 | 68.0 | 68.2 | 68.5 | 68.8 | 69.2 | 69.6 | 70.2 | 70.7 | 71.9 | 73.3 | 98.0 |
| 250 | 71.6 | 71.6 | 71.7 | 71.8 | 71.9 | 72.1 | 72.4 | 72.7 | 73.0 | 73.4 | 73.9 | 74.4 | 75.1 | 76.2 | 77.6 | 102.3 |
| 315 | 75.5 | 75.6 | 75.7 | 75.8 | 76.0 | 76.2 | 76.4 | 76.8 | 77.1 | 77.6 | 78.1 | 78.6 | 79.3 | 80.4 | 81.8 | 106.4 |
| 400 | 79.2 | 79.3 | 79.4 | 79.5 | 79.7 | 80.0 | 80.3 | 80.6 | 81.0 | 81.5 | 82.0 | 82.6 | 83.3 | 84.5 | 85.7 | 110.3 |
| 500 | 82.3 | 82.4 | 82.5 | 82.7 | 82.9 | 83.1 | 83.4 | 83.8 | 84.3 | 84.8 | 85.3 | 85.9 | 86.6 | 87.9 | 89.0 | 113.5 |
| 630 | 85.3 | 85.3 | 85.5 | 85.6 | 85.8 | 86.1 | 86.4 | 86.8 | 87.2 | 87.7 | 88.3 | 88.9 | 89.7 | 90.9 | 91.9 | 116.5 |
| 800 | 88.1 | 88.2 | 88.3 | 88.4 | 88.6 | 88.8 | 89.1 | 89.5 | 89.9 | 90.4 | 90.9 | 91.5 | 92.3 | 93.6 | 94.3 | 119.2 |
| 1000 | 90.5 | 90.6 | 90.7 | 90.8 | 91.0 | 91.2 | 91.5 | 91.8 | 92.2 | 92.7 | 93.1 | 93.7 | 94.5 | 95.8 | 96.2 | 121.4 |
| 1250 | 92.6 | 92.7 | 92.8 | 93.0 | 93.2 | 93.4 | 93.7 | 94.0 | 94.3 | 94.7 | 95.2 | 95.7 | 96.5 | 97.7 | 97.9 | 123.5 |
| 1600 | 94.6 | 94.7 | 94.8 | 95.0 | 95.2 | 95.5 | 95.8 | 96.1 | 96.4 | 96.8 | 97.2 | 97.6 | 98.5 | 99.5 | 99.4 | 125.5 |
| 2000 | 95.9 | 96.0 | 96.2 | 96.4 | 96.7 | 97.0 | 97.3 | 97.6 | 98.0 | 98.3 | 98.7 | 99.1 | 100.1 | 100.9 | 100.5 | 126.9 |
| 2500 | 96.6 | 96.8 | 97.1 | 97.4 | 97.7 | 98.1 | 98.5 | 98.8 | 99.2 | 99.6 | 100.0 | 100.4 | 101.5 | 101.9 | 101.2 | 128.1 |
| 3150 | 97.0 | 97.2 | 97.5 | 97.8 | 98.2 | 98.7 | 99.2 | 99.6 | 100.1 | 100.5 | 100.9 | 101.4 | 102.5 | 102.6 | 101.6 | 128.8 |
| 4000 | 102.7 | 101.5 | 100.1 | 99.0 | 98.6 | 98.9 | 99.4 | 99.9 | 100.5 | 101.0 | 101.4 | 102.0 | 103.0 | 102.8 | 101.5 | 129.6 |
| 5000 | 111.7 | 111.1 | 110.1 | 108.5 | 106.4 | 103.8 | 101.6 | 100.5 | 100.6 | 101.0 | 101.5 | 102.1 | 103.1 | 102.7 | 101.2 | 134.4 |
| 6300 | 111.0 | 111.5 | 111.9 | 112.0 | 111.7 | 110.8 | 109.1 | 106.8 | 104.3 | 102.5 | 101.8 | 102.0 | 102.8 | 102.2 | 100.5 | 137.4 |
| 8000 | 104.5 | 105.4 | 106.7 | 108.2 | 109.7 | 110.6 | 110.9 | 110.4 | 109.0 | 107.1 | 105.1 | 103.7 | 103.2 | 102.0 | 100.2 | 137.0 |
| 10000 | 105.9 | 105.7 | 105.3 | 105.2 | 105.7 | 107.1 | 108.7 | 109.7 | 110.0 | 109.5 | 108.4 | 107.0 | 105.7 | 104.1 | 102.4 | 136.5 |
| 12500 | 105.7 | 105.9 | 106.1 | 106.2 | 106.3 | 106.3 | 106.7 | 107.7 | 108.8 | 109.4 | 109.4 | 108.9 | 108.1 | 106.9 | 105.8 | 136.5 |
| 16000 | 103.1 | 103.4 | 103.8 | 104.3 | 104.8 | 105.3 | 105.6 | 106.0 | 106.6 | 107.4 | 108.0 | 108.2 | 108.0 | 107.4 | 106.7 | 135.2 |
| 20000 | 101.4 | 101.5 | 101.8 | 102.2 | 102.8 | 103.5 | 104.2 | 104.9 | 105.5 | 106.1 | 106.7 | 107.1 | 107.3 | 107.1 | 106.7 | 134.0 |
| 25000 | 100.1 | 100.3 | 100.5 | 100.8 | 101.2 | 101.7 | 102.4 | 103.3 | 104.1 | 104.9 | 105.6 | 106.1 | 106.4 | 106.3 | 106.1 | 132.7 |
| 31500 | 98.7 | 98.8 | 99.0 | 99.3 | 99.7 | 100.1 | 100.7 | 101.4 | 102.3 | 103.2 | 104.0 | 104.7 | 105.2 | 105.3 | 105.2 | 131.2 |
| 40000 | 96.6 | 96.7 | 96.9 | 97.2 | 97.5 | 98.0 | 98.5 | 99.1 | 99.9 | 100.8 | 101.7 | 102.5 | 103.1 | 103.4 | 103.4 | 129.1 |
| 50000 | 94.6 | 94.8 | 95.0 | 95.3 | 95.6 | 96.0 | 96.5 | 97.1 | 97.8 | 98.7 | 99.6 | 100.5 | 101.2 | 101.6 | 101.6 | 127.1 |
| 63000 | 92.1 | 92.2 | 92.4 | 92.7 | 93.0 | 93.4 | 93.9 | 94.4 | 95.1 | 95.9 | 96.8 | 97.7 | 98.6 | 99.0 | 99.0 | 124.4 |
| 80000 | 74.2 | 74.6 | 75.2 | 75.9 | 76.7 | 77.6 | 78.6 | 79.6 | 80.5 | 81.4 | 82.2 | 83.0 | 83.9 | 83.2 | 81.5 | 109.1 |
| OVERALL | 116.8 | 116.8 | 116.8 | 116.8 | 116.8 | 116.8 | 116.8 | 116.9 | 116.8 | 116.8 | 116.8 | 116.7 | 116.8 | 116.4 | 115.8 | 145.6 |
| PNL | 128.5 | 128.1 | 128.0 | 128.1 | 127.9 | 127.3 | 126.5 | 125.6 | 124.9 | 124.0 | 123.7 | 124.0 | 124.8 | 124.8 | 123.8 | |
| PNLT | 130.3 | 130.9 | 130.6 | 130.2 | 129.2 | 127.9 | 126.5 | 125.6 | 124.9 | 124.0 | 123.7 | 124.0 | 124.8 | 124.8 | 123.8 | |

Table B-6. Computational Acoustic Data for Pressure Ratio 2.5 : Total Noise Levels

| ANGLE | 20 | 30 | 40 | 50 | 60 | 70 | 80 | 90 | 100 | 110 | 120 | 130 | 140 | 150 | 160 | PWL |
|---|---|---|---|---|---|---|---|---|---|---|---|---|---|---|---|---|
| FREQ | | | | | | | | | | | | | | | | |
| 50 | 38.8 | 38.8 | 38.8 | 38.8 | 38.9 | 38.9 | 39.0 | 39.2 | 39.4 | 39.7 | 40.1 | 40.6 | 41.1 | 42.5 | 44.2 | 69.6 |
| 63 | 43.8 | 43.8 | 43.8 | 43.8 | 43.8 | 43.9 | 44.0 | 44.2 | 44.4 | 44.7 | 45.1 | 45.5 | 46.1 | 47.4 | 49.1 | 74.5 |
| 80 | 48.9 | 48.9 | 48.9 | 48.9 | 49.0 | 49.0 | 49.1 | 49.3 | 49.6 | 49.9 | 50.2 | 50.7 | 51.3 | 52.6 | 54.2 | 79.7 |
| 100 | 53.6 | 53.6 | 53.6 | 53.6 | 53.7 | 53.8 | 53.9 | 54.1 | 54.3 | 54.6 | 55.0 | 55.4 | 56.0 | 57.3 | 59.0 | 84.4 |
| 125 | 58.3 | 58.3 | 58.3 | 58.3 | 58.4 | 58.5 | 58.6 | 58.8 | 59.0 | 59.3 | 59.7 | 60.2 | 60.8 | 62.1 | 63.7 | 89.1 |
| 160 | 63.3 | 63.3 | 63.4 | 63.4 | 63.5 | 63.6 | 63.7 | 63.9 | 64.2 | 64.5 | 64.9 | 65.3 | 65.9 | 67.2 | 68.8 | 94.3 |
| 200 | 67.8 | 67.8 | 67.8 | 67.9 | 67.9 | 68.1 | 68.2 | 68.4 | 68.7 | 69.0 | 69.4 | 69.9 | 70.5 | 71.8 | 73.3 | 98.8 |
| 250 | 72.0 | 72.0 | 72.1 | 72.1 | 72.2 | 72.4 | 72.5 | 72.8 | 73.0 | 73.4 | 73.8 | 74.3 | 74.9 | 76.2 | 77.7 | 103.1 |
| 315 | 76.1 | 76.2 | 76.2 | 76.3 | 76.4 | 76.6 | 76.8 | 77.0 | 77.3 | 77.7 | 78.2 | 78.7 | 79.3 | 80.6 | 82.0 | 107.4 |
| 400 | 80.0 | 80.1 | 80.1 | 80.3 | 80.4 | 80.6 | 80.8 | 81.1 | 81.5 | 81.9 | 82.3 | 82.9 | 83.6 | 84.9 | 86.1 | 111.5 |
| 500 | 83.3 | 83.3 | 83.4 | 83.6 | 83.8 | 84.0 | 84.2 | 84.6 | 84.9 | 85.4 | 85.9 | 86.4 | 87.2 | 88.5 | 89.7 | 115.0 |
| 630 | 86.3 | 86.4 | 86.5 | 86.6 | 86.8 | 87.1 | 87.4 | 87.7 | 88.1 | 88.6 | 89.1 | 89.7 | 90.5 | 91.9 | 92.8 | 118.2 |
| 800 | 89.2 | 89.2 | 89.4 | 89.5 | 89.7 | 89.9 | 90.2 | 90.5 | 91.0 | 91.4 | 92.0 | 92.6 | 93.4 | 94.8 | 95.5 | 121.0 |
| 1000 | 91.6 | 91.7 | 91.8 | 91.9 | 92.1 | 92.3 | 92.6 | 92.9 | 93.3 | 93.7 | 94.3 | 94.8 | 95.8 | 97.0 | 97.5 | 123.4 |
| 1250 | 93.7 | 93.8 | 93.9 | 94.1 | 94.3 | 94.5 | 94.8 | 95.1 | 95.4 | 95.8 | 96.3 | 96.8 | 97.8 | 98.9 | 99.1 | 125.4 |
| 1600 | 95.7 | 95.8 | 95.9 | 96.1 | 96.3 | 96.6 | 96.9 | 97.2 | 97.5 | 97.8 | 98.3 | 98.7 | 99.8 | 100.7 | 100.5 | 127.4 |
| 2000 | 97.0 | 97.1 | 97.3 | 97.5 | 97.8 | 98.1 | 98.4 | 98.7 | 99.1 | 99.4 | 99.8 | 100.3 | 101.4 | 102.0 | 101.4 | 128.9 |
| 2500 | 97.8 | 98.0 | 98.2 | 98.5 | 98.9 | 99.2 | 99.6 | 100.0 | 100.3 | 100.7 | 101.1 | 101.5 | 102.7 | 103.0 | 102.1 | 130.0 |
| 3150 | 98.1 | 98.3 | 98.6 | 99.0 | 99.4 | 99.9 | 100.3 | 100.8 | 101.2 | 101.6 | 102.0 | 102.5 | 103.6 | 103.5 | 102.3 | 130.8 |
| 4000 | 97.9 | 98.2 | 98.5 | 99.0 | 99.5 | 100.0 | 100.6 | 101.1 | 101.7 | 102.1 | 102.6 | 103.1 | 104.2 | 103.7 | 102.1 | 131.1 |
| 5000 | 97.4 | 97.7 | 98.1 | 98.5 | 99.1 | 99.7 | 100.4 | 101.0 | 101.6 | 102.2 | 102.7 | 103.3 | 104.2 | 103.4 | 101.6 | 131.0 |
| 6300 | 96.6 | 96.9 | 97.3 | 97.8 | 98.4 | 99.1 | 99.8 | 100.5 | 101.2 | 101.8 | 102.4 | 103.1 | 103.8 | 102.7 | 100.7 | 130.6 |
| 8000 | 95.7 | 96.0 | 96.4 | 96.9 | 97.5 | 98.1 | 98.9 | 99.6 | 100.4 | 101.1 | 101.7 | 102.5 | 103.0 | 101.8 | 99.7 | 129.8 |
| 10000 | 94.8 | 95.0 | 95.4 | 95.9 | 96.5 | 97.2 | 97.9 | 98.7 | 99.4 | 100.1 | 100.8 | 101.6 | 102.1 | 100.7 | 98.7 | 129.0 |
| 12500 | 93.7 | 94.0 | 94.4 | 94.9 | 95.5 | 96.2 | 96.9 | 97.6 | 98.4 | 99.1 | 99.7 | 100.6 | 101.0 | 99.7 | 97.7 | 128.0 |
| 16000 | 92.5 | 92.8 | 93.2 | 93.7 | 94.2 | 94.9 | 95.6 | 96.4 | 97.1 | 97.8 | 98.4 | 99.3 | 99.7 | 98.4 | 96.5 | 127.0 |
| 20000 | 91.3 | 91.6 | 92.0 | 92.4 | 93.0 | 93.7 | 94.4 | 95.1 | 95.9 | 96.6 | 97.2 | 98.0 | 98.4 | 97.2 | 95.3 | 126.0 |
| 25000 | 90.1 | 90.4 | 90.8 | 91.2 | 91.8 | 92.4 | 93.1 | 93.8 | 94.5 | 95.2 | 95.8 | 96.6 | 97.0 | 95.8 | 94.0 | 125.0 |
| 31500 | 88.6 | 88.9 | 89.3 | 89.8 | 90.3 | 91.0 | 91.6 | 92.3 | 93.0 | 93.6 | 94.2 | 95.1 | 95.4 | 94.3 | 92.6 | 124.0 |
| 40000 | 86.1 | 86.4 | 86.9 | 87.5 | 88.2 | 89.0 | 89.8 | 90.5 | 91.2 | 91.9 | 92.4 | 93.2 | 93.6 | 92.6 | 90.9 | 123.0 |
| 50000 | 83.0 | 83.4 | 83.9 | 84.6 | 85.4 | 86.3 | 87.2 | 88.1 | 89.0 | 89.8 | 90.4 | 91.2 | 91.6 | 90.5 | 88.8 | 121.8 |
| 63000 | 79.0 | 79.5 | 80.0 | 80.7 | 81.6 | 82.5 | 83.6 | 84.6 | 85.7 | 86.6 | 87.4 | 88.4 | 88.8 | 87.6 | 85.8 | 120.1 |
| 80000 | 73.9 | 74.4 | 75.0 | 75.8 | 76.7 | 77.7 | 78.8 | 80.0 | 81.1 | 82.2 | 83.1 | 84.2 | 84.7 | 83.4 | 81.5 | 118.0 |
| OVERALL | 107.6 | 107.8 | 108.1 | 108.5 | 109.0 | 109.5 | 110.0 | 110.6 | 111.2 | 111.7 | 112.2 | 112.9 | 113.7 | 113.2 | 112.0 | 140.9 |
| PNL | 119.9 | 120.1 | 120.4 | 120.7 | 121.2 | 121.6 | 122.1 | 122.7 | 123.2 | 123.7 | 124.1 | 124.7 | 125.6 | 125.4 | 124.3 | |
| PNLT | 119.9 | 120.1 | 120.4 | 120.7 | 121.2 | 121.6 | 122.1 | 122.7 | 123.2 | 123.7 | 124.1 | 124.7 | 125.6 | 125.4 | 124.3 | |

Table B-7. Computational Acoustic Data for Pressure ratio 3.0 : Mixing Noise Component

| ANGLE | 20 | 30 | 40 | 50 | 60 | 70 | 80 | 90 | 100 | 110 | 120 | 130 | 140 | 150 | 160 | PWL |
|---|---|---|---|---|---|---|---|---|---|---|---|---|---|---|---|---|
| FREQ | | | | | | | | | | | | | | | | |
| 50 | 0.0 | 0.0 | 0.0 | 0.0 | 0.0 | 0.0 | 0.0 | 0.0 | 0.0 | 0.0 | 0.0 | 0.0 | 0.0 | 0.0 | 0.0 | 29.7 |
| 63 | 35.8 | 35.8 | 35.8 | 35.8 | 35.8 | 35.8 | 35.8 | 35.8 | 35.8 | 35.8 | 35.8 | 35.8 | 35.8 | 35.8 | 35.8 | 65.4 |
| 80 | 36.5 | 36.5 | 36.5 | 36.5 | 36.5 | 36.5 | 36.5 | 36.5 | 36.5 | 36.5 | 36.5 | 36.5 | 36.5 | 36.5 | 36.5 | 66.1 |
| 100 | 40.6 | 40.6 | 40.6 | 40.6 | 40.6 | 40.6 | 40.6 | 40.6 | 40.6 | 40.6 | 40.6 | 40.6 | 40.6 | 40.6 | 40.6 | 70.2 |
| 125 | 38.9 | 38.9 | 38.9 | 38.9 | 38.9 | 38.9 | 38.9 | 38.9 | 38.9 | 38.9 | 38.9 | 38.9 | 38.9 | 38.9 | 38.9 | 68.6 |
| 160 | 39.5 | 39.5 | 39.5 | 39.5 | 39.5 | 39.5 | 39.5 | 39.5 | 39.5 | 39.5 | 39.5 | 39.5 | 39.5 | 39.5 | 39.5 | 69.2 |
| 200 | 40.5 | 40.5 | 40.5 | 40.5 | 40.5 | 40.5 | 40.5 | 40.5 | 40.5 | 40.5 | 40.5 | 40.5 | 40.5 | 40.5 | 40.5 | 70.1 |
| 250 | 41.6 | 41.6 | 41.6 | 41.6 | 41.6 | 41.6 | 41.6 | 41.6 | 41.6 | 41.6 | 41.6 | 41.6 | 41.6 | 41.6 | 41.6 | 71.3 |
| 315 | 42.8 | 42.8 | 42.8 | 42.8 | 42.8 | 42.8 | 42.8 | 42.8 | 42.8 | 42.8 | 42.8 | 42.8 | 42.8 | 42.8 | 42.8 | 72.4 |
| 400 | 43.5 | 43.5 | 43.5 | 43.5 | 43.5 | 43.5 | 43.5 | 43.5 | 43.5 | 43.5 | 43.5 | 43.5 | 43.5 | 43.5 | 43.5 | 73.1 |
| 500 | 44.6 | 44.6 | 44.6 | 44.6 | 44.6 | 44.6 | 44.6 | 44.6 | 44.6 | 44.6 | 44.6 | 44.6 | 44.6 | 44.6 | 44.6 | 74.3 |
| 630 | 45.8 | 45.8 | 45.8 | 45.8 | 45.8 | 45.8 | 45.8 | 45.8 | 45.8 | 45.8 | 45.8 | 45.8 | 45.8 | 45.8 | 45.8 | 75.4 |
| 800 | 46.5 | 46.5 | 46.5 | 46.5 | 46.5 | 46.5 | 46.5 | 46.5 | 46.5 | 46.5 | 46.5 | 46.5 | 46.5 | 46.5 | 46.5 | 76.1 |
| 1000 | 47.4 | 47.4 | 47.4 | 47.4 | 47.4 | 47.4 | 47.4 | 47.4 | 47.4 | 47.4 | 47.4 | 47.4 | 47.4 | 47.4 | 47.4 | 77.1 |
| 1250 | 48.9 | 48.9 | 48.9 | 48.9 | 48.9 | 48.9 | 48.9 | 48.9 | 48.9 | 48.9 | 48.9 | 48.9 | 48.9 | 48.9 | 48.9 | 78.6 |
| 1600 | 49.5 | 49.5 | 49.5 | 49.5 | 49.5 | 49.5 | 49.5 | 49.5 | 49.5 | 49.5 | 49.5 | 49.5 | 49.5 | 49.5 | 49.5 | 79.2 |
| 2000 | 50.4 | 50.4 | 50.4 | 50.4 | 50.4 | 50.4 | 50.4 | 50.4 | 50.4 | 50.4 | 50.4 | 50.4 | 50.4 | 50.4 | 50.4 | 80.1 |
| 2500 | 74.1 | 70.3 | 64.8 | 58.0 | 52.5 | 51.6 | 51.6 | 51.6 | 51.6 | 51.6 | 51.6 | 51.6 | 51.6 | 51.6 | 51.6 | 91.8 |
| 3150 | 102.2 | 100.4 | 97.7 | 93.9 | 88.7 | 82.1 | 74.0 | 64.6 | 55.6 | 52.7 | 52.7 | 52.7 | 52.7 | 52.7 | 52.7 | 121.7 |
| 4000 | 109.5 | 109.2 | 108.4 | 107.0 | 104.7 | 101.4 | 96.8 | 91.1 | 84.2 | 76.4 | 68.1 | 60.2 | 54.7 | 53.4 | 53.4 | 132.3 |
| 5000 | 106.3 | 107.3 | 108.2 | 108.9 | 109.0 | 108.4 | 106.7 | 103.9 | 100.1 | 95.3 | 89.8 | 84.1 | 78.5 | 73.5 | 69.6 | 134.9 |
| 6300 | 99.6 | 100.0 | 101.3 | 103.4 | 105.6 | 107.4 | 108.2 | 108.0 | 106.7 | 104.4 | 101.2 | 97.6 | 93.8 | 90.3 | 87.5 | 134.6 |
| 8000 | 103.2 | 103.0 | 102.5 | 101.7 | 101.3 | 102.3 | 104.4 | 106.2 | 107.0 | 106.7 | 105.4 | 103.4 | 101.1 | 98.8 | 96.8 | 134.0 |
| 10000 | 101.8 | 102.1 | 102.4 | 102.7 | 102.7 | 102.5 | 102.4 | 103.2 | 104.7 | 105.8 | 106.0 | 105.4 | 104.3 | 102.9 | 101.6 | 133.8 |
| 12500 | 100.0 | 100.3 | 100.7 | 101.3 | 101.9 | 102.4 | 102.7 | 103.0 | 103.4 | 104.3 | 105.2 | 105.5 | 105.3 | 104.7 | 104.0 | 133.4 |
| 16000 | 98.0 | 98.2 | 98.4 | 98.7 | 99.2 | 100.0 | 100.8 | 101.5 | 102.1 | 102.7 | 103.4 | 103.9 | 104.1 | 104.0 | 103.8 | 132.0 |
| 20000 | 96.8 | 96.9 | 97.1 | 97.4 | 97.7 | 98.2 | 98.9 | 99.7 | 100.7 | 101.5 | 102.2 | 102.8 | 103.2 | 103.3 | 103.2 | 131.0 |
| 25000 | 95.6 | 95.7 | 95.9 | 96.2 | 96.5 | 96.9 | 97.4 | 98.1 | 99.0 | 100.0 | 100.9 | 101.7 | 102.2 | 102.4 | 102.5 | 130.1 |
| 31500 | 94.1 | 94.3 | 94.5 | 94.7 | 95.1 | 95.4 | 95.9 | 96.5 | 97.3 | 98.2 | 99.2 | 100.2 | 100.8 | 101.3 | 101.5 | 129.2 |
| 40000 | 92.0 | 92.2 | 92.4 | 92.6 | 93.0 | 93.3 | 93.8 | 94.4 | 95.0 | 95.9 | 96.9 | 97.9 | 98.7 | 99.2 | 99.5 | 127.9 |
| 50000 | 90.1 | 90.3 | 90.5 | 90.7 | 91.0 | 91.4 | 91.9 | 92.4 | 93.1 | 93.9 | 94.8 | 95.9 | 96.7 | 97.3 | 97.7 | 127.0 |
| 63000 | 87.6 | 87.8 | 88.0 | 88.2 | 88.5 | 88.9 | 89.4 | 89.8 | 90.5 | 91.1 | 92.1 | 93.1 | 94.1 | 94.7 | 95.0 | 125.9 |
| 80000 | 0.0 | 0.0 | 0.0 | 0.0 | 0.0 | 0.0 | 0.0 | 0.0 | 0.0 | 0.0 | 0.0 | 0.0 | 0.0 | 0.0 | 0.0 | 29.7 |
| OVERALL | 113.5 | 113.5 | 113.5 | 113.5 | 113.4 | 113.4 | 113.3 | 113.2 | 113.1 | 113.0 | 112.8 | 112.5 | 112.2 | 111.8 | 111.5 | 143.2 |
| PNL | 125.1 | 124.8 | 124.2 | 123.8 | 123.6 | 122.9 | 121.9 | 121.3 | 119.9 | 117.8 | 115.7 | 113.6 | 111.3 | 109.6 | 108.1 | |
| PNLT | 127.8 | 131.5 | 130.7 | 127.1 | 127.0 | 125.4 | 123.3 | 124.1 | 122.0 | 119.1 | 117.3 | 114.5 | 112.7 | 110.1 | 108.1 | |

Table B-8. Computational Acoustic Data for Pressure Ratio 3.0 : Shock Noise Component

| ANGLE | 20 | 30 | 40 | 50 | 60 | 70 | 80 | 90 | 100 | 110 | 120 | 130 | 140 | 150 | 160 | PWL |
|---|---|---|---|---|---|---|---|---|---|---|---|---|---|---|---|---|
| FREQ | | | | | | | | | | | | | | | | |
| 50 | 38.8 | 38.8 | 38.8 | 38.8 | 38.9 | 38.9 | 39.0 | 39.2 | 39.4 | 39.7 | 40.1 | 40.6 | 41.1 | 42.5 | 44.2 | 69.6 |
| 63 | 44.4 | 44.4 | 44.4 | 44.4 | 44.5 | 44.5 | 44.6 | 44.8 | 45.0 | 45.2 | 45.6 | 46.0 | 46.5 | 47.7 | 49.3 | 75.0 |
| 80 | 49.1 | 49.1 | 49.1 | 49.1 | 49.2 | 49.3 | 49.4 | 49.5 | 49.8 | 50.1 | 50.4 | 50.8 | 51.4 | 52.7 | 54.3 | 79.9 |
| 100 | 53.8 | 53.8 | 53.8 | 53.8 | 53.9 | 54.0 | 54.1 | 54.3 | 54.5 | 54.8 | 55.2 | 55.6 | 56.1 | 57.4 | 59.0 | 84.6 |
| 125 | 58.3 | 58.3 | 58.3 | 58.4 | 58.4 | 58.5 | 58.6 | 58.8 | 59.1 | 59.4 | 59.8 | 60.2 | 60.8 | 62.1 | 63.7 | 89.2 |
| 160 | 63.3 | 63.4 | 63.4 | 63.4 | 63.5 | 63.6 | 63.7 | 63.9 | 64.2 | 64.5 | 64.9 | 65.3 | 65.9 | 67.2 | 68.8 | 94.3 |
| 200 | 67.8 | 67.8 | 67.8 | 67.9 | 67.9 | 68.1 | 68.2 | 68.4 | 68.7 | 69.0 | 69.4 | 69.9 | 70.5 | 71.8 | 73.3 | 98.8 |
| 250 | 72.0 | 72.0 | 72.1 | 72.1 | 72.2 | 72.4 | 72.5 | 72.8 | 73.1 | 73.4 | 73.8 | 74.3 | 74.9 | 76.2 | 77.7 | 103.1 |
| 315 | 76.1 | 76.2 | 76.2 | 76.3 | 76.4 | 76.6 | 76.8 | 77.0 | 77.3 | 77.7 | 78.2 | 78.7 | 79.3 | 80.6 | 82.0 | 107.4 |
| 400 | 80.0 | 80.1 | 80.1 | 80.3 | 80.4 | 80.6 | 80.8 | 81.1 | 81.5 | 81.9 | 82.3 | 82.9 | 83.6 | 84.9 | 86.1 | 111.5 |
| 500 | 83.3 | 83.3 | 83.4 | 83.6 | 83.8 | 84.0 | 84.2 | 84.6 | 84.9 | 85.4 | 85.9 | 86.4 | 87.2 | 88.5 | 89.7 | 115.0 |
| 630 | 86.3 | 86.4 | 86.5 | 86.6 | 86.8 | 87.1 | 87.4 | 87.7 | 88.1 | 88.6 | 89.1 | 89.7 | 90.5 | 91.9 | 92.8 | 118.2 |
| 800 | 89.2 | 89.2 | 89.4 | 89.5 | 89.7 | 89.9 | 90.2 | 90.5 | 91.0 | 91.4 | 92.0 | 92.6 | 93.4 | 94.8 | 95.5 | 121.0 |
| 1000 | 91.6 | 91.7 | 91.8 | 91.9 | 92.1 | 92.3 | 92.6 | 92.9 | 93.3 | 93.7 | 94.3 | 94.8 | 95.8 | 97.0 | 97.5 | 123.3 |
| 1250 | 93.7 | 93.8 | 93.9 | 94.1 | 94.3 | 94.5 | 94.8 | 95.1 | 95.4 | 95.8 | 96.3 | 96.8 | 97.8 | 98.9 | 99.1 | 125.4 |
| 1600 | 95.7 | 95.8 | 95.9 | 96.1 | 96.3 | 96.6 | 96.9 | 97.2 | 97.5 | 97.9 | 98.3 | 98.7 | 99.8 | 100.7 | 100.5 | 127.4 |
| 2000 | 97.0 | 97.1 | 97.3 | 97.5 | 97.8 | 98.1 | 98.4 | 98.7 | 99.1 | 99.4 | 99.8 | 100.3 | 101.4 | 102.0 | 101.4 | 128.8 |
| 2500 | 97.8 | 98.0 | 98.2 | 98.5 | 98.9 | 99.2 | 99.6 | 100.0 | 100.3 | 100.7 | 101.1 | 101.5 | 102.7 | 103.0 | 102.1 | 130.0 |
| 3150 | 103.6 | 102.5 | 101.2 | 100.2 | 99.8 | 99.9 | 100.3 | 100.8 | 101.2 | 101.6 | 102.0 | 102.5 | 103.6 | 103.5 | 102.3 | 131.2 |
| 4000 | 109.8 | 109.5 | 108.8 | 107.6 | 105.8 | 103.8 | 102.1 | 101.6 | 101.7 | 102.2 | 102.6 | 103.1 | 104.2 | 103.7 | 102.1 | 134.7 |
| 5000 | 106.9 | 107.7 | 108.6 | 109.3 | 109.5 | 108.9 | 107.6 | 105.7 | 103.9 | 103.0 | 102.9 | 103.4 | 104.2 | 103.4 | 101.6 | 136.3 |
| 6300 | 101.4 | 101.7 | 102.7 | 104.5 | 106.4 | 108.0 | 108.8 | 108.7 | 107.8 | 106.3 | 104.8 | 104.2 | 104.2 | 103.0 | 100.9 | 135.9 |
| 8000 | 103.9 | 103.8 | 103.4 | 103.0 | 102.8 | 103.7 | 105.4 | 107.0 | 107.8 | 107.7 | 107.0 | 106.0 | 105.2 | 103.5 | 101.5 | 135.2 |
| 10000 | 102.6 | 102.9 | 103.2 | 103.5 | 103.7 | 103.6 | 103.7 | 104.5 | 105.8 | 106.8 | 107.2 | 106.9 | 106.3 | 105.0 | 103.4 | 134.7 |
| 12500 | 100.9 | 101.2 | 101.6 | 102.2 | 102.8 | 103.3 | 103.7 | 104.1 | 104.6 | 105.5 | 106.3 | 106.7 | 106.6 | 105.9 | 104.9 | 134.2 |
| 16000 | 99.1 | 99.3 | 99.5 | 99.9 | 100.4 | 101.1 | 101.9 | 102.7 | 103.3 | 103.9 | 104.6 | 105.2 | 105.5 | 105.1 | 104.5 | 132.6 |
| 20000 | 97.9 | 98.0 | 98.3 | 98.6 | 99.0 | 99.5 | 100.2 | 101.0 | 101.9 | 102.7 | 103.4 | 104.1 | 104.4 | 104.2 | 103.9 | 131.4 |
| 25000 | 96.7 | 96.8 | 97.1 | 97.4 | 97.7 | 98.2 | 98.8 | 99.5 | 100.3 | 101.2 | 102.1 | 102.9 | 103.3 | 103.3 | 103.1 | 130.1 |
| 31500 | 95.2 | 95.4 | 95.6 | 95.9 | 96.3 | 96.8 | 97.3 | 97.9 | 98.7 | 99.5 | 100.4 | 101.3 | 101.9 | 102.1 | 102.0 | 128.6 |
| 40000 | 93.0 | 93.2 | 93.5 | 93.8 | 94.2 | 94.7 | 95.2 | 95.9 | 96.6 | 97.3 | 98.2 | 99.2 | 99.9 | 100.1 | 100.1 | 126.5 |
| 50000 | 90.9 | 91.1 | 91.3 | 91.7 | 92.1 | 92.6 | 93.2 | 93.8 | 94.5 | 95.3 | 96.2 | 97.1 | 97.9 | 98.2 | 98.2 | 124.5 |
| 63000 | 88.1 | 88.4 | 88.6 | 89.0 | 89.3 | 89.8 | 90.4 | 91.0 | 91.7 | 92.5 | 93.4 | 94.4 | 95.2 | 95.5 | 95.5 | 121.7 |
| 80000 | 73.9 | 74.4 | 75.0 | 75.8 | 76.7 | 77.7 | 78.8 | 80.0 | 81.1 | 82.2 | 83.1 | 84.2 | 84.7 | 83.4 | 81.5 | 110.5 |
| OVERALL | 114.5 | 114.5 | 114.6 | 114.7 | 114.8 | 114.9 | 115.0 | 115.1 | 115.3 | 115.4 | 115.5 | 115.7 | 116.0 | 115.6 | 114.7 | 144.8 |
| PNL | 127.9 | 127.7 | 127.4 | 127.2 | 127.3 | 127.0 | 126.5 | 126.5 | 126.1 | 125.5 | 124.9 | 125.2 | 125.9 | 125.7 | 124.6 | |
| PNLT | 129.4 | 129.2 | 128.7 | 129.2 | 129.0 | 128.1 | 126.5 | 126.5 | 126.1 | 125.5 | 124.9 | 125.2 | 125.9 | 125.7 | 124.6 | |

Table B-9. Computational Acoustic Data for Pressure Ratio 3.0 : Total Noise Levels

| ANGLE | 20 | 30 | 40 | 50 | 60 | 70 | 80 | 90 | 100 | 110 | 120 | 130 | 140 | 150 | 160 | PWL |
|---|---|---|---|---|---|---|---|---|---|---|---|---|---|---|---|---|
| FREQ | | | | | | | | | | | | | | | | |
| 50 | 38.4 | 38.4 | 38.3 | 38.3 | 38.3 | 38.3 | 38.4 | 38.4 | 38.6 | 38.8 | 39.1 | 39.5 | 40.1 | 41.7 | 43.5 | 69.6 |
| 63 | 43.4 | 43.3 | 43.3 | 43.3 | 43.3 | 43.3 | 43.3 | 43.4 | 43.6 | 43.8 | 44.1 | 44.5 | 45.1 | 46.7 | 48.5 | 74.6 |
| 80 | 48.5 | 48.5 | 48.4 | 48.4 | 48.4 | 48.4 | 48.5 | 48.6 | 48.7 | 49.0 | 49.3 | 49.6 | 50.3 | 51.8 | 53.6 | 79.8 |
| 100 | 53.3 | 53.2 | 53.2 | 53.2 | 53.2 | 53.2 | 53.3 | 53.4 | 53.5 | 53.7 | 54.0 | 54.4 | 55.1 | 56.6 | 58.3 | 84.5 |
| 125 | 58.0 | 58.0 | 57.9 | 57.9 | 57.9 | 57.9 | 58.0 | 58.1 | 58.3 | 58.5 | 58.8 | 59.2 | 59.8 | 61.4 | 63.1 | 89.3 |
| 160 | 63.1 | 63.1 | 63.1 | 63.1 | 63.1 | 63.1 | 63.2 | 63.3 | 63.4 | 63.7 | 64.0 | 64.4 | 65.0 | 66.6 | 68.2 | 94.4 |
| 200 | 67.6 | 67.6 | 67.6 | 67.6 | 67.6 | 67.7 | 67.7 | 67.9 | 68.0 | 68.3 | 68.6 | 69.0 | 69.7 | 71.2 | 72.8 | 99.0 |
| 250 | 72.0 | 72.0 | 72.0 | 72.0 | 72.1 | 72.1 | 72.2 | 72.3 | 72.5 | 72.8 | 73.1 | 73.5 | 74.2 | 75.7 | 77.2 | 103.5 |
| 315 | 76.3 | 76.3 | 76.3 | 76.4 | 76.4 | 76.5 | 76.6 | 76.8 | 77.0 | 77.3 | 77.6 | 78.1 | 78.7 | 80.2 | 81.6 | 107.9 |
| 400 | 80.4 | 80.5 | 80.5 | 80.6 | 80.6 | 80.7 | 80.9 | 81.1 | 81.3 | 81.6 | 82.0 | 82.5 | 83.2 | 84.7 | 86.0 | 112.3 |
| 500 | 83.9 | 84.0 | 84.0 | 84.1 | 84.2 | 84.4 | 84.5 | 84.8 | 85.1 | 85.4 | 85.8 | 86.3 | 87.1 | 88.5 | 89.7 | 116.0 |
| 630 | 87.1 | 87.2 | 87.3 | 87.4 | 87.5 | 87.7 | 87.9 | 88.2 | 88.5 | 88.9 | 89.4 | 89.9 | 90.7 | 92.2 | 93.1 | 119.4 |
| 800 | 90.1 | 90.1 | 90.2 | 90.3 | 90.5 | 90.7 | 91.0 | 91.2 | 91.6 | 92.0 | 92.5 | 93.0 | 94.0 | 95.4 | 96.0 | 122.5 |
| 1000 | 92.5 | 92.6 | 92.7 | 92.8 | 93.0 | 93.2 | 93.4 | 93.7 | 94.1 | 94.5 | 95.0 | 95.5 | 96.6 | 97.8 | 98.2 | 125.0 |
| 1250 | 94.7 | 94.7 | 94.9 | 95.0 | 95.2 | 95.4 | 95.6 | 95.9 | 96.2 | 96.6 | 97.1 | 97.6 | 98.7 | 99.8 | 99.9 | 127.1 |
| 1600 | 96.6 | 96.7 | 96.9 | 97.1 | 97.3 | 97.5 | 97.7 | 98.0 | 98.3 | 98.7 | 99.1 | 99.6 | 100.7 | 101.6 | 101.3 | 129.1 |
| 2000 | 98.0 | 98.1 | 98.3 | 98.5 | 98.8 | 99.0 | 99.3 | 99.6 | 99.9 | 100.3 | 100.6 | 101.1 | 102.3 | 102.8 | 102.1 | 130.6 |
| 2500 | 98.8 | 99.0 | 99.2 | 99.5 | 99.8 | 100.2 | 100.5 | 100.9 | 101.2 | 101.6 | 101.9 | 102.4 | 103.5 | 103.7 | 102.6 | 131.7 |
| 3150 | 99.1 | 99.3 | 99.7 | 100.0 | 100.4 | 100.9 | 101.3 | 101.8 | 102.2 | 102.5 | 102.9 | 103.4 | 104.5 | 104.2 | 102.8 | 132.5 |
| 4000 | 98.9 | 99.2 | 99.6 | 100.0 | 100.5 | 101.0 | 101.6 | 102.1 | 102.6 | 103.1 | 103.4 | 104.1 | 105.0 | 104.2 | 102.5 | 132.8 |
| 5000 | 98.4 | 98.7 | 99.1 | 99.6 | 100.1 | 100.8 | 101.4 | 102.0 | 102.6 | 103.2 | 103.6 | 104.3 | 105.0 | 103.9 | 101.9 | 132.8 |
| 6300 | 97.6 | 97.9 | 98.3 | 98.8 | 99.4 | 100.1 | 100.8 | 101.5 | 102.2 | 102.8 | 103.3 | 104.1 | 104.6 | 103.2 | 101.0 | 132.3 |
| 8000 | 96.7 | 97.0 | 97.4 | 97.9 | 98.5 | 99.2 | 99.9 | 100.6 | 101.4 | 102.1 | 102.6 | 103.5 | 103.7 | 102.2 | 100.0 | 131.5 |
| 10000 | 95.7 | 96.0 | 96.4 | 96.9 | 97.5 | 98.2 | 98.9 | 99.7 | 100.4 | 101.1 | 101.7 | 102.6 | 102.8 | 101.2 | 99.0 | 130.7 |
| 12500 | 94.7 | 95.0 | 95.4 | 95.9 | 96.5 | 97.1 | 97.9 | 98.6 | 99.4 | 100.0 | 100.6 | 101.5 | 101.6 | 100.1 | 97.9 | 129.7 |
| 16000 | 93.5 | 93.7 | 94.1 | 94.6 | 95.2 | 95.9 | 96.6 | 97.4 | 98.1 | 98.8 | 99.3 | 100.2 | 100.3 | 98.8 | 96.7 | 128.6 |
| 20000 | 92.3 | 92.5 | 92.9 | 93.4 | 94.0 | 94.7 | 95.4 | 96.1 | 96.8 | 97.5 | 98.1 | 98.9 | 99.0 | 97.5 | 95.6 | 127.6 |
| 25000 | 90.9 | 91.2 | 91.6 | 92.1 | 92.7 | 93.3 | 94.0 | 94.8 | 95.5 | 96.1 | 96.7 | 97.5 | 97.6 | 96.2 | 94.3 | 126.7 |
| 31500 | 89.1 | 89.4 | 89.9 | 90.4 | 91.1 | 91.8 | 92.5 | 93.2 | 93.9 | 94.5 | 95.1 | 95.9 | 96.1 | 94.7 | 92.9 | 125.6 |
| 40000 | 86.5 | 86.9 | 87.4 | 88.0 | 88.8 | 89.6 | 90.4 | 91.2 | 92.0 | 92.6 | 93.2 | 94.0 | 94.2 | 92.9 | 91.1 | 124.4 |
| 50000 | 83.2 | 83.7 | 84.2 | 85.0 | 85.8 | 86.7 | 87.7 | 88.7 | 89.6 | 90.4 | 91.0 | 91.9 | 92.1 | 90.7 | 88.8 | 123.1 |
| 63000 | 78.7 | 79.2 | 79.9 | 80.8 | 81.7 | 82.8 | 84.0 | 85.1 | 86.2 | 87.1 | 87.9 | 88.9 | 89.1 | 87.7 | 85.7 | 121.3 |
| 80000 | 72.4 | 73.0 | 73.9 | 74.9 | 76.1 | 77.3 | 78.7 | 80.1 | 81.4 | 82.5 | 83.5 | 84.7 | 84.9 | 83.4 | 81.3 | 119.0 |
| OVERALL | 108.6 | 108.8 | 109.1 | 109.5 | 109.9 | 110.5 | 111.0 | 111.6 | 112.1 | 112.6 | 113.1 | 113.8 | 114.5 | 113.8 | 112.5 | 142.6 |
| PNL | 120.8 | 121.1 | 121.3 | 121.7 | 122.1 | 122.6 | 123.1 | 123.6 | 124.1 | 124.5 | 124.9 | 125.5 | 126.4 | 126.0 | 124.8 | |
| PNLT | 120.8 | 121.1 | 121.3 | 121.7 | 122.1 | 122.6 | 123.1 | 123.6 | 124.1 | 124.5 | 124.9 | 125.5 | 126.4 | 126.0 | 124.8 | |

Table B-10. Computational Acoustic Data for Pressure Ratio 3.62 : Mixing Noise Component

| ANGLE | 20 | 30 | 40 | 50 | 60 | 70 | 80 | 90 | 100 | 110 | 120 | 130 | 140 | 150 | 160 | PWL |
|---|---|---|---|---|---|---|---|---|---|---|---|---|---|---|---|---|
| FREQ | | | | | | | | | | | | | | | | |
| 50 | 0.0 | 0.0 | 0.0 | 0.0 | 0.0 | 0.0 | 0.0 | 0.0 | 0.0 | 0.0 | 0.0 | 0.0 | 0.0 | 0.0 | 0.0 | 30.5 |
| 63 | 35.8 | 35.8 | 35.8 | 35.8 | 35.8 | 35.8 | 35.8 | 35.8 | 35.8 | 35.8 | 35.8 | 35.8 | 35.8 | 35.8 | 35.8 | 66.3 |
| 80 | 36.5 | 36.5 | 36.5 | 36.5 | 36.5 | 36.5 | 36.5 | 36.5 | 36.5 | 36.5 | 36.5 | 36.5 | 36.5 | 36.5 | 36.5 | 67.0 |
| 100 | 40.6 | 40.6 | 40.6 | 40.6 | 40.6 | 40.6 | 40.6 | 40.6 | 40.6 | 40.6 | 40.6 | 40.6 | 40.6 | 40.6 | 40.6 | 71.0 |
| 125 | 38.9 | 38.9 | 38.9 | 38.9 | 38.9 | 38.9 | 38.9 | 38.9 | 38.9 | 38.9 | 38.9 | 38.9 | 38.9 | 38.9 | 38.9 | 69.4 |
| 160 | 39.5 | 39.5 | 39.5 | 39.5 | 39.5 | 39.5 | 39.5 | 39.5 | 39.5 | 39.5 | 39.5 | 39.5 | 39.5 | 39.5 | 39.5 | 70.0 |
| 200 | 40.5 | 40.5 | 40.5 | 40.5 | 40.5 | 40.5 | 40.5 | 40.5 | 40.5 | 40.5 | 40.5 | 40.5 | 40.5 | 40.5 | 40.5 | 70.9 |
| 250 | 41.6 | 41.6 | 41.6 | 41.6 | 41.6 | 41.6 | 41.6 | 41.6 | 41.6 | 41.6 | 41.6 | 41.6 | 41.6 | 41.6 | 41.6 | 72.1 |
| 315 | 42.8 | 42.8 | 42.8 | 42.8 | 42.8 | 42.8 | 42.8 | 42.8 | 42.8 | 42.8 | 42.8 | 42.8 | 42.8 | 42.8 | 42.8 | 73.2 |
| 400 | 43.5 | 43.5 | 43.5 | 43.5 | 43.5 | 43.5 | 43.5 | 43.5 | 43.5 | 43.5 | 43.5 | 43.5 | 43.5 | 43.5 | 43.5 | 73.9 |
| 500 | 44.6 | 44.6 | 44.6 | 44.6 | 44.6 | 44.6 | 44.6 | 44.6 | 44.6 | 44.6 | 44.6 | 44.6 | 44.6 | 44.6 | 44.6 | 75.1 |
| 630 | 45.8 | 45.8 | 45.8 | 45.8 | 45.8 | 45.8 | 45.8 | 45.8 | 45.8 | 45.8 | 45.8 | 45.8 | 45.8 | 45.8 | 45.8 | 76.3 |
| 800 | 46.5 | 46.5 | 46.5 | 46.5 | 46.5 | 46.5 | 46.5 | 46.5 | 46.5 | 46.5 | 46.5 | 46.5 | 46.5 | 46.5 | 46.5 | 77.0 |
| 1000 | 47.4 | 47.4 | 47.4 | 47.4 | 47.4 | 47.4 | 47.4 | 47.4 | 47.4 | 47.4 | 47.4 | 47.4 | 47.4 | 47.4 | 47.4 | 77.9 |
| 1250 | 48.9 | 48.9 | 48.9 | 48.9 | 48.9 | 48.9 | 48.9 | 48.9 | 48.9 | 48.9 | 48.9 | 48.9 | 48.9 | 48.9 | 48.9 | 79.4 |
| 1600 | 49.5 | 49.5 | 49.5 | 49.5 | 49.5 | 49.5 | 49.5 | 49.5 | 49.5 | 49.5 | 49.5 | 49.5 | 49.5 | 49.5 | 49.5 | 80.0 |
| 2000 | 50.4 | 50.4 | 50.4 | 50.4 | 50.4 | 50.4 | 50.4 | 50.4 | 50.4 | 50.4 | 50.4 | 50.4 | 50.4 | 50.4 | 50.4 | 80.9 |
| 2500 | 52.1 | 51.7 | 51.6 | 51.6 | 51.6 | 51.6 | 51.6 | 51.6 | 51.6 | 51.6 | 51.6 | 51.6 | 51.6 | 51.6 | 51.6 | 82.1 |
| 3150 | 58.9 | 58.4 | 57.5 | 56.1 | 54.2 | 52.8 | 52.7 | 52.7 | 52.7 | 52.7 | 52.7 | 52.7 | 52.7 | 52.7 | 52.7 | 84.9 |
| 4000 | 55.4 | 56.2 | 57.1 | 57.9 | 58.1 | 57.3 | 55.4 | 53.6 | 53.4 | 53.4 | 53.4 | 53.4 | 53.4 | 53.4 | 53.4 | 86.0 |
| 5000 | 54.5 | 54.5 | 54.5 | 54.6 | 55.4 | 56.6 | 57.4 | 57.0 | 55.4 | 54.5 | 54.5 | 54.5 | 54.5 | 54.5 | 54.5 | 86.0 |
| 6300 | 55.7 | 55.7 | 55.7 | 55.7 | 55.7 | 55.7 | 55.7 | 56.3 | 56.7 | 56.1 | 55.7 | 55.7 | 55.7 | 55.7 | 55.7 | 86.5 |
| 8000 | 56.3 | 56.3 | 56.3 | 56.3 | 56.3 | 56.3 | 56.3 | 56.3 | 56.3 | 56.3 | 56.3 | 56.3 | 56.3 | 56.3 | 56.3 | 87.0 |
| 10000 | 57.2 | 57.2 | 57.2 | 57.2 | 57.2 | 57.2 | 57.2 | 57.2 | 57.2 | 57.2 | 57.2 | 57.2 | 57.2 | 57.2 | 57.2 | 87.9 |
| 12500 | 58.5 | 58.5 | 58.5 | 58.5 | 58.5 | 58.5 | 58.5 | 58.5 | 58.5 | 58.5 | 58.5 | 58.5 | 58.5 | 58.5 | 58.5 | 89.4 |
| 16000 | 58.9 | 58.9 | 58.9 | 58.9 | 58.9 | 58.9 | 58.9 | 58.9 | 58.9 | 58.9 | 58.9 | 58.9 | 58.9 | 58.9 | 58.9 | 90.0 |
| 20000 | 59.6 | 59.6 | 59.6 | 59.6 | 59.6 | 59.6 | 59.6 | 59.6 | 59.6 | 59.6 | 59.6 | 59.6 | 59.6 | 59.6 | 59.6 | 90.9 |
| 25000 | 60.4 | 60.4 | 60.4 | 60.4 | 60.4 | 60.4 | 60.4 | 60.4 | 60.4 | 60.4 | 60.4 | 60.4 | 60.4 | 60.4 | 60.4 | 92.1 |
| 31500 | 61.0 | 61.0 | 61.0 | 61.0 | 61.0 | 61.0 | 61.0 | 61.0 | 61.0 | 61.0 | 61.0 | 61.0 | 61.0 | 61.0 | 61.0 | 93.2 |
| 40000 | 60.9 | 60.9 | 60.9 | 60.9 | 60.9 | 60.9 | 60.9 | 60.9 | 60.9 | 60.9 | 60.9 | 60.9 | 60.9 | 60.9 | 60.9 | 93.9 |
| 50000 | 61.0 | 61.0 | 61.0 | 61.0 | 61.0 | 61.0 | 61.0 | 61.0 | 61.0 | 61.0 | 61.0 | 61.0 | 61.0 | 61.0 | 61.0 | 95.1 |
| 63000 | 60.6 | 60.6 | 60.6 | 60.6 | 60.6 | 60.6 | 60.6 | 60.6 | 60.6 | 60.6 | 60.6 | 60.6 | 60.6 | 60.6 | 60.6 | 96.3 |
| 80000 | 0.0 | 0.0 | 0.0 | 0.0 | 0.0 | 0.0 | 0.0 | 0.0 | 0.0 | 0.0 | 0.0 | 0.0 | 0.0 | 0.0 | 0.0 | 30.5 |
| OVERALL | 70.7 | 70.7 | 70.7 | 70.7 | 70.7 | 70.6 | 70.6 | 70.6 | 70.5 | 70.5 | 70.5 | 70.5 | 70.5 | 70.5 | 70.5 | 103.1 |
| PNL | 79.4 | 79.2 | 78.8 | 78.9 | 78.9 | 78.5 | 78.1 | 77.8 | 77.2 | 76.9 | 76.7 | 76.7 | 76.7 | 76.7 | 76.7 | |
| PNLT | 81.1 | 80.7 | 79.9 | 78.9 | 80.1 | 78.5 | 78.1 | 77.8 | 77.2 | 76.9 | 76.7 | 76.7 | 76.7 | 76.7 | 76.7 | |

Table B-11. Computational Acoustic Data for Pressure Ratio 3.62 : Shock Noise Component

| ANGLE | 20 | 30 | 40 | 50 | 60 | 70 | 80 | 90 | 100 | 110 | 120 | 130 | 140 | 150 | 160 | PWL |
|---|---|---|---|---|---|---|---|---|---|---|---|---|---|---|---|---|
| FREQ | | | | | | | | | | | | | | | | |
| 50 | 38.4 | 38.4 | 38.3 | 38.3 | 38.3 | 38.3 | 38.4 | 38.4 | 38.6 | 38.8 | 39.1 | 39.5 | 40.1 | 41.7 | 43.5 | 69.6 |
| 63 | 44.1 | 44.0 | 44.0 | 44.0 | 44.0 | 44.0 | 44.0 | 44.1 | 44.3 | 44.4 | 44.7 | 45.0 | 45.6 | 47.0 | 48.7 | 75.2 |
| 80 | 48.8 | 48.7 | 48.7 | 48.7 | 48.7 | 48.7 | 48.7 | 48.8 | 49.0 | 49.2 | 49.5 | 49.8 | 50.5 | 52.0 | 53.7 | 80.0 |
| 100 | 53.5 | 53.5 | 53.4 | 53.4 | 53.4 | 53.4 | 53.5 | 53.6 | 53.7 | 53.9 | 54.2 | 54.6 | 55.2 | 56.7 | 58.4 | 84.7 |
| 125 | 58.0 | 58.0 | 58.0 | 58.0 | 58.0 | 58.0 | 58.0 | 58.1 | 58.3 | 58.5 | 58.8 | 59.2 | 59.9 | 61.4 | 63.1 | 89.3 |
| 160 | 63.1 | 63.1 | 63.1 | 63.1 | 63.1 | 63.1 | 63.2 | 63.3 | 63.5 | 63.7 | 64.0 | 64.4 | 65.0 | 66.6 | 68.2 | 94.5 |
| 200 | 67.6 | 67.6 | 67.6 | 67.6 | 67.6 | 67.7 | 67.8 | 67.9 | 68.1 | 68.3 | 68.6 | 69.0 | 69.7 | 71.2 | 72.8 | 99.0 |
| 250 | 72.0 | 72.0 | 72.0 | 72.0 | 72.1 | 72.1 | 72.2 | 72.3 | 72.5 | 72.8 | 73.1 | 73.5 | 74.2 | 75.7 | 77.2 | 103.5 |
| 315 | 76.3 | 76.3 | 76.3 | 76.4 | 76.4 | 76.5 | 76.6 | 76.8 | 77.0 | 77.3 | 77.6 | 78.1 | 78.7 | 80.2 | 81.6 | 107.9 |
| 400 | 80.4 | 80.5 | 80.5 | 80.6 | 80.6 | 80.7 | 80.9 | 81.1 | 81.3 | 81.6 | 82.0 | 82.5 | 83.2 | 84.7 | 86.0 | 112.3 |
| 500 | 83.9 | 84.0 | 84.0 | 84.1 | 84.2 | 84.4 | 84.5 | 84.8 | 85.1 | 85.4 | 85.8 | 86.3 | 87.1 | 88.5 | 89.7 | 116.0 |
| 630 | 87.1 | 87.2 | 87.3 | 87.4 | 87.5 | 87.7 | 87.9 | 88.2 | 88.5 | 88.9 | 89.4 | 89.9 | 90.7 | 92.2 | 93.1 | 119.4 |
| 800 | 90.1 | 90.1 | 90.2 | 90.3 | 90.5 | 90.7 | 91.0 | 91.2 | 91.6 | 92.0 | 92.5 | 93.0 | 94.0 | 95.4 | 96.0 | 122.5 |
| 1000 | 92.5 | 92.6 | 92.7 | 92.8 | 93.0 | 93.2 | 93.4 | 93.7 | 94.1 | 94.5 | 95.0 | 95.5 | 96.6 | 97.8 | 98.2 | 125.0 |
| 1250 | 94.7 | 94.7 | 94.9 | 95.0 | 95.2 | 95.4 | 95.6 | 95.9 | 96.2 | 96.6 | 97.1 | 97.6 | 98.7 | 99.8 | 99.9 | 127.1 |
| 1600 | 96.6 | 96.7 | 96.9 | 97.1 | 97.3 | 97.5 | 97.7 | 98.0 | 98.3 | 98.7 | 99.1 | 99.6 | 100.7 | 101.6 | 101.3 | 129.1 |
| 2000 | 98.0 | 98.1 | 98.3 | 98.5 | 98.8 | 99.0 | 99.3 | 99.6 | 99.9 | 100.3 | 100.6 | 101.1 | 102.3 | 102.8 | 102.1 | 130.5 |
| 2500 | 98.8 | 99.0 | 99.2 | 99.5 | 99.8 | 100.2 | 100.5 | 100.9 | 101.2 | 101.6 | 101.9 | 102.4 | 103.5 | 103.7 | 102.6 | 131.7 |
| 3150 | 99.1 | 99.3 | 99.7 | 100.0 | 100.4 | 100.9 | 101.3 | 101.8 | 102.2 | 102.5 | 102.9 | 103.4 | 104.5 | 104.2 | 102.8 | 132.4 |
| 4000 | 98.9 | 99.2 | 99.6 | 100.0 | 100.5 | 101.0 | 101.6 | 102.1 | 102.6 | 103.1 | 103.4 | 104.1 | 105.0 | 104.2 | 102.5 | 132.8 |
| 5000 | 98.4 | 98.7 | 99.1 | 99.6 | 100.1 | 100.8 | 101.4 | 102.0 | 102.6 | 103.2 | 103.6 | 104.3 | 105.0 | 103.9 | 101.9 | 132.7 |
| 6300 | 97.6 | 97.9 | 98.3 | 98.8 | 99.4 | 100.1 | 100.8 | 101.5 | 102.2 | 102.8 | 103.3 | 104.1 | 104.6 | 103.2 | 101.0 | 132.2 |
| 8000 | 96.7 | 97.0 | 97.4 | 97.9 | 98.5 | 99.2 | 99.9 | 100.6 | 101.4 | 102.1 | 102.6 | 103.5 | 103.7 | 102.2 | 100.0 | 131.4 |
| 10000 | 95.7 | 96.0 | 96.4 | 96.9 | 97.5 | 98.2 | 98.9 | 99.7 | 100.4 | 101.1 | 101.7 | 102.6 | 102.8 | 101.2 | 99.0 | 130.4 |
| 12500 | 94.7 | 95.0 | 95.4 | 95.9 | 96.5 | 97.1 | 97.9 | 98.6 | 99.4 | 100.0 | 100.6 | 101.5 | 101.6 | 100.1 | 97.9 | 129.3 |
| 16000 | 93.5 | 93.7 | 94.1 | 94.6 | 95.2 | 95.9 | 96.6 | 97.4 | 98.1 | 98.8 | 99.3 | 100.2 | 100.3 | 98.8 | 96.7 | 128.1 |
| 20000 | 92.3 | 92.5 | 92.9 | 93.4 | 94.0 | 94.7 | 95.4 | 96.1 | 96.8 | 97.5 | 98.1 | 98.9 | 99.0 | 97.5 | 95.6 | 126.8 |
| 25000 | 90.9 | 91.2 | 91.6 | 92.1 | 92.7 | 93.3 | 94.0 | 94.8 | 95.5 | 96.1 | 96.7 | 97.5 | 97.7 | 96.2 | 94.3 | 125.4 |
| 31500 | 89.1 | 89.4 | 89.9 | 90.4 | 91.1 | 91.8 | 92.5 | 93.2 | 93.9 | 94.5 | 95.1 | 95.9 | 96.1 | 94.7 | 92.9 | 123.9 |
| 40000 | 86.5 | 86.9 | 87.4 | 88.0 | 88.8 | 89.6 | 90.4 | 91.2 | 92.0 | 92.6 | 93.2 | 94.0 | 94.2 | 92.9 | 91.1 | 121.9 |
| 50000 | 83.3 | 83.7 | 84.3 | 85.0 | 85.8 | 86.7 | 87.7 | 88.7 | 89.6 | 90.4 | 91.0 | 91.9 | 92.1 | 90.7 | 88.8 | 119.4 |
| 63000 | 78.8 | 79.3 | 80.0 | 80.8 | 81.8 | 82.8 | 84.0 | 85.1 | 86.2 | 87.1 | 87.9 | 88.9 | 89.1 | 87.7 | 85.7 | 116.1 |
| 80000 | 72.4 | 73.0 | 73.9 | 74.9 | 76.1 | 77.3 | 78.7 | 80.1 | 81.4 | 82.5 | 83.5 | 84.7 | 84.9 | 83.4 | 81.3 | 111.5 |
| OVERALL | 108.6 | 108.8 | 109.1 | 109.5 | 109.9 | 110.5 | 111.0 | 111.6 | 112.1 | 112.6 | 113.1 | 113.8 | 114.5 | 113.8 | 112.5 | 142.3 |
| PNL | 120.8 | 121.1 | 121.3 | 121.7 | 122.1 | 122.6 | 123.1 | 123.6 | 124.1 | 124.5 | 124.9 | 125.5 | 126.4 | 126.0 | 124.8 | |
| PNLT | 120.8 | 121.1 | 121.3 | 121.7 | 122.1 | 122.6 | 123.1 | 123.6 | 124.1 | 124.5 | 124.9 | 125.5 | 126.4 | 126.0 | 124.8 | |

Table B-12. Computational Acoustic Data for Pressure Ratio 3.62 : Total Noise Levels

| ANGLE | 20 | 30 | 40 | 50 | 60 | 70 | 80 | 90 | 100 | 110 | 120 | 130 | 140 | 150 | 160 | PWL |
|---|---|---|---|---|---|---|---|---|---|---|---|---|---|---|---|---|
| FREQ | | | | | | | | | | | | | | | | |
| 50 | 38.6 | 38.6 | 38.6 | 38.5 | 38.5 | 38.5 | 38.5 | 38.6 | 38.7 | 38.9 | 39.2 | 39.6 | 40.3 | 41.9 | 43.8 | 70.2 |
| 63 | 43.6 | 43.6 | 43.5 | 43.5 | 43.5 | 43.5 | 43.5 | 43.6 | 43.7 | 43.9 | 44.2 | 44.6 | 45.3 | 46.9 | 48.7 | 75.2 |
| 80 | 48.7 | 48.7 | 48.7 | 48.6 | 48.6 | 48.6 | 48.6 | 48.7 | 48.9 | 49.1 | 49.4 | 49.7 | 50.4 | 52.1 | 53.8 | 80.4 |
| 100 | 53.5 | 53.5 | 53.4 | 53.4 | 53.4 | 53.4 | 53.4 | 53.5 | 53.7 | 53.9 | 54.2 | 54.5 | 55.2 | 56.8 | 58.6 | 85.1 |
| 125 | 58.2 | 58.2 | 58.2 | 58.1 | 58.1 | 58.1 | 58.2 | 58.3 | 58.4 | 58.6 | 58.9 | 59.3 | 60.0 | 61.6 | 63.3 | 89.9 |
| 160 | 63.4 | 63.4 | 63.3 | 63.3 | 63.3 | 63.3 | 63.4 | 63.4 | 63.6 | 63.8 | 64.1 | 64.5 | 65.2 | 66.8 | 68.4 | 95.1 |
| 200 | 67.9 | 67.9 | 67.9 | 67.9 | 67.9 | 67.9 | 68.0 | 68.1 | 68.2 | 68.5 | 68.8 | 69.2 | 69.9 | 71.4 | 73.0 | 99.7 |
| 250 | 72.3 | 72.3 | 72.3 | 72.3 | 72.3 | 72.4 | 72.4 | 72.6 | 72.7 | 73.0 | 73.3 | 73.7 | 74.4 | 75.9 | 77.5 | 104.2 |
| 315 | 76.7 | 76.7 | 76.7 | 76.7 | 76.8 | 76.8 | 76.9 | 77.0 | 77.2 | 77.5 | 77.8 | 78.2 | 79.0 | 80.5 | 81.9 | 108.7 |
| 400 | 80.9 | 80.9 | 80.9 | 81.0 | 81.0 | 81.1 | 81.2 | 81.4 | 81.6 | 81.9 | 82.3 | 82.7 | 83.5 | 85.0 | 86.3 | 113.0 |
| 500 | 84.5 | 84.5 | 84.5 | 84.6 | 84.7 | 84.8 | 85.0 | 85.2 | 85.4 | 85.7 | 86.1 | 86.6 | 87.4 | 88.9 | 90.0 | 116.8 |
| 630 | 87.7 | 87.8 | 87.9 | 88.0 | 88.1 | 88.2 | 88.4 | 88.7 | 89.0 | 89.3 | 89.8 | 90.2 | 91.1 | 92.6 | 93.5 | 120.3 |
| 800 | 90.7 | 90.8 | 90.9 | 91.0 | 91.1 | 91.3 | 91.6 | 91.8 | 92.2 | 92.6 | 93.0 | 93.5 | 94.5 | 95.9 | 96.6 | 123.5 |
| 1000 | 93.2 | 93.2 | 93.3 | 93.5 | 93.6 | 93.8 | 94.1 | 94.4 | 94.7 | 95.1 | 95.6 | 96.1 | 97.2 | 98.5 | 98.8 | 126.0 |
| 1250 | 95.3 | 95.4 | 95.5 | 95.7 | 95.8 | 96.0 | 96.3 | 96.5 | 96.9 | 97.3 | 97.7 | 98.3 | 99.4 | 100.5 | 100.5 | 128.2 |
| 1600 | 97.3 | 97.4 | 97.6 | 97.7 | 97.9 | 98.1 | 98.4 | 98.7 | 99.0 | 99.3 | 99.7 | 100.2 | 101.5 | 102.2 | 101.9 | 130.2 |
| 2000 | 98.7 | 98.8 | 99.0 | 99.2 | 99.4 | 99.7 | 100.0 | 100.3 | 100.6 | 100.9 | 101.2 | 101.7 | 103.0 | 103.4 | 102.7 | 131.6 |
| 2500 | 99.5 | 99.7 | 100.0 | 100.2 | 100.6 | 100.9 | 101.2 | 101.6 | 101.9 | 102.2 | 102.5 | 103.0 | 104.2 | 104.3 | 103.1 | 132.8 |
| 3150 | 100.0 | 100.2 | 100.5 | 100.8 | 101.2 | 101.6 | 102.1 | 102.5 | 102.8 | 103.2 | 103.5 | 104.0 | 105.1 | 104.7 | 103.2 | 133.6 |
| 4000 | 99.9 | 100.2 | 100.5 | 100.9 | 101.4 | 101.9 | 102.4 | 102.9 | 103.4 | 103.8 | 104.1 | 104.7 | 105.6 | 104.7 | 102.9 | 134.0 |
| 5000 | 99.6 | 99.9 | 100.2 | 100.7 | 101.2 | 101.8 | 102.4 | 103.0 | 103.5 | 103.9 | 104.3 | 105.0 | 105.6 | 104.4 | 102.4 | 134.0 |
| 6300 | 98.9 | 99.2 | 99.6 | 100.1 | 100.7 | 101.3 | 102.0 | 102.6 | 103.2 | 103.7 | 104.1 | 104.9 | 105.3 | 103.8 | 101.6 | 133.7 |
| 8000 | 98.0 | 98.3 | 98.7 | 99.2 | 99.8 | 100.5 | 101.2 | 101.9 | 102.6 | 103.2 | 103.6 | 104.4 | 104.6 | 103.0 | 100.8 | 133.1 |
| 10000 | 97.0 | 97.3 | 97.7 | 98.2 | 98.9 | 99.6 | 100.3 | 101.1 | 101.8 | 102.4 | 102.8 | 103.7 | 103.8 | 102.1 | 99.8 | 132.3 |
| 12500 | 95.8 | 96.1 | 96.6 | 97.1 | 97.7 | 98.4 | 99.2 | 100.0 | 100.7 | 101.4 | 101.9 | 102.8 | 102.7 | 101.0 | 98.8 | 131.4 |
| 16000 | 94.4 | 94.7 | 95.1 | 95.7 | 96.3 | 97.0 | 97.8 | 98.6 | 99.4 | 100.0 | 100.6 | 101.5 | 101.4 | 99.7 | 97.5 | 130.2 |
| 20000 | 93.2 | 93.5 | 93.9 | 94.4 | 95.0 | 95.7 | 96.4 | 97.2 | 98.0 | 98.6 | 99.2 | 100.1 | 100.1 | 98.3 | 96.2 | 129.1 |
| 25000 | 92.0 | 92.2 | 92.6 | 93.1 | 93.6 | 94.3 | 95.0 | 95.7 | 96.5 | 97.1 | 97.7 | 98.6 | 98.5 | 96.9 | 94.8 | 128.0 |
| 31500 | 90.3 | 90.6 | 91.0 | 91.6 | 92.2 | 92.8 | 93.5 | 94.2 | 94.9 | 95.5 | 96.0 | 96.9 | 96.8 | 95.3 | 93.4 | 127.0 |
| 40000 | 87.6 | 88.0 | 88.6 | 89.2 | 90.0 | 90.8 | 91.6 | 92.4 | 93.1 | 93.7 | 94.1 | 94.9 | 95.0 | 93.6 | 91.9 | 125.9 |
| 50000 | 84.3 | 84.8 | 85.4 | 86.1 | 87.0 | 87.9 | 88.9 | 89.9 | 90.8 | 91.5 | 92.0 | 92.9 | 93.0 | 91.7 | 89.9 | 124.6 |
| 63000 | 79.7 | 80.3 | 81.0 | 81.8 | 82.8 | 83.9 | 85.1 | 86.3 | 87.4 | 88.3 | 89.1 | 90.1 | 90.3 | 88.9 | 87.0 | 122.9 |
| 80000 | 72.9 | 73.6 | 74.5 | 75.7 | 77.0 | 78.4 | 79.8 | 81.2 | 82.5 | 83.7 | 84.6 | 85.9 | 86.2 | 84.7 | 82.7 | 120.6 |
| OVERALL | 109.5 | 109.8 | 110.1 | 110.5 | 110.9 | 111.4 | 112.0 | 112.5 | 113.0 | 113.5 | 113.9 | 114.6 | 115.2 | 114.5 | 113.0 | 143.9 |
| PNL | 121.7 | 121.9 | 122.2 | 122.6 | 123.0 | 123.5 | 123.9 | 124.4 | 124.8 | 125.2 | 125.6 | 126.2 | 127.0 | 126.5 | 125.3 | |
| PNLT | 121.7 | 121.9 | 122.2 | 122.6 | 123.0 | 123.5 | 123.9 | 124.4 | 124.8 | 125.2 | 125.6 | 126.2 | 127.0 | 126.5 | 125.3 | |

Table B-13. Computational Acoustic Data for Pressure Ratio 4.0 : Mixing Noise Component

| ANGLE | 20 | 30 | 40 | 50 | 60 | 70 | 80 | 90 | 100 | 110 | 120 | 130 | 140 | 150 | 160 | PWL |
|---|---|---|---|---|---|---|---|---|---|---|---|---|---|---|---|---|
| FREQ | | | | | | | | | | | | | | | | |
| 50 | 0.0 | 0.0 | 0.0 | 0.0 | 0.0 | 0.0 | 0.0 | 0.0 | 0.0 | 0.0 | 0.0 | 0.0 | 0.0 | 0.0 | 0.0 | 30.9 |
| 63 | 35.8 | 35.8 | 35.8 | 35.8 | 35.8 | 35.8 | 35.8 | 35.8 | 35.8 | 35.8 | 35.8 | 35.8 | 35.8 | 35.8 | 35.8 | 66.7 |
| 80 | 36.5 | 36.5 | 36.5 | 36.5 | 36.5 | 36.5 | 36.5 | 36.5 | 36.5 | 36.5 | 36.5 | 36.5 | 36.5 | 36.5 | 36.5 | 67.4 |
| 100 | 40.6 | 40.6 | 40.6 | 40.6 | 40.6 | 40.6 | 40.6 | 40.6 | 40.6 | 40.6 | 40.6 | 40.6 | 40.6 | 40.6 | 40.6 | 71.5 |
| 125 | 38.9 | 38.9 | 38.9 | 38.9 | 38.9 | 38.9 | 38.9 | 38.9 | 38.9 | 38.9 | 38.9 | 38.9 | 38.9 | 38.9 | 38.9 | 69.8 |
| 160 | 39.5 | 39.5 | 39.5 | 39.5 | 39.5 | 39.5 | 39.5 | 39.5 | 39.5 | 39.5 | 39.5 | 39.5 | 39.5 | 39.5 | 39.5 | 70.4 |
| 200 | 40.5 | 40.5 | 40.5 | 40.5 | 40.5 | 40.5 | 40.5 | 40.5 | 40.5 | 40.5 | 40.5 | 40.5 | 40.5 | 40.5 | 40.5 | 71.4 |
| 250 | 41.6 | 41.6 | 41.6 | 41.6 | 41.6 | 41.6 | 41.6 | 41.6 | 41.6 | 41.6 | 41.6 | 41.6 | 41.6 | 41.6 | 41.6 | 72.5 |
| 315 | 42.8 | 42.8 | 42.8 | 42.8 | 42.8 | 42.8 | 42.8 | 42.8 | 42.8 | 42.8 | 42.8 | 42.8 | 42.8 | 42.8 | 42.8 | 73.7 |
| 400 | 43.5 | 43.5 | 43.5 | 43.5 | 43.5 | 43.5 | 43.5 | 43.5 | 43.5 | 43.5 | 43.5 | 43.5 | 43.5 | 43.5 | 43.5 | 74.4 |
| 500 | 44.6 | 44.6 | 44.6 | 44.6 | 44.6 | 44.6 | 44.6 | 44.6 | 44.6 | 44.6 | 44.6 | 44.6 | 44.6 | 44.6 | 44.6 | 75.5 |
| 630 | 45.8 | 45.8 | 45.8 | 45.8 | 45.8 | 45.8 | 45.8 | 45.8 | 45.8 | 45.8 | 45.8 | 45.8 | 45.8 | 45.8 | 45.8 | 76.7 |
| 800 | 46.5 | 46.5 | 46.5 | 46.5 | 46.5 | 46.5 | 46.5 | 46.5 | 46.5 | 46.5 | 46.5 | 46.5 | 46.5 | 46.5 | 46.5 | 77.4 |
| 1000 | 47.4 | 47.4 | 47.4 | 47.4 | 47.4 | 47.4 | 47.4 | 47.4 | 47.4 | 47.4 | 47.4 | 47.4 | 47.4 | 47.4 | 47.4 | 78.4 |
| 1250 | 48.9 | 48.9 | 48.9 | 48.9 | 48.9 | 48.9 | 48.9 | 48.9 | 48.9 | 48.9 | 48.9 | 48.9 | 48.9 | 48.9 | 48.9 | 79.8 |
| 1600 | 49.5 | 49.5 | 49.5 | 49.5 | 49.5 | 49.5 | 49.5 | 49.5 | 49.5 | 49.5 | 49.5 | 49.5 | 49.5 | 49.5 | 49.5 | 80.4 |
| 2000 | 77.9 | 73.9 | 68.1 | 60.4 | 52.6 | 50.4 | 50.4 | 50.4 | 50.4 | 50.4 | 50.4 | 50.4 | 50.4 | 50.4 | 50.4 | 96.4 |
| 2500 | 101.6 | 100.1 | 97.7 | 94.1 | 88.9 | 81.9 | 72.9 | 62.2 | 52.9 | 51.6 | 51.6 | 51.6 | 51.6 | 51.6 | 51.6 | 122.7 |
| 3150 | 105.2 | 105.5 | 105.5 | 104.9 | 103.3 | 100.6 | 96.4 | 90.5 | 83.1 | 74.3 | 64.7 | 56.1 | 52.8 | 52.7 | 52.7 | 130.9 |
| 4000 | 95.9 | 97.9 | 100.2 | 102.4 | 103.9 | 104.5 | 103.7 | 101.5 | 97.7 | 92.6 | 86.4 | 79.6 | 72.9 | 66.9 | 62.2 | 131.2 |
| 5000 | 95.3 | 94.1 | 92.8 | 93.6 | 97.0 | 100.4 | 102.8 | 103.8 | 103.1 | 101.0 | 97.6 | 93.5 | 89.0 | 84.8 | 81.3 | 130.6 |
| 6300 | 98.9 | 99.0 | 98.9 | 98.3 | 97.0 | 95.8 | 97.3 | 100.3 | 102.4 | 102.9 | 102.0 | 100.0 | 97.4 | 94.7 | 92.4 | 130.7 |
| 8000 | 96.5 | 96.7 | 97.0 | 97.5 | 98.0 | 98.2 | 97.5 | 97.1 | 98.5 | 100.6 | 101.6 | 101.4 | 100.4 | 98.9 | 97.4 | 130.1 |
| 10000 | 94.0 | 94.3 | 94.8 | 95.5 | 96.2 | 96.9 | 97.5 | 97.7 | 97.7 | 98.4 | 99.7 | 100.6 | 100.7 | 100.2 | 99.4 | 129.3 |
| 12500 | 93.5 | 93.7 | 93.9 | 94.1 | 94.5 | 95.1 | 96.1 | 97.0 | 97.7 | 98.1 | 98.7 | 99.5 | 100.1 | 100.2 | 100.0 | 128.7 |
| 16000 | 91.9 | 92.0 | 92.2 | 92.5 | 92.8 | 93.2 | 93.7 | 94.6 | 95.6 | 96.5 | 97.3 | 98.0 | 98.6 | 98.9 | 98.9 | 127.2 |
| 20000 | 90.6 | 90.8 | 91.0 | 91.2 | 91.5 | 91.9 | 92.4 | 93.0 | 93.8 | 94.9 | 95.9 | 96.8 | 97.5 | 97.9 | 98.1 | 126.1 |
| 25000 | 89.4 | 89.6 | 89.8 | 90.0 | 90.3 | 90.7 | 91.2 | 91.7 | 92.4 | 93.3 | 94.4 | 95.4 | 96.3 | 96.9 | 97.2 | 125.2 |
| 31500 | 88.0 | 88.2 | 88.4 | 88.6 | 88.9 | 89.3 | 89.8 | 90.3 | 90.9 | 91.7 | 92.7 | 93.8 | 94.8 | 95.5 | 95.9 | 124.3 |
| 40000 | 85.9 | 86.0 | 86.2 | 86.5 | 86.8 | 87.2 | 87.7 | 88.2 | 88.8 | 89.5 | 90.5 | 91.5 | 92.5 | 93.4 | 93.9 | 122.9 |
| 50000 | 83.7 | 84.0 | 84.3 | 84.6 | 84.9 | 85.3 | 85.8 | 86.3 | 86.9 | 87.6 | 88.5 | 89.5 | 90.5 | 91.3 | 92.0 | 122.0 |
| 63000 | 77.6 | 78.6 | 79.8 | 80.9 | 81.9 | 82.6 | 83.2 | 83.7 | 84.2 | 84.9 | 85.6 | 86.8 | 87.6 | 88.6 | 89.4 | 120.7 |
| 80000 | 0.0 | 0.0 | 0.0 | 0.0 | 0.0 | 0.0 | 0.0 | 0.0 | 0.0 | 0.0 | 0.0 | 0.0 | 0.0 | 0.0 | 0.0 | 30.9 |
| OVERALL | 108.9 | 108.9 | 108.9 | 108.9 | 108.8 | 108.8 | 108.8 | 108.7 | 108.7 | 108.6 | 108.4 | 108.2 | 108.0 | 107.7 | 107.4 | 139.9 |
| PNL | 121.4 | 121.5 | 121.5 | 121.0 | 120.4 | 120.6 | 119.9 | 119.0 | 118.2 | 116.9 | 115.7 | 113.8 | 111.4 | 109.6 | 108.1 | |
| PNLT | 124.7 | 124.5 | 128.1 | 127.7 | 124.1 | 123.4 | 122.1 | 121.9 | 120.8 | 118.3 | 117.8 | 115.4 | 112.5 | 109.6 | 108.9 | |

Table B-14. Computational Acoustic Data for Pressure Ratio 4.0 : Shock Noise Component

| ANGLE | 20 | 30 | 40 | 50 | 60 | 70 | 80 | 90 | 100 | 110 | 120 | 130 | 140 | 150 | 160 | PWL |
|---|---|---|---|---|---|---|---|---|---|---|---|---|---|---|---|---|
| FREQ | | | | | | | | | | | | | | | | |
| 50 | 38.6 | 38.6 | 38.6 | 38.5 | 38.5 | 38.5 | 38.5 | 38.6 | 38.7 | 38.9 | 39.2 | 39.6 | 40.3 | 41.9 | 43.8 | 70.2 |
| 63 | 44.3 | 44.2 | 44.2 | 44.2 | 44.2 | 44.2 | 44.2 | 44.2 | 44.4 | 44.5 | 44.8 | 45.1 | 45.7 | 47.2 | 48.9 | 75.8 |
| 80 | 49.0 | 49.0 | 48.9 | 48.9 | 48.9 | 48.9 | 48.9 | 49.0 | 49.1 | 49.3 | 49.6 | 49.9 | 50.6 | 52.2 | 53.9 | 80.6 |
| 100 | 53.7 | 53.7 | 53.7 | 53.6 | 53.6 | 53.6 | 53.6 | 53.7 | 53.9 | 54.1 | 54.3 | 54.7 | 55.4 | 56.9 | 58.6 | 85.3 |
| 125 | 58.3 | 58.3 | 58.2 | 58.2 | 58.2 | 58.2 | 58.2 | 58.3 | 58.5 | 58.7 | 59.0 | 59.3 | 60.0 | 61.6 | 63.3 | 89.9 |
| 160 | 63.4 | 63.4 | 63.4 | 63.3 | 63.3 | 63.3 | 63.4 | 63.5 | 63.6 | 63.8 | 64.1 | 64.5 | 65.2 | 66.8 | 68.4 | 95.1 |
| 200 | 67.9 | 67.9 | 67.9 | 67.9 | 67.9 | 67.9 | 68.0 | 68.1 | 68.2 | 68.5 | 68.8 | 69.2 | 69.9 | 71.4 | 73.0 | 99.7 |
| 250 | 72.3 | 72.3 | 72.3 | 72.3 | 72.3 | 72.4 | 72.4 | 72.6 | 72.7 | 73.0 | 73.3 | 73.7 | 74.4 | 76.0 | 77.5 | 104.2 |
| 315 | 76.7 | 76.7 | 76.7 | 76.7 | 76.8 | 76.8 | 76.9 | 77.0 | 77.2 | 77.5 | 77.8 | 78.2 | 79.0 | 80.5 | 81.9 | 108.6 |
| 400 | 80.9 | 80.9 | 80.9 | 81.0 | 81.0 | 81.1 | 81.2 | 81.4 | 81.6 | 81.9 | 82.3 | 82.7 | 83.5 | 85.0 | 86.3 | 113.0 |
| 500 | 84.5 | 84.5 | 84.5 | 84.6 | 84.7 | 84.8 | 85.0 | 85.2 | 85.4 | 85.7 | 86.1 | 86.6 | 87.4 | 88.9 | 90.0 | 116.8 |
| 630 | 87.7 | 87.8 | 87.9 | 88.0 | 88.1 | 88.2 | 88.4 | 88.7 | 89.0 | 89.3 | 89.8 | 90.2 | 91.1 | 92.6 | 93.5 | 120.3 |
| 800 | 90.7 | 90.8 | 90.9 | 91.0 | 91.1 | 91.3 | 91.6 | 91.8 | 92.2 | 92.6 | 93.0 | 93.5 | 94.5 | 95.9 | 96.6 | 123.5 |
| 1000 | 93.2 | 93.2 | 93.3 | 93.5 | 93.6 | 93.8 | 94.1 | 94.4 | 94.7 | 95.1 | 95.6 | 96.1 | 97.2 | 98.5 | 98.8 | 126.0 |
| 1250 | 95.3 | 95.4 | 95.5 | 95.7 | 95.8 | 96.0 | 96.3 | 96.5 | 96.9 | 97.3 | 97.7 | 98.3 | 99.4 | 100.5 | 100.5 | 128.2 |
| 1600 | 97.3 | 97.4 | 97.6 | 97.7 | 97.9 | 98.1 | 98.4 | 98.7 | 99.0 | 99.3 | 99.7 | 100.2 | 101.5 | 102.2 | 101.9 | 130.1 |
| 2000 | 98.7 | 98.8 | 99.0 | 99.2 | 99.4 | 99.7 | 100.0 | 100.3 | 100.6 | 100.9 | 101.2 | 101.7 | 103.0 | 103.4 | 102.7 | 131.6 |
| 2500 | 103.7 | 102.9 | 102.0 | 101.2 | 100.8 | 100.9 | 101.2 | 101.6 | 101.9 | 102.2 | 102.5 | 103.0 | 104.2 | 104.3 | 103.1 | 133.2 |
| 3150 | 106.4 | 106.6 | 106.7 | 106.3 | 105.4 | 104.2 | 103.1 | 102.7 | 102.9 | 103.2 | 103.5 | 104.0 | 105.1 | 104.7 | 103.2 | 135.4 |
| 4000 | 101.4 | 102.2 | 103.4 | 104.7 | 105.9 | 106.4 | 106.1 | 105.3 | 104.4 | 104.1 | 104.1 | 104.7 | 105.6 | 104.7 | 102.9 | 135.8 |
| 5000 | 101.0 | 100.9 | 101.0 | 101.5 | 102.6 | 104.2 | 105.6 | 106.4 | 106.3 | 105.7 | 105.1 | 105.3 | 105.7 | 104.5 | 102.4 | 135.6 |
| 6300 | 101.9 | 102.1 | 102.3 | 102.3 | 102.2 | 102.4 | 103.2 | 104.6 | 105.8 | 106.3 | 106.2 | 106.1 | 105.9 | 104.3 | 102.1 | 135.3 |
| 8000 | 100.3 | 100.6 | 101.0 | 101.5 | 102.0 | 102.5 | 102.8 | 103.2 | 104.0 | 105.1 | 105.7 | 106.2 | 106.0 | 104.4 | 102.4 | 134.7 |
| 10000 | 98.8 | 99.1 | 99.5 | 100.1 | 100.7 | 101.4 | 102.1 | 102.7 | 103.2 | 103.8 | 104.6 | 105.4 | 105.5 | 104.2 | 102.6 | 133.8 |
| 12500 | 97.8 | 98.1 | 98.4 | 98.9 | 99.4 | 100.1 | 100.9 | 101.7 | 102.5 | 103.1 | 103.6 | 104.5 | 104.6 | 103.6 | 102.5 | 132.9 |
| 16000 | 96.3 | 96.6 | 96.9 | 97.4 | 97.9 | 98.5 | 99.2 | 100.0 | 100.9 | 101.6 | 102.2 | 103.1 | 103.2 | 102.3 | 101.3 | 131.4 |
| 20000 | 95.1 | 95.3 | 95.7 | 96.1 | 96.6 | 97.2 | 97.9 | 98.6 | 99.4 | 100.2 | 100.9 | 101.8 | 102.0 | 101.1 | 100.2 | 130.1 |
| 25000 | 93.9 | 94.1 | 94.4 | 94.8 | 95.3 | 95.9 | 96.5 | 97.2 | 97.9 | 98.6 | 99.3 | 100.3 | 100.6 | 99.9 | 99.2 | 128.7 |
| 31500 | 92.3 | 92.6 | 92.9 | 93.3 | 93.9 | 94.4 | 95.0 | 95.7 | 96.3 | 97.0 | 97.6 | 98.6 | 98.9 | 98.4 | 97.9 | 127.1 |
| 40000 | 89.9 | 90.2 | 90.6 | 91.1 | 91.7 | 92.4 | 93.1 | 93.8 | 94.5 | 95.1 | 95.7 | 96.6 | 97.0 | 96.5 | 96.0 | 125.1 |
| 50000 | 87.1 | 87.4 | 87.9 | 88.4 | 89.1 | 89.8 | 90.6 | 91.5 | 92.3 | 93.0 | 93.6 | 94.5 | 95.0 | 94.5 | 94.1 | 122.9 |
| 63000 | 81.8 | 82.5 | 83.4 | 84.4 | 85.4 | 86.4 | 87.3 | 88.2 | 89.1 | 90.0 | 90.7 | 91.7 | 92.2 | 91.7 | 91.4 | 119.8 |
| 80000 | 72.9 | 73.6 | 74.5 | 75.7 | 77.0 | 78.4 | 79.8 | 81.2 | 82.5 | 83.7 | 84.6 | 85.9 | 86.2 | 84.7 | 82.7 | 113.1 |
| OVERALL | 112.2 | 112.3 | 112.5 | 112.7 | 113.0 | 113.3 | 113.7 | 114.0 | 114.4 | 114.7 | 115.0 | 115.5 | 116.0 | 115.3 | 114.1 | 145.0 |
| PNL | 125.7 | 125.9 | 126.0 | 125.9 | 125.9 | 126.2 | 126.2 | 126.1 | 126.2 | 126.1 | 126.0 | 126.5 | 127.2 | 126.7 | 125.5 | |
| PNLT | 127.0 | 127.2 | 127.3 | 127.0 | 125.9 | 126.2 | 126.2 | 126.1 | 126.2 | 126.1 | 126.0 | 126.5 | 127.2 | 126.7 | 125.5 | |

Table B-15. Computational Acoustic Data for Pressure Ratio 4.0 : Total Noise Levels

| ANGLE | 20 | 30 | 40 | 50 | 60 | 70 | 80 | 90 | 100 | 110 | 120 | 130 | 140 | 150 | 160 | PWL |
|---|---|---|---|---|---|---|---|---|---|---|---|---|---|---|---|---|
| FREQ | | | | | | | | | | | | | | | | |
| 50 | 38.4 | 38.3 | 38.3 | 38.2 | 38.1 | 38.1 | 38.1 | 38.1 | 38.2 | 38.4 | 38.6 | 38.9 | 39.7 | 41.5 | 43.4 | 70.3 |
| 63 | 43.4 | 43.3 | 43.3 | 43.2 | 43.1 | 43.1 | 43.1 | 43.1 | 43.2 | 43.4 | 43.6 | 43.9 | 44.7 | 46.5 | 48.3 | 75.3 |
| 80 | 48.5 | 48.5 | 48.4 | 48.3 | 48.3 | 48.2 | 48.2 | 48.3 | 48.3 | 48.5 | 48.8 | 49.1 | 49.9 | 51.6 | 53.4 | 80.4 |
| 100 | 53.3 | 53.2 | 53.2 | 53.1 | 53.1 | 53.0 | 53.0 | 53.0 | 53.1 | 53.3 | 53.6 | 53.9 | 54.6 | 56.4 | 58.2 | 85.2 |
| 125 | 58.0 | 58.0 | 57.9 | 57.9 | 57.8 | 57.8 | 57.8 | 57.8 | 57.9 | 58.1 | 58.3 | 58.7 | 59.4 | 61.1 | 62.9 | 90.0 |
| 160 | 63.2 | 63.1 | 63.1 | 63.1 | 63.0 | 63.0 | 63.0 | 63.0 | 63.1 | 63.3 | 63.6 | 63.9 | 64.7 | 66.3 | 68.0 | 95.2 |
| 200 | 67.8 | 67.7 | 67.7 | 67.7 | 67.6 | 67.6 | 67.6 | 67.7 | 67.8 | 68.0 | 68.2 | 68.6 | 69.3 | 71.0 | 72.6 | 99.8 |
| 250 | 72.2 | 72.2 | 72.2 | 72.1 | 72.1 | 72.1 | 72.1 | 72.2 | 72.3 | 72.5 | 72.8 | 73.1 | 73.9 | 75.5 | 77.1 | 104.3 |
| 315 | 76.6 | 76.6 | 76.6 | 76.6 | 76.6 | 76.6 | 76.7 | 76.7 | 76.9 | 77.1 | 77.4 | 77.7 | 78.5 | 80.1 | 81.6 | 108.9 |
| 400 | 80.9 | 80.9 | 80.9 | 80.9 | 81.0 | 81.0 | 81.1 | 81.2 | 81.4 | 81.6 | 81.9 | 82.3 | 83.1 | 84.7 | 86.0 | 113.3 |
| 500 | 84.6 | 84.6 | 84.6 | 84.7 | 84.7 | 84.8 | 84.9 | 85.1 | 85.3 | 85.5 | 85.8 | 86.3 | 87.1 | 88.7 | 89.8 | 117.2 |
| 630 | 88.0 | 88.0 | 88.1 | 88.1 | 88.2 | 88.3 | 88.5 | 88.7 | 88.9 | 89.2 | 89.6 | 90.0 | 91.0 | 92.5 | 93.4 | 120.8 |
| 800 | 91.0 | 91.1 | 91.1 | 91.2 | 91.4 | 91.5 | 91.7 | 91.9 | 92.2 | 92.6 | 93.0 | 93.5 | 94.5 | 95.9 | 96.5 | 124.1 |
| 1000 | 93.5 | 93.5 | 93.6 | 93.8 | 93.9 | 94.1 | 94.3 | 94.5 | 94.9 | 95.2 | 95.7 | 96.2 | 97.3 | 98.6 | 98.9 | 126.7 |
| 1250 | 95.7 | 95.7 | 95.8 | 96.0 | 96.1 | 96.3 | 96.5 | 96.8 | 97.1 | 97.5 | 97.9 | 98.4 | 99.6 | 100.7 | 100.6 | 128.9 |
| 1600 | 97.6 | 97.7 | 97.9 | 98.0 | 98.2 | 98.4 | 98.7 | 98.9 | 99.2 | 99.5 | 99.9 | 100.4 | 101.7 | 102.4 | 102.0 | 130.9 |
| 2000 | 99.0 | 99.1 | 99.3 | 99.5 | 99.8 | 100.0 | 100.3 | 100.5 | 100.8 | 101.1 | 101.4 | 102.0 | 103.2 | 103.6 | 102.7 | 132.4 |
| 2500 | 99.8 | 100.0 | 100.2 | 100.5 | 100.8 | 101.2 | 101.5 | 101.8 | 102.1 | 102.4 | 102.7 | 103.2 | 104.4 | 104.3 | 103.1 | 133.5 |
| 3150 | 100.1 | 100.3 | 100.6 | 101.0 | 101.4 | 101.9 | 102.3 | 102.7 | 103.1 | 103.4 | 103.7 | 104.3 | 105.3 | 104.8 | 103.2 | 134.3 |
| 4000 | 99.9 | 100.2 | 100.6 | 101.0 | 101.5 | 102.0 | 102.6 | 103.1 | 103.6 | 104.0 | 104.3 | 104.9 | 105.7 | 104.7 | 102.8 | 134.6 |
| 5000 | 99.5 | 99.8 | 100.2 | 100.7 | 101.2 | 101.8 | 102.4 | 103.0 | 103.6 | 104.0 | 104.4 | 105.2 | 105.7 | 104.3 | 102.3 | 134.6 |
| 6300 | 98.9 | 99.2 | 99.6 | 100.1 | 100.6 | 101.3 | 101.9 | 102.6 | 103.2 | 103.7 | 104.1 | 105.0 | 105.2 | 103.6 | 101.6 | 134.2 |
| 8000 | 98.2 | 98.4 | 98.8 | 99.3 | 99.9 | 100.6 | 101.2 | 101.9 | 102.5 | 103.1 | 103.5 | 104.3 | 104.3 | 102.6 | 100.6 | 133.5 |
| 10000 | 97.2 | 97.5 | 97.9 | 98.5 | 99.1 | 99.7 | 100.4 | 101.1 | 101.8 | 102.3 | 102.7 | 103.6 | 103.4 | 101.6 | 99.6 | 132.8 |
| 12500 | 96.1 | 96.4 | 96.8 | 97.4 | 98.0 | 98.7 | 99.5 | 100.2 | 100.9 | 101.4 | 101.8 | 102.7 | 102.4 | 100.5 | 98.4 | 131.9 |
| 16000 | 94.6 | 94.9 | 95.4 | 96.0 | 96.6 | 97.3 | 98.1 | 98.9 | 99.6 | 100.2 | 100.6 | 101.5 | 101.2 | 99.3 | 97.1 | 130.9 |
| 20000 | 93.2 | 93.5 | 94.0 | 94.5 | 95.1 | 95.9 | 96.7 | 97.5 | 98.3 | 98.9 | 99.4 | 100.3 | 99.9 | 98.1 | 95.9 | 129.8 |
| 25000 | 92.1 | 92.4 | 92.7 | 93.2 | 93.7 | 94.4 | 95.1 | 95.9 | 96.7 | 97.4 | 97.9 | 98.8 | 98.5 | 96.6 | 94.5 | 128.7 |
| 31500 | 90.7 | 91.0 | 91.4 | 91.9 | 92.5 | 93.0 | 93.7 | 94.3 | 95.0 | 95.6 | 96.1 | 97.0 | 96.7 | 95.0 | 93.1 | 127.6 |
| 40000 | 88.1 | 88.5 | 89.1 | 89.8 | 90.5 | 91.3 | 92.0 | 92.7 | 93.3 | 93.8 | 94.2 | 95.0 | 94.9 | 93.5 | 91.7 | 126.6 |
| 50000 | 84.4 | 84.9 | 85.6 | 86.4 | 87.4 | 88.4 | 89.5 | 90.4 | 91.3 | 91.9 | 92.2 | 93.0 | 93.1 | 91.7 | 90.0 | 125.4 |
| 63000 | 79.1 | 79.7 | 80.5 | 81.5 | 82.7 | 84.0 | 85.3 | 86.7 | 87.9 | 88.8 | 89.5 | 90.4 | 90.5 | 89.0 | 87.1 | 123.7 |
| 80000 | 71.7 | 72.4 | 73.4 | 74.7 | 76.1 | 77.7 | 79.3 | 81.0 | 82.6 | 83.9 | 85.0 | 86.3 | 86.4 | 84.7 | 82.5 | 121.1 |
| OVERALL | 109.7 | 109.9 | 110.2 | 110.6 | 111.1 | 111.6 | 112.1 | 112.7 | 113.2 | 113.6 | 114.0 | 114.7 | 115.2 | 114.4 | 113.0 | 144.5 |
| PNL | 121.9 | 122.1 | 122.4 | 122.7 | 123.1 | 123.6 | 124.1 | 124.5 | 125.0 | 125.4 | 125.7 | 126.3 | 127.1 | 126.5 | 125.2 | |
| PNLT | 121.9 | 122.1 | 122.4 | 122.7 | 123.1 | 123.6 | 124.1 | 124.5 | 125.0 | 125.4 | 125.7 | 126.3 | 127.1 | 126.5 | 125.2 | |
| | | | | | | | | | | | | | | | | |
| | | | | | | | | | | | | | | | | |
| | | | | | | | | | | | | | | | | |

Table B-16. Computational Acoustic Data for Pressure Ratio 4.5 : Mixing Noise Component

| ANGLE | 20 | 30 | 40 | 50 | 60 | 70 | 80 | 90 | 100 | 110 | 120 | 130 | 140 | 150 | 160 | PWL |
|---|---|---|---|---|---|---|---|---|---|---|---|---|---|---|---|---|
| FREQ | | | | | | | | | | | | | | | | |
| 50 | 0.0 | 0.0 | 0.0 | 0.0 | 0.0 | 0.0 | 0.0 | 0.0 | 0.0 | 0.0 | 0.0 | 0.0 | 0.0 | 0.0 | 0.0 | 31.4 |
| 63 | 35.8 | 35.8 | 35.8 | 35.8 | 35.8 | 35.8 | 35.8 | 35.8 | 35.8 | 35.8 | 35.8 | 35.8 | 35.8 | 35.8 | 35.8 | 67.2 |
| 80 | 36.5 | 36.5 | 36.5 | 36.5 | 36.5 | 36.5 | 36.5 | 36.5 | 36.5 | 36.5 | 36.5 | 36.5 | 36.5 | 36.5 | 36.5 | 67.9 |
| 100 | 40.6 | 40.6 | 40.6 | 40.6 | 40.6 | 40.6 | 40.6 | 40.6 | 40.6 | 40.6 | 40.6 | 40.6 | 40.6 | 40.6 | 40.6 | 72.0 |
| 125 | 38.9 | 38.9 | 38.9 | 38.9 | 38.9 | 38.9 | 38.9 | 38.9 | 38.9 | 38.9 | 38.9 | 38.9 | 38.9 | 38.9 | 38.9 | 70.3 |
| 160 | 39.5 | 39.5 | 39.5 | 39.5 | 39.5 | 39.5 | 39.5 | 39.5 | 39.5 | 39.5 | 39.5 | 39.5 | 39.5 | 39.5 | 39.5 | 70.9 |
| 200 | 40.5 | 40.5 | 40.5 | 40.5 | 40.5 | 40.5 | 40.5 | 40.5 | 40.5 | 40.5 | 40.5 | 40.5 | 40.5 | 40.5 | 40.5 | 71.9 |
| 250 | 41.6 | 41.6 | 41.6 | 41.6 | 41.6 | 41.6 | 41.6 | 41.6 | 41.6 | 41.6 | 41.6 | 41.6 | 41.6 | 41.6 | 41.6 | 73.0 |
| 315 | 42.8 | 42.8 | 42.8 | 42.8 | 42.8 | 42.8 | 42.8 | 42.8 | 42.8 | 42.8 | 42.8 | 42.8 | 42.8 | 42.8 | 42.8 | 74.2 |
| 400 | 43.5 | 43.5 | 43.5 | 43.5 | 43.5 | 43.5 | 43.5 | 43.5 | 43.5 | 43.5 | 43.5 | 43.5 | 43.5 | 43.5 | 43.5 | 74.9 |
| 500 | 44.6 | 44.6 | 44.6 | 44.6 | 44.6 | 44.6 | 44.6 | 44.6 | 44.6 | 44.6 | 44.6 | 44.6 | 44.6 | 44.6 | 44.6 | 76.0 |
| 630 | 45.8 | 45.8 | 45.8 | 45.8 | 45.8 | 45.8 | 45.8 | 45.8 | 45.8 | 45.8 | 45.8 | 45.8 | 45.8 | 45.8 | 45.8 | 77.2 |
| 800 | 46.5 | 46.5 | 46.5 | 46.5 | 46.5 | 46.5 | 46.5 | 46.5 | 46.5 | 46.5 | 46.5 | 46.5 | 46.5 | 46.5 | 46.5 | 77.9 |
| 1000 | 47.4 | 47.4 | 47.4 | 47.4 | 47.4 | 47.4 | 47.4 | 47.4 | 47.4 | 47.4 | 47.4 | 47.4 | 47.4 | 47.4 | 47.4 | 78.9 |
| 1250 | 48.9 | 48.9 | 48.9 | 48.9 | 48.9 | 48.9 | 48.9 | 48.9 | 48.9 | 48.9 | 48.9 | 48.9 | 48.9 | 48.9 | 48.9 | 80.3 |
| 1600 | 56.0 | 51.9 | 49.6 | 49.5 | 49.5 | 49.5 | 49.5 | 49.5 | 49.5 | 49.5 | 49.5 | 49.5 | 49.5 | 49.5 | 49.5 | 81.5 |
| 2000 | 97.9 | 95.0 | 90.5 | 84.2 | 75.7 | 64.8 | 53.3 | 50.4 | 50.4 | 50.4 | 50.4 | 50.4 | 50.4 | 50.4 | 50.4 | 117.7 |
| 2500 | 111.3 | 110.7 | 109.5 | 107.3 | 103.7 | 98.4 | 91.1 | 81.7 | 70.5 | 58.2 | 51.7 | 51.6 | 51.6 | 51.6 | 51.6 | 134.7 |
| 3150 | 108.2 | 109.4 | 110.7 | 111.5 | 111.5 | 110.3 | 107.6 | 103.2 | 97.0 | 89.3 | 80.5 | 71.1 | 62.2 | 55.5 | 53.0 | 138.5 |
| 4000 | 94.8 | 96.4 | 99.8 | 103.7 | 107.1 | 109.5 | 110.5 | 109.9 | 107.5 | 103.4 | 98.1 | 91.9 | 85.6 | 79.8 | 75.1 | 137.6 |
| 5000 | 104.8 | 104.1 | 102.7 | 100.6 | 99.3 | 102.1 | 106.2 | 108.9 | 109.8 | 108.9 | 106.5 | 103.0 | 99.0 | 95.1 | 91.7 | 137.2 |
| 6300 | 103.9 | 104.3 | 104.8 | 105.1 | 104.8 | 103.6 | 102.2 | 103.7 | 106.9 | 108.7 | 108.9 | 107.7 | 105.6 | 103.2 | 101.0 | 137.3 |
| 8000 | 101.5 | 101.9 | 102.4 | 102.8 | 103.4 | 104.1 | 104.3 | 103.6 | 103.5 | 105.3 | 107.1 | 107.7 | 107.2 | 106.1 | 104.9 | 136.5 |
| 10000 | 100.0 | 100.0 | 100.1 | 100.5 | 101.3 | 102.2 | 103.1 | 103.7 | 103.9 | 104.0 | 105.0 | 106.2 | 106.7 | 106.6 | 106.1 | 135.5 |
| 12500 | 99.2 | 99.4 | 99.6 | 99.9 | 100.2 | 100.6 | 101.3 | 102.4 | 103.3 | 104.0 | 104.5 | 105.2 | 105.9 | 106.3 | 106.3 | 134.9 |
| 16000 | 97.6 | 97.7 | 97.9 | 98.2 | 98.5 | 98.9 | 99.4 | 100.0 | 101.0 | 102.1 | 103.0 | 103.7 | 104.4 | 104.8 | 105.0 | 133.4 |
| 20000 | 96.4 | 96.5 | 96.7 | 96.9 | 97.3 | 97.6 | 98.1 | 98.6 | 99.4 | 100.3 | 101.4 | 102.5 | 103.3 | 103.8 | 104.1 | 132.3 |
| 25000 | 95.2 | 95.3 | 95.5 | 95.7 | 96.1 | 96.4 | 96.9 | 97.4 | 98.1 | 98.9 | 99.9 | 101.0 | 102.0 | 102.7 | 103.1 | 131.4 |
| 31500 | 93.7 | 93.9 | 94.1 | 94.3 | 94.6 | 95.0 | 95.5 | 96.0 | 96.6 | 97.3 | 98.3 | 99.4 | 100.4 | 101.2 | 101.8 | 130.5 |
| 40000 | 91.6 | 91.8 | 92.0 | 92.2 | 92.5 | 92.9 | 93.4 | 93.9 | 94.5 | 95.2 | 96.1 | 97.1 | 98.2 | 99.1 | 99.7 | 129.1 |
| 50000 | 88.6 | 89.1 | 89.6 | 90.1 | 90.6 | 91.0 | 91.5 | 92.0 | 92.6 | 93.3 | 94.1 | 95.1 | 96.1 | 97.1 | 97.7 | 128.2 |
| 63000 | 78.8 | 80.6 | 82.7 | 84.7 | 86.5 | 87.8 | 88.8 | 89.3 | 89.9 | 90.5 | 91.3 | 92.4 | 93.3 | 94.3 | 95.0 | 126.7 |
| 80000 | 0.0 | 0.0 | 0.0 | 0.0 | 0.0 | 0.0 | 0.0 | 0.0 | 0.0 | 0.0 | 0.0 | 0.0 | 0.0 | 0.0 | 0.0 | 31.4 |
| OVERALL | 115.0 | 115.0 | 115.1 | 115.1 | 115.1 | 115.1 | 115.0 | 115.0 | 114.9 | 114.8 | 114.7 | 114.6 | 114.3 | 114.1 | 113.8 | 146.6 |
| PNL | 127.0 | 126.7 | 127.2 | 127.6 | 127.5 | 126.7 | 126.7 | 126.0 | 125.0 | 124.0 | 122.8 | 121.3 | 119.3 | 117.0 | 115.6 | |
| PNLT | 133.7 | 133.3 | 131.1 | 131.0 | 130.3 | 133.4 | 130.3 | 128.6 | 128.2 | 126.7 | 124.6 | 122.3 | 121.2 | 118.5 | 116.7 | |

Table B-17. Computational Acoustic Data for Pressure Ratio 4.5 : Shock Noise Component

| ANGLE | 20 | 30 | 40 | 50 | 60 | 70 | 80 | 90 | 100 | 110 | 120 | 130 | 140 | 150 | 160 | PWL |
|---|---|---|---|---|---|---|---|---|---|---|---|---|---|---|---|---|
| FREQ | | | | | | | | | | | | | | | | |
| 50 | 38.4 | 38.3 | 38.3 | 38.2 | 38.1 | 38.1 | 38.1 | 38.1 | 38.2 | 38.4 | 38.6 | 38.9 | 39.7 | 41.5 | 43.4 | 70.3 |
| 63 | 44.1 | 44.0 | 44.0 | 43.9 | 43.9 | 43.8 | 43.8 | 43.8 | 43.9 | 44.1 | 44.3 | 44.6 | 45.2 | 46.8 | 48.6 | 75.9 |
| 80 | 48.8 | 48.7 | 48.7 | 48.6 | 48.6 | 48.5 | 48.5 | 48.5 | 48.6 | 48.8 | 49.0 | 49.3 | 50.0 | 51.7 | 53.5 | 80.7 |
| 100 | 53.5 | 53.5 | 53.4 | 53.3 | 53.3 | 53.3 | 53.3 | 53.3 | 53.4 | 53.5 | 53.8 | 54.1 | 54.8 | 56.5 | 58.2 | 85.4 |
| 125 | 58.1 | 58.0 | 58.0 | 57.9 | 57.9 | 57.8 | 57.8 | 57.9 | 58.0 | 58.1 | 58.4 | 58.7 | 59.5 | 61.2 | 62.9 | 90.0 |
| 160 | 63.2 | 63.2 | 63.1 | 63.1 | 63.0 | 63.0 | 63.0 | 63.0 | 63.1 | 63.3 | 63.6 | 63.9 | 64.7 | 66.3 | 68.0 | 95.2 |
| 200 | 67.8 | 67.7 | 67.7 | 67.7 | 67.6 | 67.6 | 67.6 | 67.7 | 67.8 | 68.0 | 68.2 | 68.6 | 69.3 | 71.0 | 72.6 | 99.8 |
| 250 | 72.2 | 72.2 | 72.2 | 72.1 | 72.1 | 72.1 | 72.1 | 72.2 | 72.3 | 72.5 | 72.8 | 73.1 | 73.9 | 75.6 | 77.1 | 104.3 |
| 315 | 76.7 | 76.6 | 76.6 | 76.6 | 76.6 | 76.6 | 76.7 | 76.7 | 76.9 | 77.1 | 77.4 | 77.7 | 78.5 | 80.1 | 81.6 | 108.9 |
| 400 | 80.9 | 80.9 | 80.9 | 80.9 | 81.0 | 81.0 | 81.1 | 81.2 | 81.4 | 81.6 | 81.9 | 82.3 | 83.1 | 84.7 | 86.0 | 113.3 |
| 500 | 84.6 | 84.6 | 84.6 | 84.7 | 84.7 | 84.8 | 84.9 | 85.1 | 85.3 | 85.5 | 85.8 | 86.3 | 87.1 | 88.7 | 89.8 | 117.2 |
| 630 | 88.0 | 88.0 | 88.1 | 88.1 | 88.2 | 88.3 | 88.5 | 88.7 | 88.9 | 89.2 | 89.6 | 90.0 | 91.0 | 92.5 | 93.4 | 120.8 |
| 800 | 91.0 | 91.1 | 91.1 | 91.2 | 91.4 | 91.5 | 91.7 | 91.9 | 92.2 | 92.6 | 93.0 | 93.5 | 94.5 | 95.9 | 96.5 | 124.1 |
| 1000 | 93.5 | 93.5 | 93.6 | 93.8 | 93.9 | 94.1 | 94.3 | 94.5 | 94.9 | 95.2 | 95.7 | 96.2 | 97.3 | 98.6 | 98.9 | 126.7 |
| 1250 | 95.7 | 95.7 | 95.8 | 96.0 | 96.1 | 96.3 | 96.5 | 96.8 | 97.1 | 97.5 | 97.9 | 98.4 | 99.6 | 100.7 | 100.6 | 128.9 |
| 1600 | 97.6 | 97.7 | 97.9 | 98.0 | 98.2 | 98.4 | 98.7 | 98.9 | 99.2 | 99.5 | 99.9 | 100.4 | 101.7 | 102.4 | 102.0 | 130.9 |
| 2000 | 101.5 | 100.5 | 99.8 | 99.6 | 99.8 | 100.0 | 100.3 | 100.5 | 100.8 | 101.1 | 101.4 | 102.0 | 103.2 | 103.6 | 102.7 | 132.5 |
| 2500 | 111.6 | 111.1 | 110.0 | 108.1 | 105.5 | 103.0 | 101.9 | 101.9 | 102.1 | 102.4 | 102.7 | 103.2 | 104.4 | 104.3 | 103.1 | 137.1 |
| 3150 | 108.8 | 109.9 | 111.1 | 111.9 | 111.9 | 110.9 | 108.7 | 106.0 | 104.0 | 103.6 | 103.7 | 104.3 | 105.3 | 104.8 | 103.2 | 139.8 |
| 4000 | 101.1 | 101.7 | 103.2 | 105.5 | 108.2 | 110.2 | 111.2 | 110.7 | 108.9 | 106.7 | 105.2 | 105.1 | 105.7 | 104.7 | 102.9 | 139.3 |
| 5000 | 105.9 | 105.4 | 104.6 | 103.6 | 103.3 | 105.0 | 107.7 | 109.9 | 110.7 | 110.1 | 108.6 | 107.2 | 106.5 | 104.8 | 102.7 | 139.0 |
| 6300 | 105.1 | 105.5 | 106.0 | 106.3 | 106.2 | 105.6 | 105.1 | 106.2 | 108.4 | 109.9 | 110.1 | 109.5 | 108.4 | 106.4 | 104.3 | 138.9 |
| 8000 | 103.2 | 103.5 | 104.0 | 104.4 | 105.0 | 105.7 | 106.0 | 105.9 | 106.0 | 107.3 | 108.7 | 109.4 | 109.0 | 107.7 | 106.3 | 138.1 |
| 10000 | 101.8 | 102.0 | 102.2 | 102.6 | 103.3 | 104.1 | 104.9 | 105.6 | 106.0 | 106.2 | 107.0 | 108.1 | 108.4 | 107.8 | 107.0 | 137.1 |
| 12500 | 100.9 | 101.1 | 101.4 | 101.8 | 102.2 | 102.8 | 103.5 | 104.4 | 105.3 | 105.9 | 106.3 | 107.1 | 107.5 | 107.3 | 106.9 | 136.3 |
| 16000 | 99.4 | 99.6 | 99.8 | 100.2 | 100.7 | 101.2 | 101.8 | 102.5 | 103.4 | 104.2 | 105.0 | 105.8 | 106.1 | 105.9 | 105.6 | 134.7 |
| 20000 | 98.1 | 98.3 | 98.5 | 98.9 | 99.3 | 99.9 | 100.5 | 101.1 | 101.9 | 102.7 | 103.5 | 104.5 | 104.9 | 104.8 | 104.7 | 133.4 |
| 25000 | 96.9 | 97.1 | 97.3 | 97.7 | 98.1 | 98.5 | 99.1 | 99.7 | 100.4 | 101.2 | 102.0 | 103.0 | 103.6 | 103.6 | 103.7 | 132.1 |
| 31500 | 95.5 | 95.7 | 96.0 | 96.3 | 96.7 | 97.2 | 97.7 | 98.2 | 98.9 | 99.6 | 100.3 | 101.3 | 102.0 | 102.2 | 102.3 | 130.5 |
| 40000 | 93.2 | 93.5 | 93.8 | 94.2 | 94.6 | 95.2 | 95.7 | 96.3 | 96.9 | 97.6 | 98.2 | 99.2 | 99.8 | 100.1 | 100.3 | 128.5 |
| 50000 | 90.0 | 90.5 | 91.1 | 91.7 | 92.3 | 92.9 | 93.6 | 94.3 | 95.0 | 95.6 | 96.3 | 97.2 | 97.9 | 98.2 | 98.4 | 126.4 |
| 63000 | 81.9 | 83.2 | 84.7 | 86.4 | 88.0 | 89.3 | 90.4 | 91.2 | 92.0 | 92.8 | 93.5 | 94.5 | 95.1 | 95.5 | 95.6 | 123.3 |
| 80000 | 71.7 | 72.4 | 73.4 | 74.7 | 76.1 | 77.7 | 79.3 | 81.0 | 82.6 | 83.9 | 85.0 | 86.3 | 86.4 | 84.7 | 82.5 | 113.6 |
| OVERALL | 116.1 | 116.2 | 116.3 | 116.4 | 116.5 | 116.7 | 116.8 | 117.0 | 117.1 | 117.3 | 117.4 | 117.7 | 117.8 | 117.2 | 116.4 | 148.4 |
| PNL | 129.3 | 129.0 | 129.6 | 130.0 | 130.1 | 129.7 | 129.9 | 129.7 | 129.2 | 129.0 | 128.5 | 128.3 | 128.1 | 127.2 | 126.0 | |
| PNLT | 131.4 | 131.0 | 132.6 | 132.8 | 131.8 | 131.1 | 131.7 | 129.7 | 129.2 | 129.0 | 128.5 | 128.3 | 128.1 | 127.2 | 126.0 | |
| | | | | | | | | | | | | | | | | |
| | | | | | | | | | | | | | | | | |
| | | | | | | | | | | | | | | | | |

Table B-18. Computational Acoustic Data for Pressure Ratio 4.5 : Total Noise Levels

| ANGLE | 20 | 30 | 40 | 50 | 60 | 70 | 80 | 90 | 100 | 110 | 120 | 130 | 140 | 150 | 160 | PWL |
|---|---|---|---|---|---|---|---|---|---|---|---|---|---|---|---|---|
| FREQ | | | | | | | | | | | | | | | | |
| 50 | 38.3 | 38.2 | 38.2 | 38.1 | 38.0 | 37.9 | 37.9 | 37.9 | 37.9 | 38.1 | 38.3 | 38.6 | 39.5 | 41.4 | 43.3 | 70.6 |
| 63 | 43.3 | 43.2 | 43.1 | 43.1 | 43.0 | 42.9 | 42.9 | 42.9 | 42.9 | 43.1 | 43.3 | 43.6 | 44.5 | 46.4 | 48.3 | 75.5 |
| 80 | 48.4 | 48.4 | 48.3 | 48.2 | 48.1 | 48.1 | 48.0 | 48.0 | 48.1 | 48.2 | 48.5 | 48.8 | 49.6 | 51.5 | 53.4 | 80.7 |
| 100 | 53.2 | 53.1 | 53.1 | 53.0 | 52.9 | 52.9 | 52.8 | 52.8 | 52.9 | 53.0 | 53.3 | 53.6 | 54.4 | 56.3 | 58.1 | 85.5 |
| 125 | 57.9 | 57.9 | 57.8 | 57.8 | 57.7 | 57.6 | 57.6 | 57.6 | 57.7 | 57.8 | 58.0 | 58.4 | 59.2 | 61.0 | 62.8 | 90.2 |
| 160 | 63.1 | 63.1 | 63.0 | 63.0 | 62.9 | 62.8 | 62.8 | 62.8 | 62.9 | 63.0 | 63.3 | 63.6 | 64.5 | 66.3 | 68.0 | 95.5 |
| 200 | 67.8 | 67.7 | 67.7 | 67.6 | 67.5 | 67.5 | 67.5 | 67.5 | 67.6 | 67.7 | 67.9 | 68.3 | 69.1 | 70.9 | 72.6 | 100.1 |
| 250 | 72.2 | 72.2 | 72.2 | 72.1 | 72.1 | 72.0 | 72.0 | 72.0 | 72.1 | 72.3 | 72.5 | 72.9 | 73.7 | 75.5 | 77.0 | 104.7 |
| 315 | 76.7 | 76.7 | 76.7 | 76.6 | 76.6 | 76.6 | 76.6 | 76.6 | 76.7 | 76.9 | 77.1 | 77.5 | 78.4 | 80.1 | 81.5 | 109.2 |
| 400 | 81.1 | 81.1 | 81.1 | 81.0 | 81.0 | 81.0 | 81.1 | 81.1 | 81.3 | 81.5 | 81.7 | 82.1 | 83.0 | 84.7 | 86.0 | 113.7 |
| 500 | 84.8 | 84.8 | 84.8 | 84.9 | 84.9 | 84.9 | 85.0 | 85.1 | 85.3 | 85.5 | 85.8 | 86.1 | 87.1 | 88.7 | 89.9 | 117.7 |
| 630 | 88.3 | 88.3 | 88.4 | 88.4 | 88.5 | 88.6 | 88.7 | 88.8 | 89.0 | 89.3 | 89.6 | 90.0 | 91.0 | 92.6 | 93.5 | 121.4 |
| 800 | 91.4 | 91.4 | 91.5 | 91.6 | 91.7 | 91.9 | 92.0 | 92.2 | 92.5 | 92.8 | 93.1 | 93.6 | 94.7 | 96.1 | 96.7 | 124.8 |
| 1000 | 93.9 | 93.9 | 94.0 | 94.2 | 94.3 | 94.5 | 94.7 | 94.9 | 95.2 | 95.6 | 96.0 | 96.4 | 97.6 | 98.9 | 99.2 | 127.5 |
| 1250 | 95.9 | 96.0 | 96.2 | 96.3 | 96.5 | 96.7 | 96.9 | 97.2 | 97.5 | 97.9 | 98.3 | 98.8 | 100.1 | 101.1 | 101.0 | 129.8 |
| 1600 | 97.8 | 97.9 | 98.1 | 98.3 | 98.5 | 98.8 | 99.0 | 99.3 | 99.6 | 99.9 | 100.3 | 100.9 | 102.2 | 102.9 | 102.2 | 131.8 |
| 2000 | 99.0 | 99.2 | 99.4 | 99.7 | 99.9 | 100.2 | 100.5 | 100.8 | 101.1 | 101.5 | 101.8 | 102.4 | 103.7 | 103.9 | 102.9 | 133.2 |
| 2500 | 99.8 | 100.0 | 100.2 | 100.6 | 100.9 | 101.3 | 101.7 | 102.0 | 102.4 | 102.7 | 103.0 | 103.6 | 104.8 | 104.5 | 103.1 | 134.2 |
| 3150 | 100.0 | 100.2 | 100.6 | 101.0 | 101.4 | 101.9 | 102.4 | 102.8 | 103.2 | 103.6 | 103.9 | 104.5 | 105.5 | 104.7 | 102.9 | 134.9 |
| 4000 | 99.7 | 100.0 | 100.4 | 100.9 | 101.4 | 102.0 | 102.6 | 103.1 | 103.6 | 104.0 | 104.4 | 105.1 | 105.8 | 104.5 | 102.3 | 135.1 |
| 5000 | 99.2 | 99.5 | 99.9 | 100.4 | 101.0 | 101.6 | 102.3 | 103.0 | 103.6 | 104.1 | 104.4 | 105.3 | 105.6 | 103.9 | 101.4 | 134.9 |
| 6300 | 98.4 | 98.7 | 99.1 | 99.7 | 100.3 | 101.0 | 101.7 | 102.4 | 103.1 | 103.7 | 104.1 | 105.0 | 105.0 | 103.0 | 100.4 | 134.4 |
| 8000 | 97.5 | 97.8 | 98.2 | 98.7 | 99.4 | 100.1 | 100.8 | 101.6 | 102.3 | 102.9 | 103.4 | 104.3 | 104.0 | 101.9 | 99.3 | 133.6 |
| 10000 | 96.6 | 96.9 | 97.3 | 97.8 | 98.4 | 99.1 | 99.9 | 100.6 | 101.4 | 102.0 | 102.4 | 103.4 | 102.9 | 100.8 | 98.2 | 132.8 |
| 12500 | 95.5 | 95.8 | 96.3 | 96.8 | 97.4 | 98.1 | 98.8 | 99.6 | 100.3 | 100.9 | 101.4 | 102.3 | 101.8 | 99.7 | 97.2 | 131.8 |
| 16000 | 93.9 | 94.3 | 94.8 | 95.4 | 96.1 | 96.8 | 97.6 | 98.4 | 99.1 | 99.7 | 100.1 | 101.0 | 100.5 | 98.4 | 95.9 | 130.7 |
| 20000 | 92.2 | 92.6 | 93.0 | 93.6 | 94.4 | 95.2 | 96.1 | 97.0 | 97.8 | 98.4 | 98.8 | 99.7 | 99.2 | 97.1 | 94.7 | 129.6 |
| 25000 | 91.0 | 91.3 | 91.7 | 92.1 | 92.7 | 93.4 | 94.3 | 95.2 | 96.1 | 96.8 | 97.3 | 98.2 | 97.7 | 95.6 | 93.1 | 128.4 |
| 31500 | 89.5 | 89.8 | 90.3 | 90.8 | 91.4 | 92.0 | 92.6 | 93.3 | 94.1 | 94.8 | 95.4 | 96.3 | 95.8 | 93.8 | 91.6 | 127.1 |
| 40000 | 86.4 | 86.9 | 87.5 | 88.3 | 89.2 | 90.1 | 90.9 | 91.6 | 92.3 | 92.8 | 93.2 | 94.1 | 93.7 | 92.1 | 90.1 | 125.9 |
| 50000 | 81.5 | 82.2 | 83.1 | 84.2 | 85.5 | 86.8 | 88.0 | 89.2 | 90.1 | 90.8 | 91.2 | 92.0 | 91.8 | 90.2 | 88.1 | 124.5 |
| 63000 | 73.9 | 74.8 | 76.1 | 77.6 | 79.3 | 81.2 | 83.0 | 84.8 | 86.3 | 87.5 | 88.2 | 89.2 | 89.0 | 87.2 | 84.7 | 122.5 |
| 80000 | 63.4 | 64.4 | 65.9 | 67.7 | 69.9 | 72.4 | 74.9 | 77.5 | 79.8 | 81.8 | 83.2 | 84.7 | 84.4 | 82.1 | 79.1 | 119.2 |
| OVERALL | 109.4 | 109.7 | 110.0 | 110.4 | 110.9 | 111.4 | 112.0 | 112.6 | 113.1 | 113.6 | 114.0 | 114.7 | 115.1 | 114.2 | 112.5 | 144.8 |
| PNL | 121.7 | 122.0 | 122.3 | 122.6 | 123.1 | 123.6 | 124.1 | 124.6 | 125.0 | 125.5 | 125.8 | 126.5 | 127.2 | 126.4 | 124.9 | |
| PNLT | 121.7 | 122.0 | 122.3 | 122.6 | 123.1 | 123.6 | 124.1 | 124.6 | 125.0 | 125.5 | 125.8 | 126.5 | 127.2 | 126.4 | 124.9 | |

Table B-19. Computational Acoustic Data for Pressure Ratio 5.0 : Mixing Noise Component

| ANGLE | 20 | 30 | 40 | 50 | 60 | 70 | 80 | 90 | 100 | 110 | 120 | 130 | 140 | 150 | 160 | PWL |
|---|---|---|---|---|---|---|---|---|---|---|---|---|---|---|---|---|
| FREQ | | | | | | | | | | | | | | | | |
| 50 | 0.0 | 0.0 | 0.0 | 0.0 | 0.0 | 0.0 | 0.0 | 0.0 | 0.0 | 0.0 | 0.0 | 0.0 | 0.0 | 0.0 | 0.0 | 31.9 |
| 63 | 35.8 | 35.8 | 35.8 | 35.8 | 35.8 | 35.8 | 35.8 | 35.8 | 35.8 | 35.8 | 35.8 | 35.8 | 35.8 | 35.8 | 35.8 | 67.7 |
| 80 | 36.5 | 36.5 | 36.5 | 36.5 | 36.5 | 36.5 | 36.5 | 36.5 | 36.5 | 36.5 | 36.5 | 36.5 | 36.5 | 36.5 | 36.5 | 68.4 |
| 100 | 40.6 | 40.6 | 40.6 | 40.6 | 40.6 | 40.6 | 40.6 | 40.6 | 40.6 | 40.6 | 40.6 | 40.6 | 40.6 | 40.6 | 40.6 | 72.4 |
| 125 | 38.9 | 38.9 | 38.9 | 38.9 | 38.9 | 38.9 | 38.9 | 38.9 | 38.9 | 38.9 | 38.9 | 38.9 | 38.9 | 38.9 | 38.9 | 70.8 |
| 160 | 39.5 | 39.5 | 39.5 | 39.5 | 39.5 | 39.5 | 39.5 | 39.5 | 39.5 | 39.5 | 39.5 | 39.5 | 39.5 | 39.5 | 39.5 | 71.4 |
| 200 | 40.5 | 40.5 | 40.5 | 40.5 | 40.5 | 40.5 | 40.5 | 40.5 | 40.5 | 40.5 | 40.5 | 40.5 | 40.5 | 40.5 | 40.5 | 72.3 |
| 250 | 41.6 | 41.6 | 41.6 | 41.6 | 41.6 | 41.6 | 41.6 | 41.6 | 41.6 | 41.6 | 41.6 | 41.6 | 41.6 | 41.6 | 41.6 | 73.5 |
| 315 | 42.8 | 42.8 | 42.8 | 42.8 | 42.8 | 42.8 | 42.8 | 42.8 | 42.8 | 42.8 | 42.8 | 42.8 | 42.8 | 42.8 | 42.8 | 74.6 |
| 400 | 43.5 | 43.5 | 43.5 | 43.5 | 43.5 | 43.5 | 43.5 | 43.5 | 43.5 | 43.5 | 43.5 | 43.5 | 43.5 | 43.5 | 43.5 | 75.4 |
| 500 | 44.6 | 44.6 | 44.6 | 44.6 | 44.6 | 44.6 | 44.6 | 44.6 | 44.6 | 44.6 | 44.6 | 44.6 | 44.6 | 44.6 | 44.6 | 76.5 |
| 630 | 45.8 | 45.8 | 45.8 | 45.8 | 45.8 | 45.8 | 45.8 | 45.8 | 45.8 | 45.8 | 45.8 | 45.8 | 45.8 | 45.8 | 45.8 | 77.7 |
| 800 | 46.5 | 46.5 | 46.5 | 46.5 | 46.5 | 46.5 | 46.5 | 46.5 | 46.5 | 46.5 | 46.5 | 46.5 | 46.5 | 46.5 | 46.5 | 78.4 |
| 1000 | 47.4 | 47.4 | 47.4 | 47.4 | 47.4 | 47.4 | 47.4 | 47.4 | 47.4 | 47.4 | 47.4 | 47.4 | 47.4 | 47.4 | 47.4 | 79.3 |
| 1250 | 48.9 | 48.9 | 48.9 | 48.9 | 48.9 | 48.9 | 48.9 | 48.9 | 48.9 | 48.9 | 48.9 | 48.9 | 48.9 | 48.9 | 48.9 | 80.8 |
| 1600 | 76.1 | 70.9 | 63.3 | 54.0 | 49.5 | 49.5 | 49.5 | 49.5 | 49.5 | 49.5 | 49.5 | 49.5 | 49.5 | 49.5 | 49.5 | 95.0 |
| 2000 | 107.3 | 105.3 | 101.9 | 96.9 | 89.8 | 80.3 | 68.3 | 54.9 | 50.4 | 50.4 | 50.4 | 50.4 | 50.4 | 50.4 | 50.4 | 128.5 |
| 2500 | 114.1 | 114.1 | 113.8 | 112.7 | 110.4 | 106.5 | 100.6 | 92.5 | 82.3 | 70.4 | 58.0 | 51.7 | 51.6 | 51.6 | 51.6 | 139.7 |
| 3150 | 105.5 | 107.7 | 110.1 | 112.2 | 113.6 | 113.7 | 112.3 | 109.1 | 104.0 | 97.2 | 89.0 | 80.2 | 71.4 | 63.6 | 57.9 | 141.2 |
| 4000 | 100.2 | 98.3 | 97.3 | 100.5 | 105.4 | 109.5 | 112.0 | 112.7 | 111.5 | 108.4 | 103.8 | 98.2 | 92.2 | 86.6 | 82.0 | 140.0 |
| 5000 | 107.9 | 107.7 | 107.1 | 105.6 | 103.2 | 101.8 | 105.4 | 109.5 | 111.7 | 111.8 | 110.2 | 107.3 | 103.7 | 100.0 | 96.8 | 140.0 |
| 6300 | 105.5 | 105.7 | 106.2 | 106.9 | 107.4 | 107.0 | 105.5 | 104.6 | 107.3 | 110.1 | 111.2 | 110.6 | 109.0 | 106.9 | 104.9 | 139.9 |
| 8000 | 102.7 | 103.1 | 103.8 | 104.5 | 105.1 | 105.8 | 106.4 | 106.4 | 105.7 | 106.5 | 108.6 | 109.8 | 109.8 | 109.0 | 107.9 | 138.9 |
| 10000 | 102.0 | 102.1 | 102.3 | 102.4 | 102.8 | 103.7 | 104.7 | 105.6 | 106.1 | 106.1 | 106.7 | 107.9 | 108.8 | 108.9 | 108.6 | 137.9 |
| 12500 | 101.2 | 101.3 | 101.5 | 101.8 | 102.1 | 102.5 | 103.0 | 104.0 | 105.1 | 105.9 | 106.5 | 107.1 | 107.9 | 108.4 | 108.5 | 137.3 |
| 16000 | 99.5 | 99.7 | 99.9 | 100.1 | 100.4 | 100.8 | 101.3 | 101.9 | 102.7 | 103.8 | 104.9 | 105.7 | 106.4 | 106.9 | 107.1 | 135.8 |
| 20000 | 98.3 | 98.4 | 98.6 | 98.9 | 99.2 | 99.6 | 100.0 | 100.6 | 101.2 | 102.1 | 103.2 | 104.3 | 105.2 | 105.8 | 106.2 | 134.7 |
| 25000 | 97.1 | 97.2 | 97.4 | 97.7 | 98.0 | 98.4 | 98.8 | 99.4 | 100.0 | 100.7 | 101.7 | 102.8 | 103.9 | 104.7 | 105.2 | 133.8 |
| 31500 | 95.7 | 95.8 | 96.0 | 96.3 | 96.6 | 97.0 | 97.4 | 97.9 | 98.6 | 99.3 | 100.1 | 101.2 | 102.3 | 103.2 | 103.8 | 132.9 |
| 40000 | 93.5 | 93.7 | 93.9 | 94.2 | 94.5 | 94.9 | 95.3 | 95.8 | 96.4 | 97.1 | 98.0 | 99.0 | 100.1 | 101.0 | 101.7 | 131.5 |
| 50000 | 89.0 | 89.9 | 90.8 | 91.7 | 92.4 | 92.9 | 93.4 | 93.9 | 94.5 | 95.2 | 96.0 | 97.0 | 98.0 | 99.0 | 99.7 | 130.5 |
| 63000 | 75.6 | 78.1 | 81.1 | 84.2 | 86.8 | 88.9 | 90.4 | 91.2 | 91.8 | 92.5 | 93.2 | 94.1 | 95.0 | 96.1 | 96.9 | 128.8 |
| 80000 | 0.0 | 0.0 | 0.0 | 0.0 | 0.0 | 0.0 | 0.0 | 0.0 | 0.0 | 0.0 | 0.0 | 0.0 | 0.0 | 0.0 | 0.0 | 31.9 |
| OVERALL | 117.2 | 117.3 | 117.3 | 117.4 | 117.4 | 117.4 | 117.4 | 117.3 | 117.3 | 117.2 | 117.1 | 117.0 | 116.8 | 116.5 | 116.2 | 149.4 |
| PNL | 129.6 | 129.7 | 129.4 | 129.1 | 129.8 | 129.8 | 128.9 | 128.9 | 127.8 | 127.0 | 125.5 | 124.4 | 122.7 | 120.6 | 118 | |
| PNLT | 133.0 | 136.3 | 136.1 | 135.8 | 133.5 | 132.8 | 135.5 | 132.4 | 130.0 | 130.1 | 127.8 | 126.2 | 122.7 | 122.6 | 120 | |
| | | | | | | | | | | | | | | | | |
| | | | | | | | | | | | | | | | | |
| | | | | | | | | | | | | | | | | |

Table B-20. Computational Acoustic Data for Pressure Ratio 5.0 : Shock Noise Component

| ANGLE | 20 | 30 | 40 | 50 | 60 | 70 | 80 | 90 | 100 | 110 | 120 | 130 | 140 | 150 | 160 | PWL |
|---|---|---|---|---|---|---|---|---|---|---|---|---|---|---|---|---|
| FREQ | | | | | | | | | | | | | | | | |
| 50 | 38.3 | 38.2 | 38.2 | 38.1 | 38.0 | 37.9 | 37.9 | 37.9 | 37.9 | 38.1 | 38.3 | 38.6 | 39.5 | 41.4 | 43.3 | 70.6 |
| 63 | 44.0 | 43.9 | 43.9 | 43.8 | 43.7 | 43.7 | 43.7 | 43.7 | 43.7 | 43.8 | 44.0 | 44.3 | 45.0 | 46.7 | 48.5 | 76.2 |
| 80 | 48.7 | 48.6 | 48.6 | 48.5 | 48.4 | 48.4 | 48.3 | 48.3 | 48.4 | 48.5 | 48.7 | 49.0 | 49.9 | 51.6 | 53.5 | 80.9 |
| 100 | 53.4 | 53.4 | 53.3 | 53.2 | 53.2 | 53.1 | 53.1 | 53.1 | 53.1 | 53.3 | 53.5 | 53.8 | 54.6 | 56.4 | 58.2 | 85.7 |
| 125 | 58.0 | 58.0 | 57.9 | 57.8 | 57.7 | 57.7 | 57.7 | 57.7 | 57.7 | 57.9 | 58.1 | 58.4 | 59.3 | 61.1 | 62.8 | 90.3 |
| 160 | 63.2 | 63.1 | 63.1 | 63.0 | 62.9 | 62.9 | 62.8 | 62.8 | 62.9 | 63.1 | 63.3 | 63.6 | 64.5 | 66.3 | 68.0 | 95.5 |
| 200 | 67.8 | 67.7 | 67.7 | 67.6 | 67.5 | 67.5 | 67.5 | 67.5 | 67.6 | 67.7 | 67.9 | 68.3 | 69.2 | 70.9 | 72.6 | 100.1 |
| 250 | 72.2 | 72.2 | 72.2 | 72.1 | 72.1 | 72.0 | 72.0 | 72.0 | 72.1 | 72.3 | 72.5 | 72.9 | 73.8 | 75.5 | 77.0 | 104.7 |
| 315 | 76.7 | 76.7 | 76.7 | 76.6 | 76.6 | 76.6 | 76.6 | 76.6 | 76.7 | 76.9 | 77.1 | 77.5 | 78.4 | 80.1 | 81.5 | 109.2 |
| 400 | 81.1 | 81.1 | 81.1 | 81.0 | 81.0 | 81.0 | 81.1 | 81.1 | 81.3 | 81.5 | 81.7 | 82.1 | 83.0 | 84.7 | 86.0 | 113.7 |
| 500 | 84.8 | 84.8 | 84.8 | 84.9 | 84.9 | 84.9 | 85.0 | 85.1 | 85.3 | 85.5 | 85.8 | 86.1 | 87.1 | 88.7 | 89.9 | 117.7 |
| 630 | 88.3 | 88.3 | 88.4 | 88.4 | 88.5 | 88.6 | 88.7 | 88.8 | 89.0 | 89.3 | 89.6 | 90.0 | 91.0 | 92.6 | 93.5 | 121.4 |
| 800 | 91.4 | 91.4 | 91.5 | 91.6 | 91.7 | 91.9 | 92.0 | 92.2 | 92.5 | 92.8 | 93.1 | 93.6 | 94.7 | 96.1 | 96.7 | 124.8 |
| 1000 | 93.9 | 93.9 | 94.0 | 94.2 | 94.3 | 94.5 | 94.7 | 94.9 | 95.2 | 95.6 | 96.0 | 96.4 | 97.6 | 98.9 | 99.2 | 127.5 |
| 1250 | 95.9 | 96.0 | 96.2 | 96.3 | 96.5 | 96.7 | 96.9 | 97.2 | 97.5 | 97.9 | 98.3 | 98.8 | 100.1 | 101.1 | 101.0 | 129.8 |
| 1600 | 97.8 | 97.9 | 98.1 | 98.3 | 98.5 | 98.8 | 99.0 | 99.3 | 99.6 | 99.9 | 100.3 | 100.9 | 102.2 | 102.9 | 102.2 | 131.7 |
| 2000 | 107.9 | 106.2 | 103.8 | 101.5 | 100.3 | 100.3 | 100.5 | 100.8 | 101.1 | 101.5 | 101.8 | 102.4 | 103.7 | 103.9 | 102.9 | 134.4 |
| 2500 | 114.2 | 114.3 | 114.0 | 113.0 | 110.9 | 107.6 | 104.2 | 102.5 | 102.4 | 102.7 | 103.0 | 103.6 | 104.8 | 104.5 | 103.1 | 140.7 |
| 3150 | 106.6 | 108.4 | 110.5 | 112.5 | 113.8 | 114.0 | 112.7 | 110.0 | 106.6 | 104.5 | 104.0 | 104.6 | 105.5 | 104.7 | 102.9 | 142.0 |
| 4000 | 103.0 | 102.2 | 102.1 | 103.7 | 106.8 | 110.2 | 112.5 | 113.2 | 112.1 | 109.8 | 107.1 | 105.9 | 105.9 | 104.6 | 102.3 | 141.1 |
| 5000 | 108.4 | 108.3 | 107.8 | 106.8 | 105.3 | 104.7 | 107.1 | 110.4 | 112.3 | 112.5 | 111.3 | 109.4 | 107.7 | 105.4 | 102.7 | 141.1 |
| 6300 | 106.3 | 106.5 | 107.0 | 107.6 | 108.1 | 108.0 | 107.0 | 106.7 | 108.7 | 111.0 | 111.9 | 111.7 | 110.4 | 108.4 | 106.2 | 140.9 |
| 8000 | 103.8 | 104.2 | 104.8 | 105.5 | 106.1 | 106.8 | 107.5 | 107.6 | 107.3 | 108.1 | 109.7 | 110.8 | 110.8 | 109.7 | 108.5 | 139.9 |
| 10000 | 103.1 | 103.3 | 103.5 | 103.7 | 104.1 | 105.0 | 105.9 | 106.8 | 107.3 | 107.6 | 108.1 | 109.2 | 109.8 | 109.6 | 109.0 | 138.8 |
| 12500 | 102.2 | 102.4 | 102.6 | 103.0 | 103.4 | 103.8 | 104.4 | 105.3 | 106.3 | 107.1 | 107.7 | 108.4 | 108.8 | 108.9 | 108.8 | 138.0 |
| 16000 | 100.6 | 100.8 | 101.0 | 101.4 | 101.8 | 102.3 | 102.8 | 103.5 | 104.3 | 105.2 | 106.1 | 107.0 | 107.4 | 107.4 | 107.4 | 136.4 |
| 20000 | 99.3 | 99.4 | 99.7 | 100.0 | 100.4 | 100.9 | 101.5 | 102.2 | 102.8 | 103.7 | 104.6 | 105.6 | 106.2 | 106.4 | 106.5 | 135.0 |
| 25000 | 98.1 | 98.2 | 98.5 | 98.8 | 99.1 | 99.6 | 100.1 | 100.8 | 101.5 | 102.2 | 103.1 | 104.1 | 104.8 | 105.2 | 105.4 | 133.7 |
| 31500 | 96.6 | 96.8 | 97.0 | 97.4 | 97.7 | 98.2 | 98.7 | 99.2 | 99.9 | 100.6 | 101.4 | 102.4 | 103.2 | 103.7 | 104.1 | 132.1 |
| 40000 | 94.3 | 94.5 | 94.8 | 95.2 | 95.6 | 96.1 | 96.7 | 97.2 | 97.8 | 98.5 | 99.2 | 100.2 | 101.0 | 101.5 | 102.0 | 130.0 |
| 50000 | 89.7 | 90.6 | 91.5 | 92.4 | 93.2 | 93.9 | 94.5 | 95.2 | 95.9 | 96.6 | 97.3 | 98.2 | 98.9 | 99.5 | 100.0 | 127.8 |
| 63000 | 77.8 | 79.8 | 82.3 | 85.0 | 87.5 | 89.6 | 91.1 | 92.1 | 92.9 | 93.7 | 94.4 | 95.3 | 96.0 | 96.6 | 97.1 | 124.5 |
| 80000 | 63.4 | 64.4 | 65.9 | 67.7 | 69.9 | 72.4 | 74.9 | 77.5 | 79.8 | 81.8 | 83.2 | 84.7 | 84.4 | 82.1 | 79.1 | 111.6 |
| OVERALL | 117.9 | 118.0 | 118.1 | 118.2 | 118.3 | 118.4 | 118.5 | 118.6 | 118.7 | 118.8 | 118.8 | 119.0 | 119.0 | 118.5 | 117.8 | 150.4 |
| PNL | 131.3 | 131.3 | 131.2 | 131.1 | 131.8 | 131.9 | 131.3 | 131.6 | 131.1 | 130.7 | 130.1 | 129.8 | 129.4 | 128.2 | 126.7 | |
| PNLT | 134.8 | 134.5 | 133.5 | 133.1 | 134.8 | 134.3 | 132.8 | 133.4 | 131.1 | 130.7 | 130.1 | 129.8 | 129.4 | 128.2 | 126.7 | |

Table B-21. Computational Acoustic Data for Pressure Ratio 5.0 : Total Noise Levels

# REPORT DOCUMENTATION PAGE

*Form Approved*
*OMB No. 0704-0188*



| 1. AGENCY USE ONLY (*Leave blank*) | 2. REPORT DATE | 3. REPORT TYPE AND DATES COVERED |
|---|---|---|
| | June 1996 | Final Contractor Report |

**4. TITLE AND SUBTITLE**

Computational Study of a Contoured Plug-Nozzle as a Supersonic Jet Noise Suppressor

**5. FUNDING NUMBERS**

WU–537–05–21
G–NAG3–1563

**6. AUTHOR(S)**

I.S. Das, A. Khavaran, and A.P. Das

**7. PERFORMING ORGANIZATION NAME(S) AND ADDRESS(ES)**

Pennsylvania State University
University Park, Pennsylvania 16802–1009

**8. PERFORMING ORGANIZATION REPORT NUMBER**

E–10147

**9. SPONSORING/MONITORING AGENCY NAME(S) AND ADDRESS(ES)**

National Aeronautics and Space Administration
Lewis Research Center
Cleveland, Ohio 44135–3191

**10. SPONSORING/MONITORING AGENCY REPORT NUMBER**

NASA CR–198462

**11. SUPPLEMENTARY NOTES**

I.S. Das, Pennsylvania State University, University Park, Pennsylvania 16802 (work funded under NASA Grant NAG3–1563); A. Khavaran, NYMA, Inc., 2001 Aerospace Parkway, Brook Park, Ohio 44142 (work funded under NASA Contract NAS3–27186); A.P. Das, Youngstown State University, Youngstown, Ohio 44555. Project Manager, Eugene A. Krejsa, Propulsion Systems Division, NASA Lewis Research Center, organization code 2770, (216) 433–3951.

**12a. DISTRIBUTION/AVAILABILITY STATEMENT**

Unclassified - Unlimited
Subject Category 71

This publication is available from the NASA Center for Aerospace Information, (301) 621–0390.

**12b. DISTRIBUTION CODE**

**13. ABSTRACT** (*Maximum 200 words*)

The report summarizes a computational jet noise study of an ideal contoured plug-nozzle (CPN), The gasdynamics of the jet flows have been predicted using the CFD code, NPARC with k-ε turbulence model; these data are then used as inputs to perform the noise computations based on the modified version of General Electric MGB code. The study covers a range of operating pressure ratio, $2.0 \le \xi \le 5.0$ (shockless flow at design pressure ratio, $\xi_d = 3.62$). The agreement of the computational aeroacoustics results with the available experimental data may be considered to be favorable. The computational results indicate consistent noise reduction effectiveness of the CPN at all operating pressure ratios. At the design pressure ratio (shockless), the codes predict overall sound pressure levels within +3.0dB of the experimental data. But at the off-design pressure ratios (flows with shocks), the agreement is rather mixed. The theory overpredicts the OASPL's at all pressure ratios except at lower angles to the jet axis in overexpanded mode ($\xi \le \xi_d$), the deviations being within 4.5dB. The mechanism of shock formations in the CPN jet flows is noted to be basically different from those in the convergent-divergent nozzle jet flows.

**14. SUBJECT TERMS**

Acoustics; Jet aircraft noise

**15. NUMBER OF PAGES**

80

**16. PRICE CODE**

A05

| 17. SECURITY CLASSIFICATION OF REPORT | 18. SECURITY CLASSIFICATION OF THIS PAGE | 19. SECURITY CLASSIFICATION OF ABSTRACT | 20. LIMITATION OF ABSTRACT |
|---|---|---|---|
| Unclassified | Unclassified | Unclassified | |

National Aeronautics and
Space Administration

**Lewis Research Center**
21000 Brookpark Rd.
Cleveland, OH 44135-3191